



VYSOKÉ UČENÍ TECHNICKÉ V BRNĚ  
BRNO UNIVERSITY OF TECHNOLOGY



FAKULTA STROJNÍHO INŽENÝRSTVÍ  
ÚSTAV MECHANIKY TĚLES, MECHATRONIKY A  
BIOMECHANIKY

FACULTY OF MECHANICAL ENGINEERING  
INSTITUTE OF SOLID MECHANICS, MECHATRONICS AND  
BIOMECHANICS

# FRACTURE BEHAVIOR OF WELDED POLYOLEFIN PIPES

LOMOVÉ CHOVÁNÍ SVAŘOVANÝCH POLYOLEFINOVÝCH TRUBEK

DIPLOMOVÁ PRÁCE  
MASTER'S THESIS

AUTOR PRÁCE  
AUTHOR

Bc. JAKUB MIKULA

VEDOUCÍ PRÁCE  
SUPERVISOR

Ing. MARTIN ŠEVÍK, Ph.D.

BRNO 2015



Vysoké učení technické v Brně, Fakulta strojního inženýrství

Ústav mechaniky těles, mechatroniky a biomechaniky

Akademický rok: 2014/2015

## **ZADÁNÍ DIPLOMOVÉ PRÁCE**

student(ka): Bc. Jakub Mikula

který/která studuje v **magisterském navazujícím studijním programu**

obor: **Inženýrská mechanika a biomechanika (3901T041)**

editel ústavu Vám v souladu se zákonem 111/1998 o vysokých školách a se Studijním a  
zkušebním řádem VUT v Brně určuje následující téma diplomové práce:

### **Lomové chování svařovaných polyolefinových trubek**

v anglickém jazyce:

### **Fracture behavior of welded polyolefin pipes**

Stručná charakteristika problematiky úkolu:

Cílem diplomové práce je popis lomového chování polyolefinového potrubí, které je ovlivněno  
tupým svarovým spojem. V průběhu svařovacího procesu dochází ke změně geometrie potrubí a  
změně materiálových vlastností. Poškození potrubí pak může být způsobeno iniciací a růstem  
radiální nebo axiální trhliny rostoucí v blízkosti svarového spoje. Nezbytné numerické analýzy  
budou provedeny v konečnoprvkovém systému ANSYS.

Cíle diplomové práce:

Diplomová práce bude obsahovat:

- 1) Úvod do lomové mechaniky
- 2) Literární rešerše zaměřenou na poškození polyolefinových trubek
- 3) Vývoj 2D a 3D numerických modelů homogenního potrubí obsahující trhlinu
- 4) Vývoj 3D numerického modelu svarového spoje dvou trubek
- 5) Zahrnutí vlivu materiálové nehomogenity, způsobené svařovacím procesem, do numerického modelu
- 6) Diskuzi získaných výsledků
- 7) Závěr

Seznam odborné literatury:

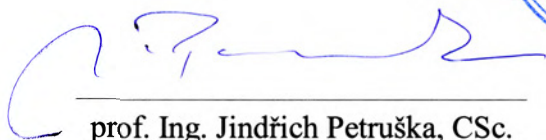
- [1] JANSON, L.-E. Plastic Pipes for Water Supply and Sewage Disposal. Neste, 1989.
- [2] ANDERSON, T.L.: Fracture Mechanics – Fundamentals and Applications, 2nd edition, CRC Press Inc, 1995.
- [3] FRANK, A. et al. A fracture mechanics concept for the accelerated characterization of creep crack growth in PE-HD pipe grades. Engineering Fracture Mechanics. 2009-12, Vol. 76, No. 18, p. 2780–2787.
- [4] HUTAŘ, P. et al. A numerical methodology for lifetime estimation of HDPE pressure pipes. Engineering Fracture Mechanics. 2011-12, Vol. 78, No. 17, p. 3049–3058.
- [5] LESKOVICS, K.; KOLLÁR, M.; BÁRCZY, P. A study of structure and mechanical properties of welded joints in polyethylene pipes. Materials Science and Engineering: A. 2006-03-15, Vol. 419, No. 1–2, p. 138–143.

Vedoucí diplomové práce: Ing. Martin Ševčík, Ph.D.

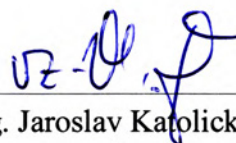
Termín odevzdání diplomové práce je stanoven časovým plánem akademického roku 2014/15.

V Brně, dne 24.11.2014





prof. Ing. Jindřich Petruška, CSc.  
Ředitel ústavu



doc. Ing. Jaroslav Katolický, Ph.D.  
Děkan

## Abstract

The purpose of this diploma thesis is to introduce fracture behavior of welded polyolefin pipes. This study is focused on numerical modelling of the quasi-brittle failure which is a direct result of slow creep crack growth. Welding of polyolefin pipes causes material inhomogeneity in the welded region and the weld bead shape introduces geometric stress raisers. The aim of the thesis is to evaluate these influences on the welded pipe lifespan and its assessment. Different experimental tests (mainly CRB and PENT tests) which allow measuring of material properties describing the crack growth kinetics are presented in the thesis. The results of numerical modelling are presented for a polyethylene pipe (PE 100 110 x 6.3 SDR 17.6). Polyethylene is one of the most common material used in the pipeline industry, but the results of the thesis can be used for any other polyolefin material as well. Lifetime prediction of polyolefin pipes is based on the Linear Elastic Fracture Mechanics (LEFM) using the concept of the stress intensity factor. The thesis complements the existing methodology of pipe lifetime assessment, specifically lifetime prediction of welded polyolefin pipes and a possible direction for future related research is given.

## Keywords

Polyolefin pipes, Finite Element Method (FEM), Fracture mechanics, Creep crack growth

## Abstrakt

Cílem této diplomové práce je řešit problematiku poškozování svařovaných polyolefinových potrubí. Prezentovaná práce je zaměřena na numerické modelování kvazi-křehkého porušování, které je přímým důsledkem šíření creepové trhliny. Svařování polyolefinových potrubí vnáší do oblasti svaru nehomogenní rozložení materiálových vlastností a tvar svarového výronku způsobuje vznik geometrických koncentrátorů napětí. Posouzení těchto vlivů na životnost svarového spoje a výpočet polyolefinových potrubí je hlavním cílem této práce. V práci je uveden popis několika experimentálních testů (především CRB a PENT) k určení materiálových vlastností popisujících kinetiku trhliny. Výsledky práce jsou prezentovány pro polyetylenové potrubí (PE 100 110 x 6.3 SDR 17.6). Polyetylen je jeden z nejčastěji používaných materiálů právě v oblasti potrubních systémů. Prezentované výsledky práce mohou být použity i pro jiný polyolefinový materiál. Predikce životnosti polyolefinových potrubí je založena na lineárně elastické lomové mechanice (LELM) a koncepci faktoru intenzity napětí. Diplomová práce doplňuje tuto metodologii výpočtu životnosti o výpočet svařovaných polyolefinových potrubí z pohledu lomové mechaniky s náznakem možnosti budoucího výzkumu.

## Klíčové slová

Polyolefinové potrubia, Metóda konečných prvkov (MKP), Lomová mechanika, Šírenie creepovej trhliny

MIKULA, Jakub. Fracture behavior of welded polyolefin pipes: master's thesis. Brno: Brno University of Technology, Faculty of Mechanical Engineering, Institute of Solid Mechanics, Mechatronics and Biomechanics, 2015. 111 p. Supervised by Ing. Martin Ševčík, Ph.D.

# Declaration

I declare that I have written my master's thesis, *Fracture Behavior of Welded Polyolefin Pipes*, independently, under the guidance of the master's thesis supervisor. All technical literature and other sources of information used in the thesis have been cited within the text and detailed in the bibliography. As the author of the master's thesis, I furthermore declare that I have not infringed any copyright. In particular, I have not unlawfully encroached on anyone's personal and/or ownership rights, and I am fully aware of the consequences in the case of breaking Regulation S 11 and the Copyright Act No 121/2000 Sb., and of the rights related to intellectual property and changes in the Intellectual Property Act formulated in later regulations, inclusive of the possible consequences resulting from the provisions of Criminal Act No 40/2009 Sb., Section 2, Head VI, Part 4.

© Jakub Mikula, 2015

Institute of Solid Mechanics, Mechatronics and Biomechanics  
Faculty of Mechanical Engineering  
Brno University of Technology

and

Institute of Physics of Materials  
Academy of Sciences of the Czech Republic, v. v. i.  
Brno

mikula@ipm.cz  
mikula.jakub@centrum.sk  
tel.: +420 607 881 232





## Acknowledgements

I would like to express my deepest gratitude to my supervisor, Ing. Martin Ševčík, Ph.D. for his professional guidance, consultations, patience, and insightful suggestions during the completion of this thesis. I offer my heartfelt thanks to doc. Ing. Pavel Hutař, Ph.D. for his frequent consultations, useful advice, and critical evaluation of my writing and problem solving. Also I would like to thank my colleagues from the Institute of Physics of Materials (IPM), including Katka Štegnarová, Pavel Pokorný, Ján Poduška, and Vír Horník, who supported and motivated me with their insights, suggestions, and helpful advice. Last but not least, I want to thank all who helped make my studies simultaneously interesting and challenging, and who gave me the opportunity to make it an interesting and challenging experience for others. For a lot of grammatical corrections I would like to offer a huge thanks to Jessica.



The research was supported by the Ministry of Education, Youth and Sports of the Czech Republic throughout the project No. CZ.1.07/2.3.00/30.0063 Talented postdocs for scientific excellence in physics of materials and by CEITEC – Central European Institute of Technology with research infrastructure supported by the project CZ.1.05/1.1.00/02.0068 financed from European Regional Development Fund. This research was also supported by the Czech Science Foundation by grant No. P108/12/1560



# Contents

<b>1</b>	<b>Introduction</b>	<b>15</b>
<b>2</b>	<b>Polyolefin Pipes</b>	<b>17</b>
2.1	Material of Choice . . . . .	17
2.2	Basic Polyethylene Pipe Parameters . . . . .	18
2.3	Material Properties of Basic Pipe Material . . . . .	19
2.3.1	Viscoelastic Behaviour of Polyolefin Pipes . . . . .	19
2.3.2	Creep Modulus . . . . .	20
2.4	Joining of Polyolefin Pipes . . . . .	20
2.4.1	Butt Welding . . . . .	20
2.4.2	Electro-Fusion Welding . . . . .	22
2.5	Correlation Between Structure and Properties of Welded Region . . . . .	22
2.6	Failure Mechanisms of Pressurized Pipes . . . . .	23
2.6.1	Creep Crack Growth . . . . .	25
2.7	Experimental Testing of Polyolefins . . . . .	26
2.7.1	Hydrostatic Pressure Test . . . . .	27
2.7.2	CRB Test . . . . .	28
2.7.3	PENT test . . . . .	29
<b>3</b>	<b>Theoretical Background on Fracture Mechanics</b>	<b>31</b>
3.1	Introduction . . . . .	31
3.2	Linear Elastic Fracture Mechanics . . . . .	31
3.2.1	Mathematical Background on Crack-Like Discontinuities . . . . .	32
3.2.2	Numerical Methods on the Stress Intensity Factor Assessment . . . . .	35
3.2.3	Estimation of the Crack Propagation Direction . . . . .	38
3.2.4	Plastic Zone Size . . . . .	39
<b>4</b>	<b>Problem Formulation and Aims of Diploma Thesis</b>	<b>41</b>
<b>5</b>	<b>Semi-Analytical Solutions of SIF in a cracked Pipe</b>	<b>43</b>
5.1	Semi-Elliptical Surface Crack in a Pipe . . . . .	43
5.2	Full Circumferential Crack in a Pipe . . . . .	45
5.3	Axial Through-Thickness Crack in a Pipe . . . . .	46
<b>6</b>	<b>Numerical Models Description</b>	<b>49</b>
6.1	Description of the Pipe Geometry . . . . .	50

6.2	Description of the Crack Front Shape . . . . .	51
<b>7</b>	<b>Optimal Welding Conditions</b>	<b>55</b>
7.1	Optimal Welding Procedure of PE 100 . . . . .	55
7.2	Material Inhomogeneity Implementation . . . . .	56
7.3	Different Locations of Crack Initiation . . . . .	57
7.4	Stress Intensity Factor Assessment . . . . .	59
7.4.1	Weld Bead Removed - Axial Crack Propagation . . . . .	60
7.4.2	Weld Bead Removed - Circumferential Crack Propagation . . . . .	61
7.4.3	Weld Bead Kept - Axial Crack Propagation . . . . .	63
7.4.4	Weld Bead Kept - Circumferential Crack Propagation . . . . .	63
7.5	Accuracy of the Obtained Results . . . . .	65
7.5.1	Accuracy for Axial Cracks . . . . .	65
7.5.2	Accuracy for Circumferential Cracks . . . . .	66
7.6	Crack Trajectories in Optimal Butt Welded Pipes . . . . .	67
<b>8</b>	<b>Comparison of the Optimal Butt Welding Pipe Failure Modes</b>	<b>69</b>
<b>9</b>	<b>Non-Optimal Welding Conditions</b>	<b>71</b>
9.1	Influence of Weld Bead Shape . . . . .	72
9.2	Influence of Weld Bead Radius . . . . .	73
9.3	Crack Trajectories for Various Welding Conditions . . . . .	74
<b>10</b>	<b>Crack Propagation in Electro-Fusion Welded Pipes</b>	<b>77</b>
10.1	Numerical Model . . . . .	78
10.2	Crack Propagation . . . . .	79
10.3	Comparison of the Electro-Fusion and Butt Welding Joint Failure Modes . .	79
<b>11</b>	<b>Lifetime Prediction of PE 100</b>	<b>81</b>
11.1	Material Properties of PE 100 . . . . .	81
11.1.1	PE 100 Short Term Properties . . . . .	81
11.1.2	PE 100 Long Term Properties . . . . .	82
11.2	Lifetime Prediction Based on the Numerical Models . . . . .	83
11.2.1	Time to Failure of Butt Welded Pipes (Optimal Welding Conditions)	85
11.2.2	Time to Failure of Butt Welded Pipes (Non-Optimal Welding Conditions)	87
11.2.3	Time to Failure of Electro-Fusion Welded Pipes . . . . .	88
<b>12</b>	<b>Conclusion</b>	<b>89</b>
<b>13</b>	<b>Author's Contributions</b>	<b>93</b>
	<b>Bibliography</b>	<b>101</b>
	<b>List of Abbreviations</b>	<b>103</b>
	<b>List of Symbols and Physical Constants</b>	<b>105</b>

<b>List of Appendices</b>	<b>107</b>
<b>A Flow Diagrams</b>	<b>109</b>
A.1 Algorithm of Axial Crack Propagation . . . . .	109
A.2 Algorithm of Circumferential Crack Propagation . . . . .	110
<b>B APDL Scripts</b>	<b>111</b>
B.1 Material Inhomogeneity Implementation . . . . .	111



# Chapter 1

## Introduction

Polyolefin pipes have significant applications in water and gas transportation. They are characterized mainly by the advantages of being highly resistant to corrosion. Due to their flexibility, excellent flow characteristics, suitability for welding, polyolefin pipes are preferable to other materials for use in pipeline industries.

An important aspect of pipeline system installation is connecting pipes. The most common connection being used for a wide range of pipe diameters is the butt welding joint created by applying heat and pressure. This standardized welding process, outlined in ISO 21307 [1], involves a change of material properties and results in a weld bead geometry. Another very well known procedure for connecting pipes is electro-fusion which melts pipes together by sending a current through a closely fitted heating coil.

Optimizing the longevity and functionality of pipes is a source of competition in the pipeline industry. Recently developed materials such as High Density Polyethylene (HDPE) provide full functionality of a system for over fifty years. A better understanding the pipe life-cycle may lead to further optimization and design of the connection process or pipes themselves. Although it is possible to predict the life expectancy of welded pipes by performing a hydrostatic pressure test, such as in EN ISO 9080 [2], the procedure is extremely time consuming. Numerical predictions [3] of pipeline life expectancy are therefore highly valuable speeding up the process of weld bead technology development, as well as safety assessment.

Understanding the vulnerabilities of welded pipes is essential to the optimization process. Damage to a pipeline system may be a consequence of a number of factors, such as the flowing medium exerting high pressure on the inner pipe walls, chemical degradation, or slow creep crack growth. Highlighting the last factor, this thesis shows that slow crack growth (SCG) caused by creep is the most common type of damage found in experiments and real applications under normal working conditions.

It is shown that the process of creep crack growth in polyolefin pipes may be characterized using the Linear Elastic Fracture Mechanics (LEFM). It was verified by many experiments that this approach is relevant to analyzing slow crack growth propagating with the small plastic zone at the crack tip.

The main aim of the thesis is to describe the influence of welding on the lifespan of polyolefin pipes. A large portion of the thesis is focused on polyethylene as one of the most frequently used polyolefin materials in pipelines. Building upon the LEFM methodology for pipe lifespan assessment, numerical simulations of welding polyolefin pipes under different conditions are created and analyzed using the commercial package ANSYS. Different ANSYS Parametric Design Language (APDL) codes are created to simulate crack propagation in pipes for different welding conditions. Crack propagation in 2D numerical models is simulated based on the APDL algorithm proposed in the author's bachelor's thesis [4] improved here of analysing axisymmetric bodies.

The thesis may be divided into three general sections. The first section (*Chapter 2, Polyolefin Pipes*) is devoted to the background of polyolefin pipe material, pipe failure mechanisms, and the two most common welding procedures (butt welding and electro-fusion welding). The end of the chapter is devoted to the experimental testing of polyolefins, giving descriptions of the basic experimental tests involved (Cracked Round Bar (CRB) and Pennsylvania Edge Notched Tensile (PENT) tests).

The second section (*Chapter 3, Theoretical Background of Fracture Mechanics*) provides the basics of LEFM. It begins with a short introduction, followed by a description of basic mathematical formulas, numerical methods, and restrictions.

As the third section, the remainder of the thesis discusses various numerical models and provides an analysis of their results. Simple analytical solutions are introduced and compared to numerical models for optimal and non-optimal welding conditions, followed by a discussion of the electro-fusion welding joint. The end of the section is devoted to an analysis of lifespan estimation for welded polyethylene pipes, specifically PE 100 110x6.3 SDR 17.6, and with a short description of recently measured material properties of the welded region.

Finally, all major aspects of the thesis, including a summary of all experimental results, results of numerical calculations and recommendations, are summarized in the conclusion.



# Chapter 2

## Polyolefin Pipes

### 2.1 Material of Choice

Polyolefin is a thermoplastic material (a class of polymers) which is produced by polymerization (chemical linking) of simple olefins. The most common olefins are ethylene and propylene, which can be polymerized to create polyethylene (PE) or polypropylene (PP). Polyolefins consist only of carbon and hydrogen atoms, and they are usually processed by extrusion or molding. Figure 2.1 illustrates polyethylene molecular chain production. After converting methane gas into ethylene, heat and pressure is added to produce polyethylene.

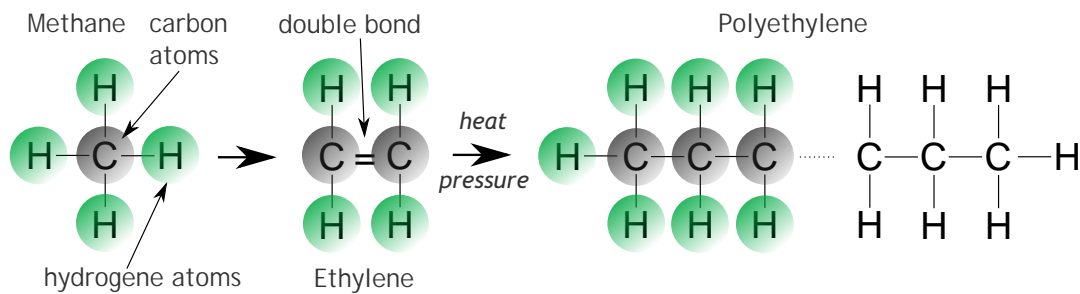


FIGURE 2.1: Polyethylene molecular chain [5]

As a polyolefin, polyethylene is highly resistant to corrosion, abrasion, and chemical attack. However, it is often combined with colorants, stabilizers, anti-oxidants, and other ingredients to protect or improve material properties. In addition to these advantages, polyethylene is flexible, light-weight, provides good insulation, and has successfully substituted steel and cast iron in many applications of pipeline industries [6].

Polyethylene has become one of the world's most widely used and recognized thermoplastic materials in pipelines. Already in 1955, a pipe made from High Density Polyethylene (HDPE) was first produced. Karl Ziegler was awarded the 1963 Nobel Prize in Chemistry for his invention of HDPE. Due to the emergence of additional common polyethylene materials, such as Medium Density polyethylene (MDPE) and Low Density Polyethylene (LDPE), polyethylene materials are now categorized according to density under the standardized

classification, as in ASTM D 3350 [7]. MDPE is usually used for low-pressure gas pipelines, and LDPE is typically used for small-diameter water-distribution pipes [5]. HDPE has less flexibility but greater strength, ideal for use in larger pipe systems which must withstand high internal pressure. Typical applications are found in drainage systems, oil and gas production, and water and gas distribution.

## 2.2 Basic Polyethylene Pipe Parameters

Polyethylene piping is in general very suitable for places where vibrations occur or where aggressive ground conditions are present. In the pipeline industry, several types of polyethylene are characterized by their minimal required stress value,

$$MRS = \frac{p_{in} \cdot d}{2 \cdot s}, \quad (2.1)$$

where  $p_{in}$  is the inner pressure in  $MPa$ ,  $d$  is the pipe's nominal outer diameter, and  $s$  is the nominal wall thickness. The most common types are PE 80 and PE 100.

Another important parameter is the Standard Dimensional Ratio (SDR), measuring pipe durability under pressure. It is a rounded number expressing the ratio between the nominal outer diameter and nominal thickness,

$$SDR = \frac{d}{s}. \quad (2.2)$$

Figure 2.2 illustrates three typical examples of SDR. A lower ratio is an indication that the pipe can withstand higher pressures, since the pipe wall is thicker in comparison to the diameter.

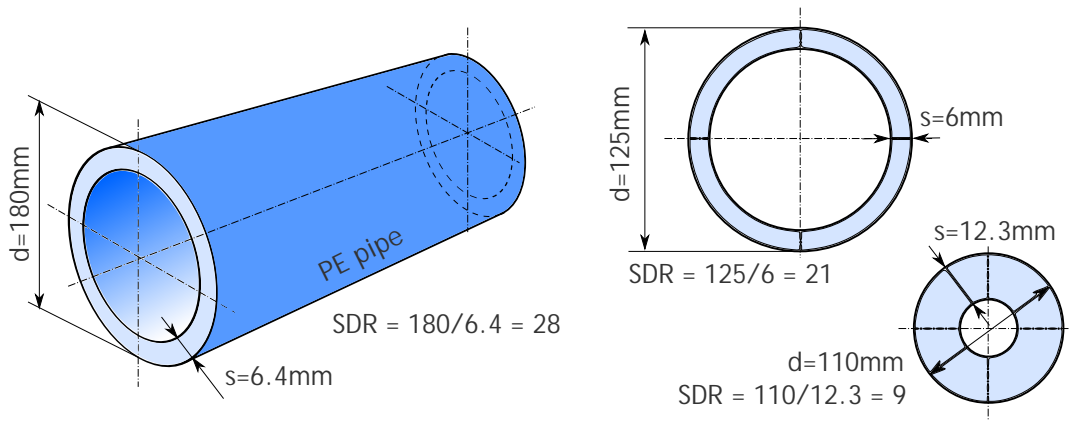


FIGURE 2.2: Standard Dimensional Ratio (SDR)

Long term behavior of polyolefins in pipe systems has been studied extensively for many years. Pipes made from HDPE can maintain perfect working conditions for over fifty years.

There is, however, a demand for pipes to last more than 100 years. One way to achieve this goal is to enhance the material properties of the pipes by designing new materials, connections, and welding techniques. Understanding both the weaknesses and strengths of pipe physical limitations will benefit the pipe system optimization process, leading to increased pipe life expectancy, as well as potential environmental and economical growth. The influence of pipe welding and related factors, particularly their impact on the lifespan of welded pipe systems, is discussed throughout the thesis.

## 2.3 Material Properties of Basic Pipe Material

This chapter introduces the basic material properties of polyolefin materials. (See Chapter 2.5 for an introduction to material properties of welded regions).

### 2.3.1 Viscoelastic Behaviour of Polyolefin Pipes

Polyolefin materials in general exhibit viscoelastic behavior. This means that the stress response, or the deformation response, are time-dependent. The viscoelastic nature of polyolefin results into two unique characteristics - creep and stress relaxation, which are described below.

#### creep

Creep is the time-dependent deformation due to a constant amount of stress. When the viscoelastic material is subjected to a constant static load (constant stress), it deforms with time. If the stress is too great, the material may rupture. See Figure 2.3 (left).

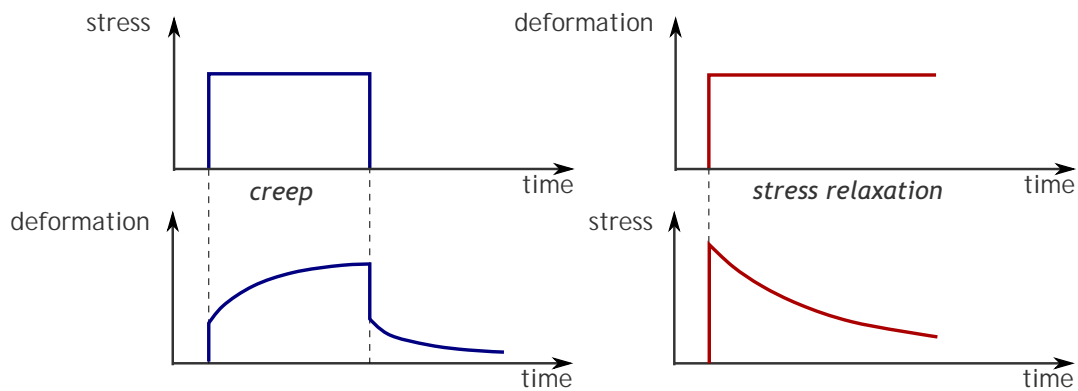


FIGURE 2.3: Stress and deformation response of viscoelastic materials

#### stress relaxation

When the viscoelastic material is subjected to a constant deformation (constant strain), the stress caused by the initial deformation slowly decreases with time. This phenomenon is called stress relaxation, the decreasing amount of stress resulting from constant deformation. See Figure 2.3 (right).

Viscoelastic materials are typically modeled using springs and dashpots, or other devices representing viscous and elastic behavior.

### 2.3.2 Creep Modulus

Under short-term loading, the modulus of elasticity describes the linear part of the stress-strain curve (Hooke's law), and characterizes the stiffness of the material.

However, viscoelastic material loading, especially long-term loading, exhibits a non-linear stress-strain curve. This kind of deformation is usually described by the creep modulus  $E_C$ ,

$$E_C = E_C(\sigma, t, T) = \frac{\sigma}{\varepsilon(\sigma, t, T)}, \quad (2.3)$$

which depends on the applied load force  $\sigma$ , deformation time  $t$  and temperature  $T$ . Although the creep modulus does not give a complete description of the material stiffness, it is a useful ratio comparing the force and the deformation.

## 2.4 Joining of Polyolefin Pipes

Making well-formed pipe connections is the key factor ensuring the reliability of a pipe system. Poorly-crafted joints may cause installation delays and/or result in system leakage.

Polyolefin pressure piping products are connected via fusion or mechanical methods. Heat fusion is a weather-independent process often requiring electrically powered equipment. The most common types of heat fusion used for pipe welding are butt welding and electrofusion welding. This thesis examines the pros and cons of both techniques in terms of slow crack propagation, which is the primary cause of pipe rupture. A brief introduction to the technological procedures is described in the following chapters.

### 2.4.1 Butt Welding

Butt welding is the most widely used method for joining of PE pipes, and the only option for connecting pipes with diameter larger than 500mm [8].

Two pipes of the same diameter and wall thickness are joined using heat and pressure action. The process usually takes a few minutes. (See Figure 2.6 for a simplified schematic of a typical procedure.) The method is considered to be fast, cheap, and easy to operate. There are many standards describing this welding procedure, but the most commonly used are the German standard DVS 2207-1 [9] (single pressure procedure) and ISO 21307 [1] (dual pressure procedure).

Figure 2.4 and Figure 2.5 feature real-world examples of the installation and butt welding process joining huge pipes. Two pipes of the same diameter and wall thickness are heated to



FIGURE 2.4: Welding and installation [8]

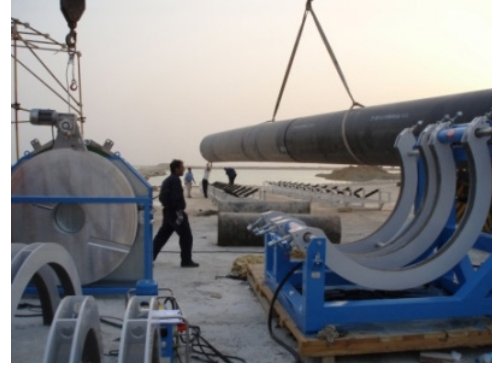


FIGURE 2.5: Butt welding fittings [8]

a molten state and pressed together. The surfaces of the pipes are heated using electrically heated plates (see the plate in Figure 2.5 on the left). After a prescribed time, the pipes are cooled until a solid bond is formed.

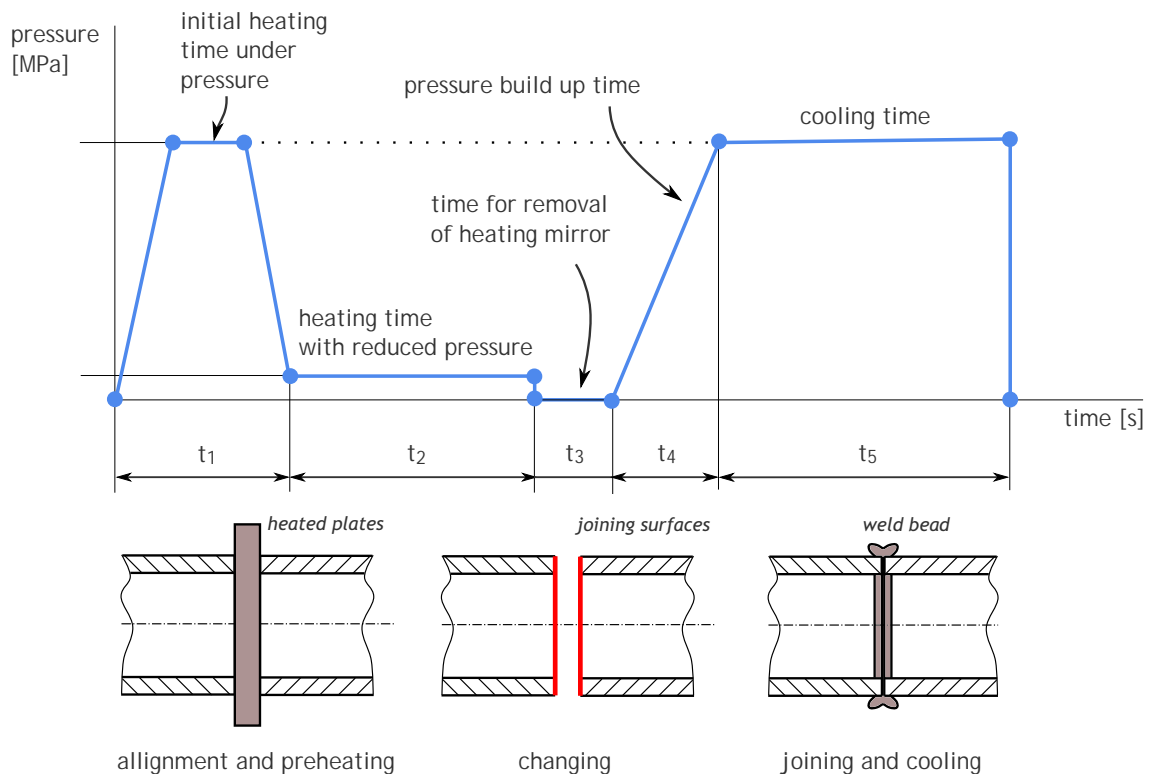


FIGURE 2.6: Butt welding procedure

Changes in material properties, as well as the resulting weld bead geometry, are typical to each welding procedure. Usually, the correct welding procedure leads to the so-called optimal weld bead shape. Figure 2.7 depicts an example of the optimal bead geometry on a pipe wall.

Nowadays, the butt welding process is usually controlled by Computer Numerical Control (CNC) machines, which automates both the welding and data recording.



FIGURE 2.7: Optimal weld bead geometry in a pipe wall

### 2.4.2 Electro-Fusion Welding

Although it uses the same principle of heat fusion, electro-fusion welding of polyolefin pipes is somewhat different than butt welding. Electro-fusion requires a special fitting (see Figure 2.8) in which electrical current is applied to a wire coil, causing the adjacent materials to melt. The pipes are welded only in the region where the coil is placed. The fitting becomes a permanent part of the connection, which is then cooled until a solid joint is created. Welding pipes with different wall thickness can be done only via electro-fusion welding.

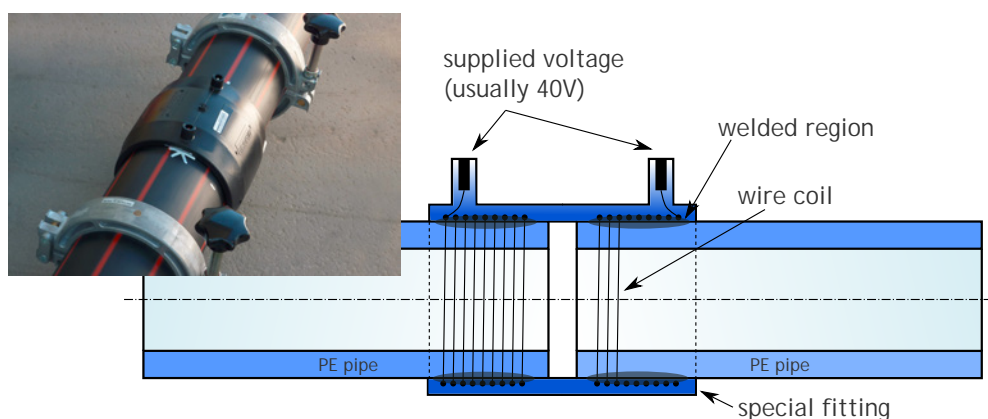


FIGURE 2.8: Electro-fusion weld description (the left figure taken from [10])

## 2.5 Correlation Between Structure and Properties of Welded Region

Knowledge of the correlation between structure and properties of polymer welds is essential for estimating the lifespan of welded pipes. Despite the high number of papers dealing with the relationship between morphology and mechanical behavior of bulk polyethylene (e.g., [11], [12], [13], [14]), the constitution of the welding joints has not been thoroughly investigated [15], [16], [17].

An example of a welded connection in polarized light with well visible changes in microstructure can be seen in Figure 2.9. The degree of crystallinity is highest at the center of the welding joint (indicated by the red color), and lowest in the non-heated pipe areas.

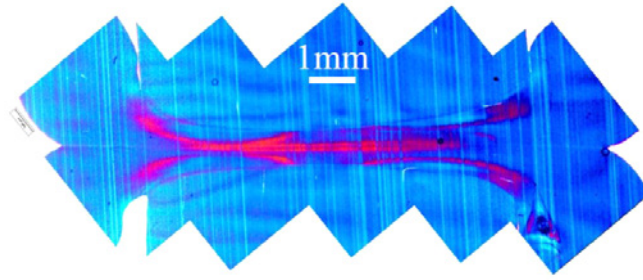


FIGURE 2.9: Welded connection in polarized light [17]

The greater the proportion of crystals, the higher the density and brittleness of the resin [5]. This may lead to stress cracking, increased permeability, reduced impact strength, and lower resistance to slow crack growth. On the other hand, stiffness, tensile strength, creep resistance, and resistance to chemicals are increased [18].

The above trends correlate well with the results of micro-hardness tests performed at the Martin-Luther University Halle-Wittenberg, Germany [17]. The correlation between hardness and stiffness (Young's modulus) is easily detected. Figure 2.10 and Figure 2.11 illustrate the inhomogeneous distribution of Young's modulus according to the micro-hardness tests of polyethylene and polypropylene, respectively. (Refer to Chapter 7.2 for more specific details.)

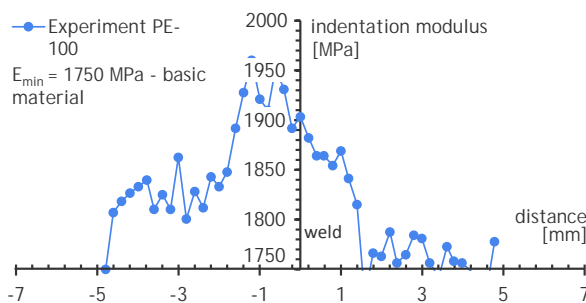


FIGURE 2.10: Young's modulus correlation with micro-hardness tests of PE [17]

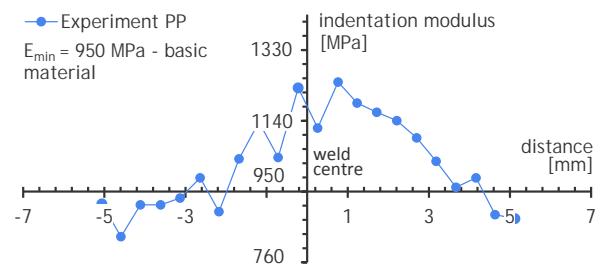


FIGURE 2.11: Young's modulus correlation with micro-hardness tests of PP [17]

## 2.6 Failure Mechanisms of Pressurized Pipes

The lifespan of polyolefin pipes is reduced by structural weakness and overloading. By considering only the pressure exerted by a medium on the inner walls of a pipe, pipe failure mechanisms can be generalized by one of the following three stages: ductile failure, quasi-brittle failure, and brittle failure. Figure 2.12 and the following descriptions illustrate when these three stages occur in the pipe degradation process caused by stress over time.

### region A

As seen in Figure 2.12, the first stage (region A) is characterized by a high amount



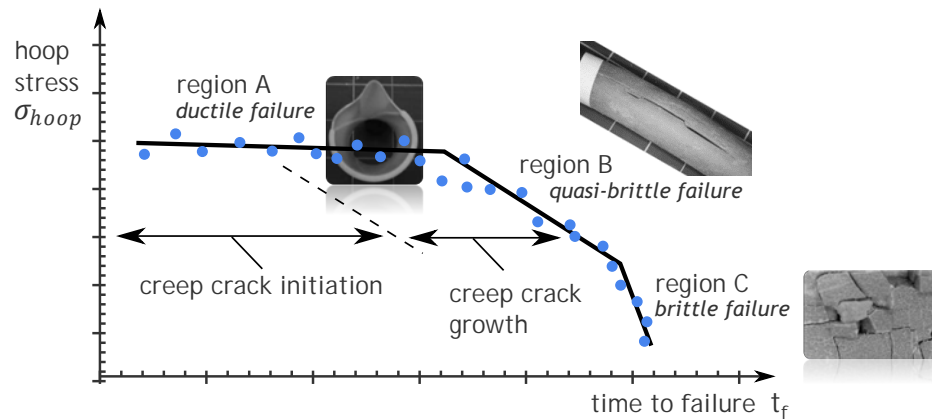


FIGURE 2.12: Polyolefin pipe failure stages

of hoop stress (tangential stress resulting from radial pressure of inner medium). This leads to instability of pipe wall and huge irreversible pipe deformations. Application of excessive pressure at this stage can then cause instant pipe failure. This phenomenon is called ductile failure, and is rare. Two examples of ductile failure are shown in Figure 2.13 and Figure 2.14.

FIGURE 2.13: Ductile failure of a pipe  
(photo author: Jiri Sadilek, Polymer Institute Brno )FIGURE 2.14: Ductile failure of a pipe  
(photo author: Jiri Sadilek, Polymer Institute Brno )

### region B

The second stage (region B) is the so-called quasi-brittle failure which is a direct consequence of crack initiation followed by Creep Crack Growth (CCG). The hoop stress is mild and the crack propagation may take many years. Chapter 2.6.1 describes this type of failure process in more detail. As the most common failure mechanism, CCG has been discussed in many publications, for instance [19], [20], [21], [22].

### region C

In the last stage (region C), material degradation is a consequence of thermo-oxidation over a long period of time. This is known as brittle fracture. The pipe can be protected using chemical stabilizers inhibiting oxidation. Figure 2.15 and Figure 2.16 illustrate examples of brittle failure in the form of Stress Corrosion Cracking (SCC).



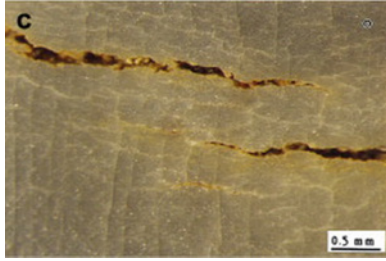


FIGURE 2.15: Microcrack network of SCC on the inner surface of a polybutylene pipe [23]

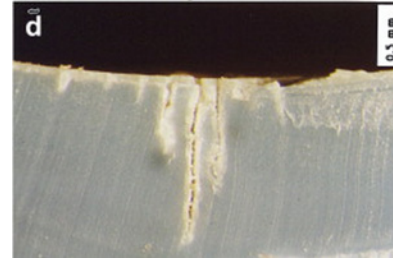


FIGURE 2.16: Observation of SCC in radial direction of a polybutylene pipe [23]

### 2.6.1 Creep Crack Growth

As mentioned in the previous section, the majority of the failures of polyethylene (PE) pipes in real service are attributed to Slow Crack Growth (SCG) which is characterized by stable crack growth and small plastic zone initiated at the crack tip. In the presence of these conditions, Linear Elastic Fracture Mechanics (LEFM) can be used to describe the crack behavior. (See Chapter 3 for a description of the basics of LEFM). Numerous studies have dealt with creep fracture mechanisms by SCG in polyolefin materials [24], [25], [26].

Already in 1983, it was observed by Chan and Williams [27] that the rate of slow crack growth in high density polyethylene can be described by a function analogous to the Paris-Erdogan equation [28],

$$\frac{da}{dt} = CK^m, \quad (2.4)$$

where  $da/dt$  describes crack kinetics (crack growth rate),  $C$  is a constant for a given resin and temperature, and  $K$  is the stress intensity factor. Chan and Williams proposed the exponent  $m = 4$ , but the exponent varies in practice from 2.6 to 4.8 depending heavily on the type of PE and depending only slightly on the temperature [29].

The crack propagation under fatigue loading from morphological point of view is usually characterized by striations. In metals, this phenomenon is easily recognizable as bands on the fracture surface. A similar effect can be observed in polymer materials as well [30], [31]. Creep crack growth can be discontinuous even under static loading. Cyclic loading, which can accelerate creep crack growth, is usually used in testing of the material.

In pressurized polyethylene pipes under normal conditions, creep crack propagation is slow and the plastic deformation at the crack tip is just local [32], [6]. Depending on the polyolefin, localized geometry, and loading conditions, the plastic zone constitutes of crazes and microcracks (brittle defects), or microvoids and shearbands (ductile defects). These micro-defects increase material compliance near the crack front and decrease high elastic stresses. The formation and evolution of these micro-defects is closely coupled with the crack propagation.

Two main yielding mechanisms are responsible for crack propagation in polyolefin materials. Contrary to metals, which yield by dislocation motion, polymer materials exhibit either shear

yielding or crazing. Shear yielding is characterized by molecules sliding with respect to one another when subjected to a critical shear stress [33].

The craze zone usually forms perpendicular to maximum principal stresses and resembles what a strip-yield model (originally proposed for metals) predicts. According to Oxborough and Bowden's craze criterion [34] the critical strain for crazing decreases with increasing modulus and hydrostatic stress, making the welding joint more pivotal in crack propagation. The proposed craze criterion is,

$$\varepsilon_1 = \frac{\beta(t, T)}{E} + \frac{\gamma(t, T)}{3\sigma_m}, \quad (2.5)$$

where  $\varepsilon_1$  is the maximum nominal principal strain,  $\beta$  and  $\gamma$  parameters (functions of time and temperature),  $E$  represents the Young's modulus, and  $\sigma_m$  is the hydrostatic stress.

A craze zone schematic with unbroken fibers is shown in Figure 2.17 and a photo of the craze zone is depicted in Figure 2.18.

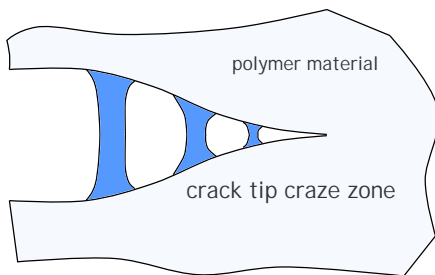


FIGURE 2.17: Schematic crack tip craze zone

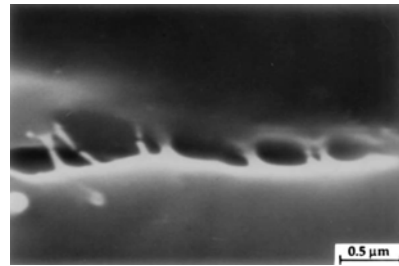


FIGURE 2.18: Craze zone in polypropylene (photo author: M.Cayard )

Crack propagates when individual fibers rupture. The process is therefore discontinuous causing striations to resemble fatigued metals. The amount of shear yielding or crazing depends on the stress state, temperature, and molecular structure.

## 2.7 Experimental Testing of Polyolefins

Knowing material properties is essential for lifetime prediction of polyolefin pipes. The service-life of the pipe is closely connected with the slow crack growth resistance of the pipe material [35]. Even though, polymer materials exhibit viscoelastic (non-linear) behaviour, the linear elastic fracture mechanics can be used to estimate the reliability of a polyolefin pipe. However, this concept requires the knowledge of the crack resistance and the kinetics of Creep Crack Growth (CCG) [32].

Mechanical behaviour can significantly differ between static and cyclic loading. Polyolefin pipes usually fail due to creep crack growth caused by the inner pressure of the flowing medium. The inner pressure acting on the pipe walls may be considered to be constant (static loading). Some experimental tests, however, utilize cyclic loading to accelerate creep crack

growth in order to retrieve material properties in a reasonable time frame. Experimental tests can be further divided into short or long term tests giving short (e.g. resistance against stable crack propagation) or long term (e.g. resistance to creep crack growth) properties.

Short term tests can give relevant results only for applications with high deformation rates ( $\dot{\epsilon}$ ), but for many materials (viscoelastic materials) the deformation or the stress response in real service is relatively small, so short term tests are more appropriate for the lifespan characterization.

A traditional way for determining the long term properties of PE pipes is by performing internal hydrostatic pressure tests. When the information about the CCG is required, these tests are quite expensive and time-consuming. Due to this fact numerous other methods have been developed to simulate the CCG behaviour in a reasonable time frame. Relevant tests for these purposes are Cracked Round Bar (CRB) tests [36] or Pennsylvania Edge Notched Tensile (PENT) tests. These tests are described in more detail in the following sections. Another often used tests are Notch Pipe Tests (NPT), Full Notch Creep Tests (FNCT) or Double Edge Notched Tensile Tests (DENT) [37],[38].

Properties of the PE 100 material used in this thesis were obtained on CRB and PENT tests and are given in Chapter 11.1.

### 2.7.1 Hydrostatic Pressure Test

Hydrostatic pressure tests measure pipe's resistance to hydrostatic pressure. The testing pipes are filled with water and their behaviour is investigated for different temperatures.

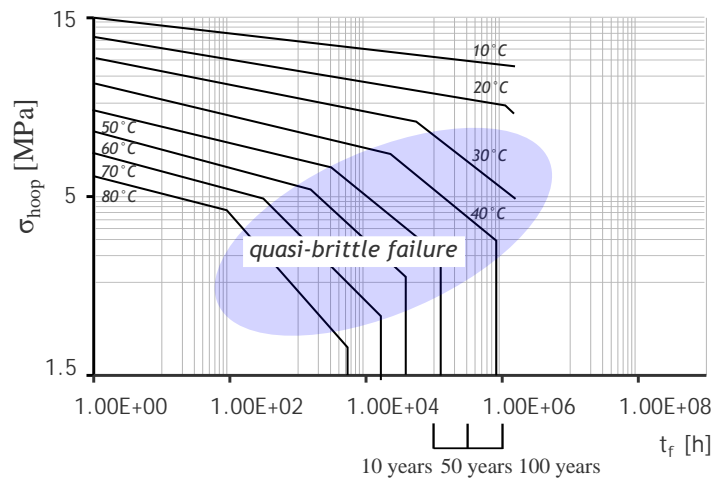


FIGURE 2.19: Hydrostatic pressure curves for HDPE according to DIN 8075 [39]

The temperature is controlled by water bath in which the pipe is placed. The results are plotted in stress vs. time diagrams transformed into log-log coordinates. Typical hydrostatic pressure curves for different temperatures are shown in Figure 2.19. For higher temperatures (e.g. 80°C) the graph typically shows 3 stages (see also Figure 2.12). For higher temperatures the quasi-brittle failure becomes shifted into longer times so the results for normal working

conditions in real applications are extrapolated from temperature-accelerated experimental tests. The test procedure is standardized for instance in ČSN EN ISO 1167-1 [40].

### 2.7.2 CRB Test

Cracked Round Bar (CRB) tests are performed using round bar specimens which are circumferentially notched. Reports first published on these specimens were in Japan [41], [42]. Later work in Europe [43], [44], has shown that CRB tests are able to characterize the crack growth resistance of polymer pipes. This information is very important when assessing lifespan of a pipe. The CRB tests describe the crack kinetics (creep crack growth rate) as a function of the applied loading (usually expressed in terms of the stress intensity factor). The experiment is usually conducted as given below.

A CRB specimen is loaded with a given sinusoidal frequency with a given R-ratio where,

$$R = \frac{F_{min}}{F_{max}} = \frac{K_{I,min}}{K_{I,max}}. \quad (2.6)$$

For different specimens the ratio between the maximum loading force  $F_{max}$  and the minimum loading force  $F_{min}$  is different. Cyclic loading with a higher ratio accelerates crack propagation more.

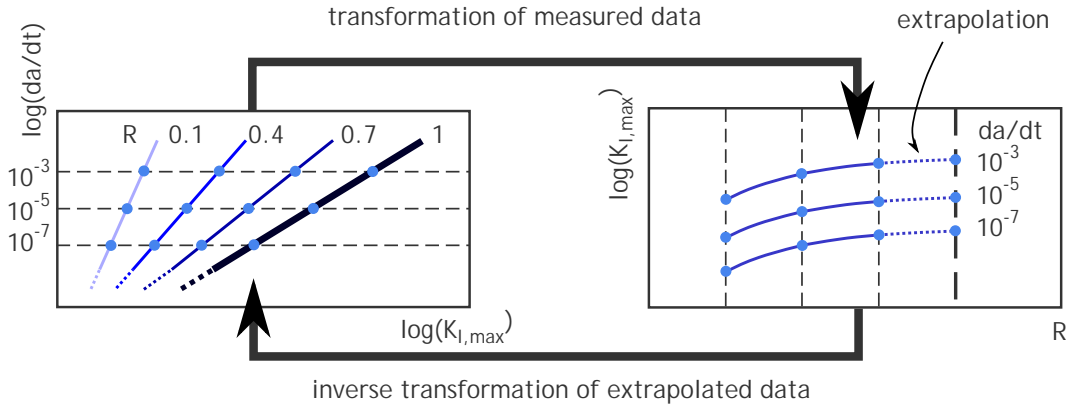


FIGURE 2.20: CRB test data extrapolation [45]

The tests may be accelerated also by increasing the temperature or using stress cracking liquids. Since the static loading for which  $R = 1$  is a very time consuming procedure this state is approached by extrapolating the measurements for different R-ratio approaching one. The extrapolation is shown in Figure 2.20.

Based on the extrapolation methodology proposed by [46], [47], the Fatigue Crack Growth (FCG) curves for different R-ratios (left graph in Figure 2.20) are transformed into the diagram of constant crack rates (right graph in Figure 2.20). In this diagram, they are extrapolated to  $R = 1$ , and this extrapolation is mapped back into the diagram of FCG curves. FCG curves show crack propagation rate as a function of the stress intensity factor

$K_I$ . Based on this curve, the Paris-Erdogan constants,  $C$  and  $m$  (see Equation 2.4) can be calculated. These constants are material properties and can be used to calculate time of slow crack growth using an equivalent equation (Equation 2.4) to the Paris-Erdogan law [28].

A typical fracture surface of a CRB specimen and CRB specimen geometry is presented in Figure 2.21.

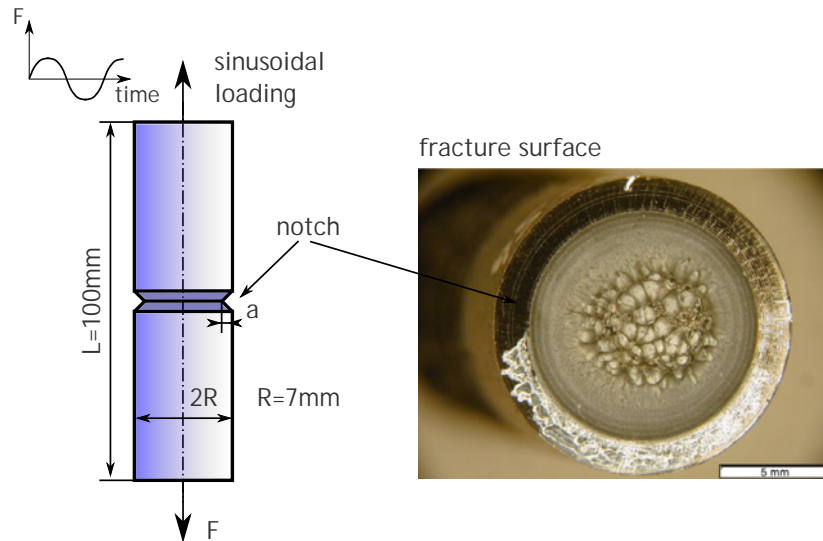


FIGURE 2.21: Typical CRB specimen geometry (left), striations on the brittle fracture surface of a CRB specimen of PE 100-D after fatigue loading [38] (right)

Crack propagates symmetrically from the initial razor blade notch, creating a brittle fracture surface, and fails into a fully ductile fracture surface (center of the CRB specimen in Figure 2.21). The striations are created because of the cyclic loading with the purpose of accelerating the crack growth.

A main advantage of the method is a simple geometry (manufacturable from moulded plates or extruded pipes). CRB specimens provide near plane strain conditions which keep the plastic zone size on its minimum and this way very realistically simulate the real conditions near the crack front in a pressurized pipe.

### 2.7.3 PENT test

Pennsylvania Edge Notched Tensile (PENT) tests are used to determine the resistance to slow crack growth by measuring the total time to failure. PENT test specimens are rectangular and notched on three sides (see Figure 2.22).

The primary purpose of the notch is to introduce a triaxial stress state which would consequently lead to a brittle fracture. The loading is constant and the temperature during the test is increased. The experiment measures the evolution of the Crack Opening Displacement (COD) with respect to time (see Figure 11.3).

Similar to the CRB tests the PENT tests give information about time of slow crack propagation. CRB tests describe the crack growth rate and PENT test time to failure. Each

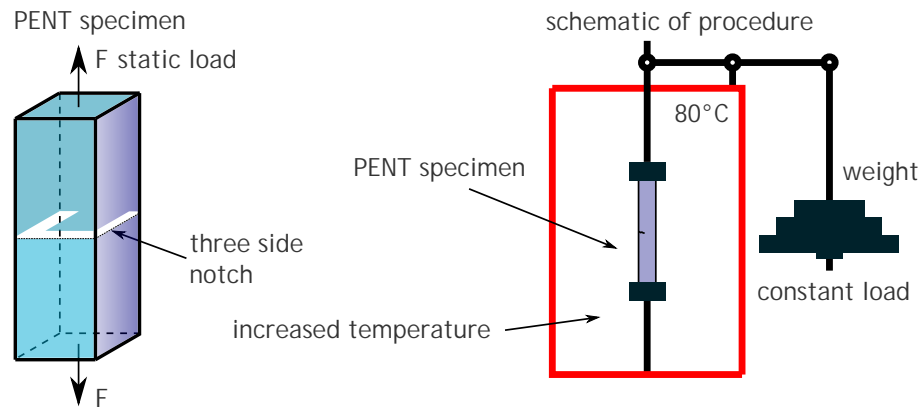


FIGURE 2.22: PENT test specimen and loading

long term test should reveal the same conclusion about the crack resistance. This might not agree with short term test because the mechanism of the deformation is different.

Measured properties of PE 100 (short as well as long term properties) performed by the CRB and PENT tests are given in Chapter 11.1 linked with the pipe lifetime assessment.

# Chapter 3

## Theoretical Background on Fracture Mechanics

### 3.1 Introduction

Fracture mechanics was raised in the nineteenth century when the Industrial Revolution had brought many accidents with loss of lives. Many of the failures had been caused by cyclic loading even though the loading amplitude was significantly below the yield strength of the material. Later it was discovered that the structures failed due to pre-existing flaws from which a crack was able to initiate, consequently causing the structure to rupture.

In the course of time the fracture mechanics has developed into two main disciplines - Linear Elastic Fracture Mechanics (LEFM) and Elasto Plastic Fracture Mechanics (EPFM). LEFM is valid for so called Small Scale Yielding (SSY) conditions when the plastic zone size at the crack tip is negligibly small, and the material obeys the Hook's law. This issue is discussed in more details in the following sections. The theory behind the EPFM is more complex and it allows to solve problems when the plastic zone size is beyond the restrictions of LEFM. In this case the material does not necessarily need to behave linearly. It will be shown that the use of the LEFM is in many cases satisfactory when solving problems of reliability of polyolefin pipes.

### 3.2 Linear Elastic Fracture Mechanics

Linear elastic fracture mechanics was first based on energetic approaches. The energy balance in an infinite plate with a crack was first proposed by Griffith already in 1920 [48]. Due to impracticalities of this concept a new approach - stress intensity approach - was proposed by Irwin in 1950s. Owing to this, the stress field near the crack front can be described using one parameter called the Stress Intensity Factor (SIF),  $K[MPa.m^{1/2}]$ . This parameter is a function of external loading and geometry of the structure and crack.

More parameters can be used to describe the stress field near the crack front and the LEFM can be then usually divided into one, two or more parametric LEFM, based on how many parameters are being used. The second parameter often taken into account is the T-stress,  $T[MPa]$ . More to these will be discussed in the following.

### 3.2.1 Mathematical Background on Crack-Like Discontinuities

When a solid body with a crack-like defect is subjected to loading, it generally produces high stresses near the crack tip. Crack tip is a point on the crack front. The basic crack terminology is explained in Figure 3.1.

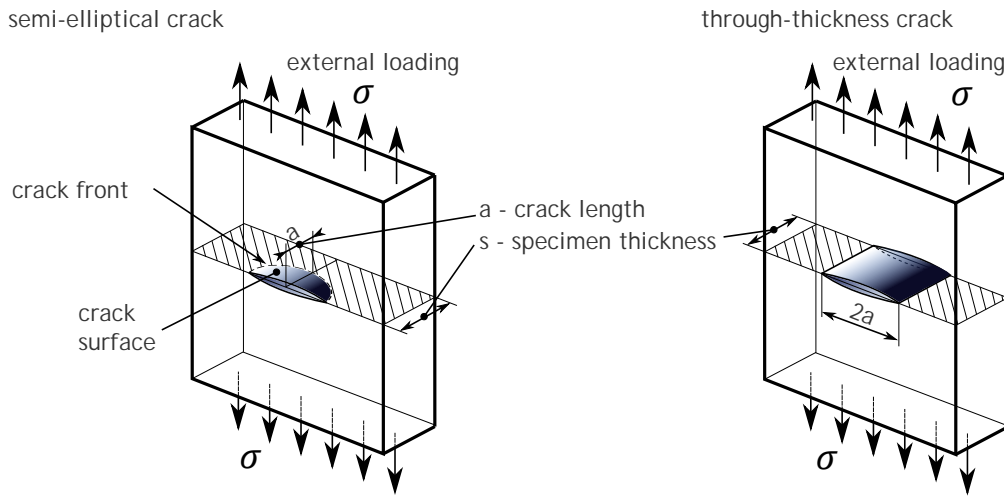


FIGURE 3.1: Basic crack terminology, semi-elliptical crack (left), through-thickness crack (right)

Within the concept of LEFM the stresses near the crack front in a loaded body go to infinity. This paradox in compare to reality is caused by assuming the linear elastic model of material having no limitations in stress. The crack front in reality is not perfectly sharp, as assumed by mathematical models. Actually, the material near the crack tip will undergo plastic deformations, and the crack tip will get blunted producing much lower stresses at the crack tip.

However, when using the linear elastic mathematical model, the components of the stress tensor reveal an exponential dependence,

$$\sigma_{ij} \approx \frac{A}{r^p}, \quad (3.1)$$

where the denominator exponent  $p$  is called the stress singularity exponent, as it describes the local degree of stress singularity, and  $A$  is a constant which describes the amplitude of the stress singularity. Generally the singularity exponent can vary in the interval  $0 < p < 1$ . The singularity with the exponent  $p = 1/2$  is often called as the square-root singularity and it usually dominates over the others.



The amplitude of the singular term is finite and the root singularity is coupled just with the stress intensity factor - the most important parameter of the LEFM. Stress distribution of the stress singularity of  $p = 1/2$  in a cracked body is plot in Figure 3.2.

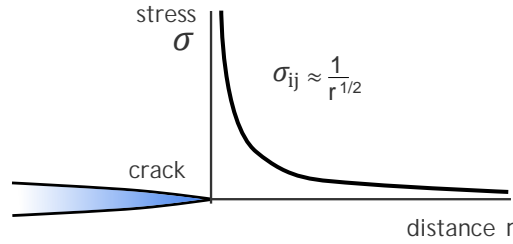


FIGURE 3.2: Stress singularity near the crack front of the linear elastic material

The exponent  $p$  may change within the given interval when the crack front approaches another material (like in a composite) or when the crack is very close to a free surface. Generally any elastic mismatch causes this kind of change. The dominance of the stress intensity factor which is coupled with the square-root singularity is then suppressed and the stress field near a general stress concentrator can be described by the Generalized Stress Intensity Factor (GSIF), denoted as  $H$ .

The T-stress, as the second fracture-mechanics parameter, is a non-singular quantity, often characterizing the influence of the body geometry, or the constraint effect at the crack tip.

For an infinitely large solid body with a center through-thickness crack, as one shown in Figure 3.1 on the right, Williams derived an equation for the stress field near the crack front in form of an infinite series [49]. The stress tensor components can according to the Williams expansion be written as,

$$\sigma_{ij} = \left( \frac{K}{\sqrt{2\pi r}} \right) f_{ij}(\varphi) + \sum_{m=0}^{\infty} A_m r^{\frac{m}{2}} g_{ij}^{(m)}(\varphi). \quad (3.2)$$

The parameters of the series are explained in the following figures. The functions  $f_{ij}(\varphi)$  or  $g_{ij}^{(m)}(\varphi)$  are goniometric functions dependent only on the angle  $\varphi$  in the polar coordinate system.

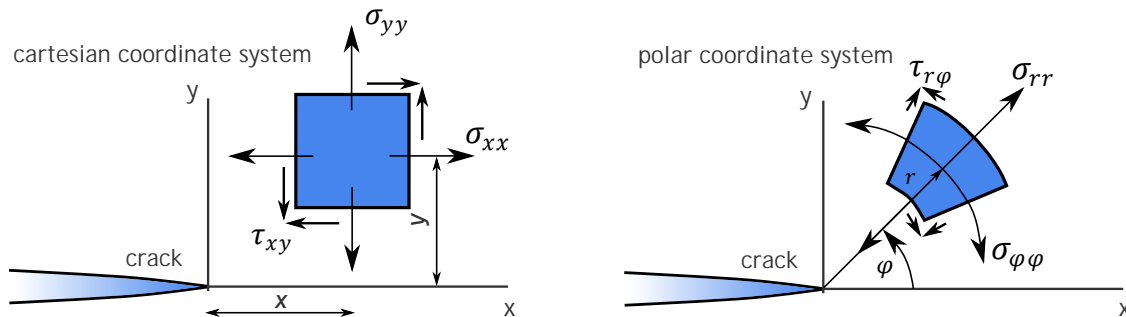


FIGURE 3.3: Stress components for the Cartesian and polar coordinate system

The first constant of the Williams expansion, as written in Equation 3.2, represents the stress intensity factor  $K$ . As seen from the expansion, this is the only singular term in the series. The second constant  $A_0$  is related to the T-stress. Similarly some other constants could be derived. Usually only the first term of the expansion (SIF) is taken into account and the others are neglected, allowing a simple description of the stress field near the crack front just by one finite parameter.

Irwin defined the SIF as,

$$K_i = \lim_{r \rightarrow 0} \sqrt{2\pi r} \sigma_i(r, 0), \quad (3.3)$$

where  $\sigma_i(r, 0)$  is the crack opening stress in a distance  $r$  in front of the crack tip, and the subscript  $i$  denotes the loading mode  $I$ ,  $II$  or  $III$ . One loading mode represents a simple crack opening. General crack propagation can be superimposed by different basic modes. Three basic modes are illustrated in Figure 3.4.

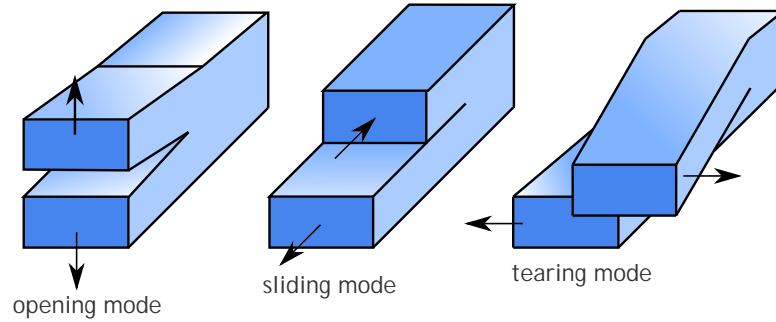


FIGURE 3.4: Three modes of loading that can be applied to a crack

The first mode is the opening mode  $I$ . This mode is usually the most energetically efficient, so cracks usually tend to curve into the direction where they are loaded under this mode. The second case in the figure illustrates the sliding mode  $II$ , and the third case illustrates the tearing mode  $III$ .

In the vicinity of the crack, where the singular term prevails and the other terms of the Williams expansion can be neglected, the stress tensor can be defined depending on the mode in which the crack propagates,

$$\sigma_{ij}(r, \varphi)^{(I,II,III)} = \frac{K_{(I,II,III)}}{\sqrt{2\pi r}} f_{ij}(\varphi). \quad (3.4)$$

Subscripts  $(I, II, III)$  denote one of the loading mode. The term  $f_{ij}(\varphi)$  represents goniometric functions in polar coordinate system. Combining different modes, the stress intensity factors or consequently stress tensors can be superimposed as given in the following relation,

$$\sigma_{ij}^{total} = \sigma_{ij}^{(I)} + \sigma_{ij}^{(II)} + \sigma_{ij}^{(III)}. \quad (3.5)$$

### 3.2.2 Numerical Methods on the Stress Intensity Factor Assessment

Unfortunately only a few cases exist, when analytical solutions can be used to estimate the stress intensity factor. Analytical solutions can be derived only for simple geometries and so more complex geometries require numerical calculations to be used. In the course of time, many different finite element methods for the stress intensity factor assessment have been developed, each one having their pros and cons.

A brief description of selected methods is given in the following subsections.

#### Displacement extrapolation methods

This method is used to calculate the stress intensity factor  $K$  by knowing displacements on the crack surface. To improve the square root singularity at the crack tip, the collapsed quarter-point elements are widely used. Using of these elements leads to a better description of the stress field and accuracy of the results near the crack front. Various quarter-point extrapolations were published by Barsoum [50] and Rhee [51], [52].

The finite element mesh using the quadratic quarter-point elements is shown in Figure 3.5.

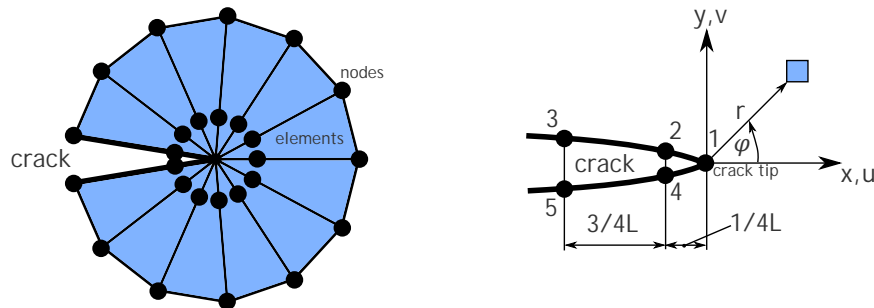


FIGURE 3.5: Quarter-point quadratic elements

The stress intensity factor expressed in terms of the opening displacements can be written as [53],

$$K_I = \frac{E}{3(1+\mu)(1+\kappa)} \sqrt{\frac{2\pi}{2}} \left[ 4(v_2 - v_4) - \frac{v_3 - v_5}{2} \right], \quad (3.6)$$

$$K_{II} = \frac{E}{3(1+\mu)(1+\kappa)} \sqrt{\frac{2\pi}{2}} \left[ 4(u_2 - u_4) - \frac{u_3 - u_5}{2} \right], \quad (3.7)$$

where the parameter  $\kappa$  is  $\kappa = 3 - 4\mu$  for plane stress conditions, and  $\kappa = (3 - \mu)/(1 + \mu)$  for plane strain conditions. Node displacement in x-direction is denoted as  $u$ , and node displacement in y-direction is denoted as  $v$ . The subscripts are related to the individual nodes as shown in Figure 3.5.

The method usually is implemented in commercial packages. Specifically in ANSYS the command KCALC can be searched [53]. Since usually the displacements are the solution of the finite element method, the extrapolation of displacements is more accurate than extrapolation of stresses which are recalculated from the displacements. The method is easily programmable since it consists only of the two previous equations, but the knowledge of the stress state (plane stress or plain strain) is required.

### Direct methods

The advantage of direct methods is that they are easily programmable, but usually not implemented within standard finite element packages. The numerical results of the stresses or displacements in front of the crack tip are extrapolated on analytical solutions. The stress intensity factor is estimated from this extrapolation.

The opening stress near the crack tip for the first (opening) mode and for a crack situated in the coordinate system shown in Figure 3.3 on the right (see the Williams series in Equation 3.2) is,

$$\sigma_{yy} = \frac{K_I}{\sqrt{2\pi r}} \cos \frac{\varphi}{2} \left[ 1 + \sin \frac{\varphi}{2} \sin \frac{3\varphi}{2} \right] + (\text{neglected terms}) \approx \frac{K_I}{\sqrt{2\pi r}} f_{yy}(\varphi). \quad (3.8)$$

However, the stress intensity factor can be derived just from the previous equation, when neglecting all, but the singular terms,

$$K_I = \sigma_{yy} \frac{\sqrt{2\pi r}}{f_{yy}(\varphi)}. \quad (3.9)$$

The stress intensity factor can be estimated from a different stress component as well.

By taking the numerically calculated stress field not far from the crack tip, the stress intensity factor is directly estimated from Equation 3.9. The results are valid only in the area very close the crack front where the singular term dominates.

The accuracy of the method can be improved by refining the finite element mesh or by plotting the calculated stress intensity factor  $K_I$ , (3.9) as a function of the distance  $r$ , and extrapolating this function for  $r = 0$ , [54]. In the extrapolation the results near the crack tip are discarded due to huge numerical errors caused by the singularity (see Equation 3.3 where  $r$  approaching zero is multiplied by  $\sigma$  approaching infinity). The process of the extrapolation is shown in Figure 3.6.

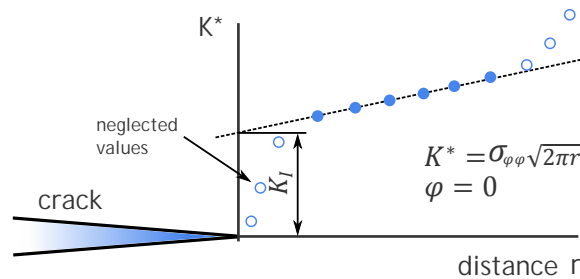


FIGURE 3.6: Direct method extrapolation

### J-integral

This method is usually implemented in commercial packages as ANSYS or ABAQUS. J-integral is a parameter of the elasto plastic fracture mechanics. It was first introduced by Rice [55], [56]. The J-integral is basically derived from an energetic approach, but rather than assuming the elasto plastic material, only the non-linear material behaviour is assumed. Loading a solid body cannot distinguish between this two cases, because the stress-strain curve might look the same for both of them. Unloading is, however, different for both of these material models, so the non-linear behaviour can simulate elasto plastic material only when no unloading at the crack tip happens. J-integral thus cannot describe crack propagation. This has to be taken with care. It was proved that for small scale yielding conditions assuming linear elastic case, the J-integral is equal to the crack driving force and consequently to the stress intensity factor,

$$J = G = \frac{K_I^2}{E'}, \quad (3.10)$$

where for plane stress  $E' = E$ , and for plane strain  $E' = E/(1 - \mu^2)$ , and  $\mu$  is the Poisson's ratio.

In ANSYS the command JINT can be searched. More information can be found also in the ANSYS manual [53].

### Crack driving force

Crack driving force was introduced in Equation 3.10 from which the stress intensity factor can be derived. Crack driving force is an energetic parameter and it can be calculated from the strain energy stored in a loaded body with a crack. For two different configurations with different crack lengths the energy stored in the body differs. Crack driving force can be calculated subtracting these two energies based on the following equation,

$$G \approx \frac{[U(a) - U(a + \delta a)]}{\delta a \cdot B}, \quad (3.11)$$

where  $U(a)$  represents the strain energy for the initial crack configuration,  $U(a + \delta a)$  represents the strain energy in the solid body where the crack has grown for a small length  $\delta a$  and  $B$  is the body thickness.

Knowing the crack driving force, Equation 3.10 can be used to calculate the stress intensity factor.

The first three methods can be used also for a 3D crack configuration where the stress intensity factor is calculated for a chosen point on the crack front. The method based on the crack driving force can in 3D solid body give only an average value of the SIF along the crack front.

### 3.2.3 Estimation of the Crack Propagation Direction

The angle of the next crack increment in a 2D body can be calculated iteratively by knowing the stress intensity factors for the first and the second loading mode. The basic criteria for assessment of the next crack increment are described in the following:

- **maximal tangential criterion**

This criterion was proposed by Erdogan and Sih [57]. The main idea is that the crack propagates in the direction of the maximal tangential stress. It is possible to derive an analytical solution which takes the following form,

$$\theta = 2 \arctan \left( \frac{1}{4} \frac{K_I}{K_{II}} \pm \frac{1}{4} \sqrt{\left( \frac{K_I}{K_{II}} \right)^2 + 8} \right), \quad (3.12)$$

where  $\theta$  is the angle by which the crack direction will change with respect to the previous direction,  $K_I$  and  $K_{II}$  are the stress intensity factors for the first and the second loading mode, separately. This criterion is the most simple one and it was used to simulate crack propagation in this thesis.

- **maximal strain density criterion**

The criterion was proposed by Sih [58]. According to this criterion the crack propagates in the direction where the strain energy density is maximal. Strain energy density can be expressed in terms of stress intensity factors,

$$w = \frac{1}{2} \sigma_{ij} \varepsilon_{ij} = \frac{S(K_{(I,II)})}{r}, \quad (3.13)$$

where  $S$  is a function of  $K_I$ ,  $K_{II}$  and goniometric terms.

The angle can be found by looking for the stationary points,

$$\left( \frac{\partial S}{\partial \theta} \right)_{\theta=\theta_0} = 0, \quad \left( \frac{\partial^2 S}{\partial \theta^2} \right)_{\theta=\theta_0} < 0. \quad (3.14)$$

Another theories on crack growth direction are for instance the modified maximal tangential stress criterion [57], [59] or the maximum strain energy release rate criterion [60].

Crack propagation in the commercial package ANSYS was described in the author's bachelor's thesis [4]. The algorithm proposed in the bachelor's thesis was expanded of solving axisymmetric problems and used for herein solved 2D problems. Testing of the algorithm was performed on many examples for which analytical solutions are known. Detailed description, testing and accuracy is given in [4].

### 3.2.4 Plastic Zone Size

Linear elastic fracture mechanics is usually restricted in the size of the plastic zone. The plastic zone should be relatively small and therefore the LEFM is valid mostly for brittle materials. The size of the plastic zone can be calculated using different approaches. The most simplified ones assuming the plastic zone to have the shape of a circle were proposed by Irwin,

$$r_y = \frac{1}{2\pi} \left( \frac{K_I}{\sigma_y} \right)^2, \quad (3.15)$$

where  $r_y$  is plastic zone radius as shown in Figure 3.7,  $K_I$  is the stress intensity factor for the first opening mode,  $\sigma_y$  is the uniaxial yield strength of the material.

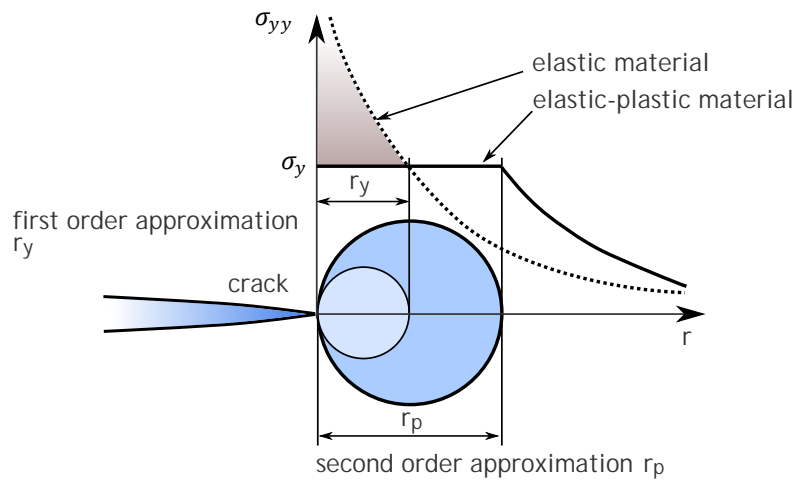


FIGURE 3.7: First and second order approximation of plastic zone size

This relation was derived from the linear elastic model of material. A more realistic approach is to take an elasto plastic material which has a restriction on stresses. The plastic zone considering the plane strain conditions would be now twice as big as in the previous case.

It was observed that for many polymer materials the strip-yield model first proposed by Dugdale [61] and Barenblatt [62] can be used to simulate crazing at the crack tip. Crazing is a mechanism by which a crack in polymer materials usually propagates. In this model the strip-yield plastic zone in an infinite plate is modeled by assuming a crack of length  $2a + 2\rho$ . The length  $\rho$  represents the size of plastic zone with a closure stress equal to the yield strength of the material  $\sigma_y$  applied at the crack tip. This situation is shown in Figure 3.8

This model superimposes two elastic solutions, one where the crack is in tension and another one where the crack is loaded with closure stresses at the tip. In this model the stresses are finite and the crack tip cannot be described by the singularity  $r^{1/2}$ . The size of the plastic zone is then calculated in the way that the stress intensity factors from these two superimposed solutions cancel. The solution of this approach is,

$$\frac{a}{a + \rho} = \cos \left( \frac{\pi \sigma}{2\sigma_y} \right). \quad (3.16)$$

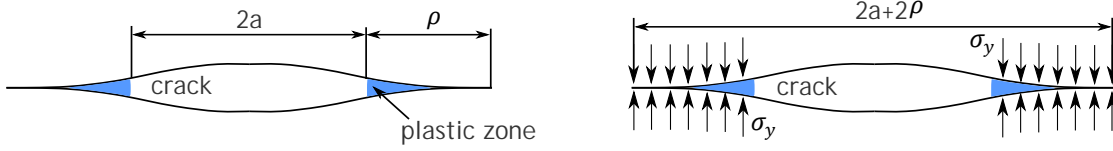


FIGURE 3.8: Strip yield model

Applying Taylor series expansion to the equation and neglecting higher terms, the plastic zone size is,

$$\rho = \frac{\pi}{8} \left( \frac{K_I}{\sigma_y} \right)^2. \quad (3.17)$$

Real shape of the plastic zone in an infinite plate can be analytically obtained for instance by the von Mises Yield Criterion. Using the first order approximation of the plastic zone (3.15) the shape can be estimated as follows,

$$r(\varphi)_{plane \ strain} = r_y \left( \frac{3}{4} \sin^2(\varphi) + \frac{1}{2} (1 - 2\mu)^2 (1 + \cos(\varphi)) \right). \quad (3.18)$$

To properly describe the size and the shape of the plastic zone at the same time is extremely difficult. For more complex problems the finite element analyses can be used.

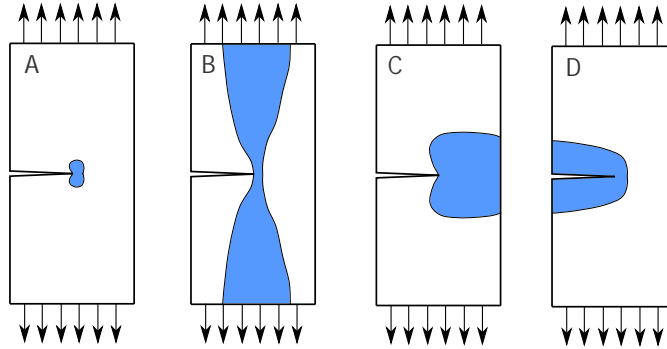


FIGURE 3.9: Plastic zone shapes

Size of the plastic zone is of a huge importance when applying the linear elastic fracture mechanics. The restriction for this approach to describe the crack properly is that the plastic zone is relatively small and it can be neglected. There are four examples in Figure 3.9 showing different sizes and shapes of the plastic zone where only the first one (case A) is relevant for LEFM usage.



# Chapter 4

## Problem Formulation and Aims of Diploma Thesis

Developing numerical tools and methodologies which would allow simple engineering calculations of pipe systems is important. The current research has been dealing mostly with the basic pipe material and the constitution of the joints of welded polyolefin pipes has been only rarely investigated, so a more complex study of different failure modes in welded pipes is still not yet available.

A typical lifespan of polyolefin pipes is approximately fifty years. Changes due to welding introduce material inhomogeneity and stress raisers leading to lower resistance against creep crack growth. This thesis is aimed to find the constitution of the connections using the existing numerical tools (Finite Element Method (FEM), commercial package ANSYS) and to introduce a basic procedure for a welded pipe lifetime prediction.

The main goals of the thesis can be summarized as,

- development of a 2D axisymmetrical model simulating growth of a circumferential crack in the basic pipe material,
- development of a 3D axisymmetrical model simulating growth of an axial semi-elliptical crack in the basic pipe material,
- introduction of material inhomogeneity into the models to find the constitution of material properties on crack behavior,
- introduction of weld bead geometry (butt welding joint, electro-fusion welding joint) into the models to find the constitution of the geometrical configuration on crack behavior near the welded connections,
- estimation of residual lifetime of welded pipe systems based on the methodology of Linear Elastic Fracture Mechanics (LEFM) using the concept of the Stress Intensity Factor (SIF),
- discussion over the results and future related research possibilities.



# Chapter 5

## Semi-Analytical Solutions of SIF in a cracked Pipe

Analytical solutions of the Stress Intensity Factor (SIF) for pipes with a crack are difficult to obtain, especially when it comes to a more complex geometry. A few solutions are possible to derive, but they usually combine extrapolations from finite element method calculations and simple analytical formulas.

Three simple examples are shown and derived in the following sections. The results of the final solutions can be used for simple engineering calculations or they can be used for checking the correctness of numerical solutions, and mesh refinement sufficiency in more complex geometries.

### 5.1 Semi-Elliptical Surface Crack in a Pipe

A semi-elliptical surface crack represents a 3D case, in which the crack front takes an elliptical shape, with the major axis being situated on the intersection of the inner pipe wall cylinder and the cross section in which the crack propagates. A semi-elliptical surface crack in a pipe is illustrated in Figure 5.1. The crack propagates only in the cross section plane.

Assuming the wall thickness to be negligible small in compare to the radius of the pipe, the shell theory can be used to describe the stress field in the pipe. The tangential stress in this case takes the following form,

$$\sigma_{hoop} = \frac{p_{in}R}{s}, \quad (5.1)$$

where  $p_{in}$  is the inner pressure acting on the pipe wall,  $R$  denotes the mid-surface radius and  $s$  is the wall thickness.

The stress intensity factor for a semi-elliptical crack in a solid body externally loaded can be calculated based on the results of Raju and Newman [63],

$$K_I = \frac{C\sigma\sqrt{\pi a}}{\Theta}, \quad (5.2)$$

where  $C$  is a constant depending on the ratio  $a/b$  (major and minor axis of the ellipse), on the specimen thickness  $a/s$  and on the point on the crack front  $\varphi$  (see Figure 5.1). Neglecting both of the constants in Equation 5.2, the relation describes a small through-thickness central crack in an infinitely large solid body, as the well-known equation for this case is  $K_I = \sigma\sqrt{\pi a}$ .

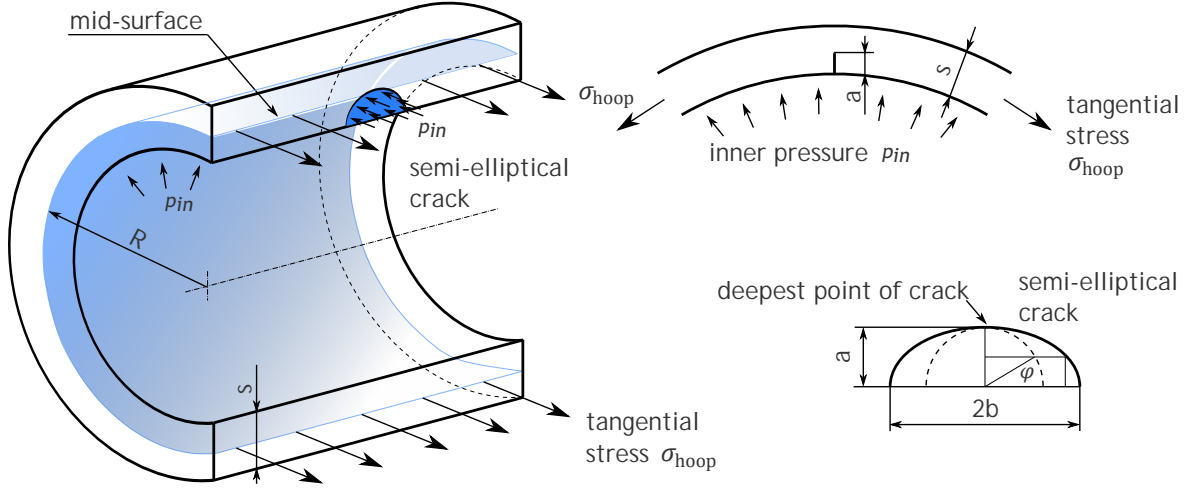


FIGURE 5.1: Axial crack in a pressurized pipe with crack shape description

The constant  $C$  was derived by Raju and Newman using the finite element calculations and it basically characterises the finite dimensions of the body and the crack front shape. The constant  $\Theta$  follows from the elliptical integral of the second kind. For a circular crack it holds  $\Theta = \frac{\pi}{2}$ . A small crack in a large solid body is negligibly effected by the boundaries of the body and the constant  $C$  vanishes. Further, in the case of a semi-circular crack front shape it approaches one. The stress intensity factor for a small circular crack in a large 3D body is therefore  $K_I = \frac{2}{\pi}\sigma\sqrt{\pi a}$ .

A general solution for the stress intensity factor in the deepest point ( $\varphi = 90^\circ$ ) of a semi-circular crack ( $a/b = 1$ ) in a pressurized pipe is,

$$K_I = C\left(\frac{a}{b} = 1, \frac{a}{s}, \varphi = 90^\circ\right) \frac{2}{\pi} \frac{p_{in} R}{s} \sqrt{\pi a}. \quad (5.3)$$

There is also pressure acting on the crack itself and this contribution has to be accounted for,

$$K_I = C\left(\frac{a}{b} = 1, \frac{a}{s}, \varphi = 90^\circ\right) \frac{2}{\pi} p_{in} \sqrt{\pi a}. \quad (5.4)$$

The final equation superimposes the previous stress intensity factors (Equation 5.3 and Equation 5.4), as the superposition for linear problems is possible,

$$K_I = C \left( \frac{a}{s} \right) \frac{2}{\pi} p_{in} \left( 1 + \frac{R}{s} \right) \sqrt{\pi a}. \quad (5.5)$$

For a semi-circular crack front shape and the stress intensity factor estimation in the deepest point of the crack, the constant  $C$  is depended only on the ratio  $a/s$ . This ratio can be estimated from the results of Raju and Newman [63]. For only semi-circular cracks and the SIF estimation in the deepest point of the crack front (see Figure 5.1) the results of Raju and Newman can be fitted using the leas-square method by the following function,

$$C \left( \frac{a}{s} \right) = 1.014 + 0.167 \left( \frac{a}{s} \right) - 0.05 \left( \frac{a}{s} \right)^2. \quad (5.6)$$

The final equation for an estimation of the stress intensity factor of an axial semi-circular crack in a pipe wall is,

$$K_I = \frac{2p_{in}}{\pi} \left( 1 + \frac{R}{s} \right) \sqrt{\pi a} \left[ 1.014 + 0.167 \left( \frac{a}{s} \right) - 0.05 \left( \frac{a}{s} \right)^2 \right]. \quad (5.7)$$

When the crack shape changes from semi-circular to semi-elliptical the constant  $C$  and consequently the stress intensity factor get higher. The worst crack shape (the ratio  $a/c = 0$ ) would make the result of the elliptical integral  $\Theta = 1$ . This case would represent a crack with the straight crack front for which a 2D model considering plane strain state could be used. The stress intensity factor for this case would possibly be calculated using the results of the single edge notched specimen.

The presented equation (Equation 5.7) is valid only for small cracks where the crack front shape is close to a semi-circular shape and the crack is not influenced by boundaries of the studied body.

## 5.2 Full Circumferential Crack in a Pipe

Full circumferential crack in a pipe is shown in Figure 5.2. The axial stress opening the crack following from the shell theory is twice as small as the tangential stress,

$$\sigma_{axial} = \frac{p_{in} R}{2s}, \quad (5.8)$$

where the notation is the same as in the previous example ( $p$  - inner pressure,  $R$  - pipe radius (mid-surface),  $s$  - wall thickness).

The stress intensity factor can be calculated as,

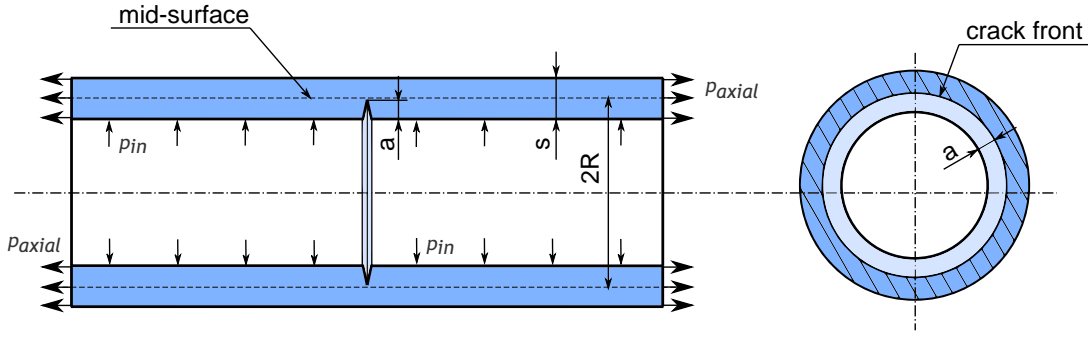


FIGURE 5.2: Circumferential crack in a pressurized pipe

$$K_I = p_{in} \left( \frac{R}{2s} + 1 \right) \sqrt{\pi a} \cdot Y(a/s), \quad (5.9)$$

where the function  $Y(a/s)$  describing the geometry can be replaced by a function for the single edge notched plate. The sum in the left bracket has the same meaning as explained in the previous case - superimposition of the stress intensity factors, from the pressure acting on the pipe wall, as well as on the crack surfaces. The final equation is,

$$K_I = p_{in} \left( \frac{R}{2s} + 1 \right) \sqrt{\pi a} \left( 1.122 - 0.231 \left( \frac{a}{s} \right) + 10.550 \left( \frac{a}{s} \right)^2 - 21.710 \left( \frac{a}{s} \right)^3 + 30.382 \left( \frac{a}{s} \right)^4 \right). \quad (5.10)$$

Accuracy for the function  $Y(a/s)$  is 0.5% for  $a/W < 0.6$  [64].

### 5.3 Axial Through-Thickness Crack in a Pipe

When the semi-elliptical crack shown in the first example has outgrown the outer pipe wall it starts to propagate in the axial direction, causing a through-thickness defect. This case breaks the leak-tightness of the pipe. The crack shape and a short description is given in Figure 5.3. The tangential stress in a thin-wall pipe is represented by Equation 5.1.

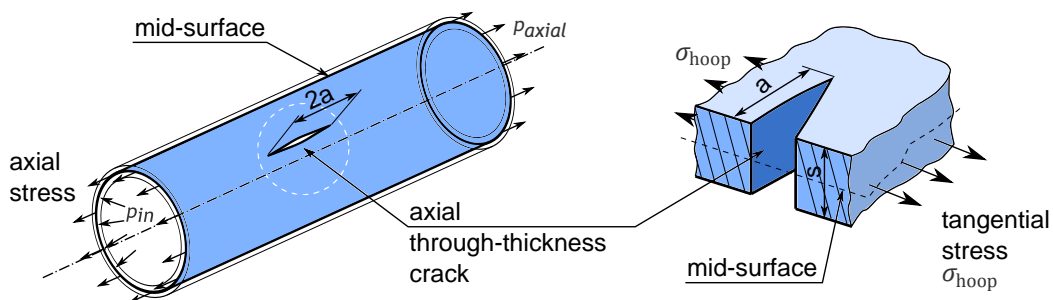


FIGURE 5.3: Axial through-thickness crack in a pipe

Assuming a very long pipe, the solution for the stress intensity factor follows the equation for a large solid body with a small crack,

$$K_I = \sigma_{hoop} \sqrt{\pi a} = \frac{p_{in} R}{s} \sqrt{\pi a}. \quad (5.11)$$

To this equation Folias [65] introduced a correction factor  $M_f$  for bulging of the crack flanks,

$$M_f = \sqrt{1 + 1.225 \frac{a^2}{R s} - 0.0135 \frac{a^4}{R^2 s^2}}, \quad (5.12)$$

$$K_I = \sigma_{hoop} \sqrt{\pi a} \cdot M_f, \quad (5.13)$$

$$K_I = \frac{p_{in} R}{s} \sqrt{\pi a \left( 1 + 1.225 \frac{a^2}{R s} - 0.0135 \frac{a^4}{R^2 s^2} \right)}. \quad (5.14)$$

More complex geometries require using of numerical methods to find the stress intensity factor solutions.





# Chapter 6

## Numerical Models Description

To achieve the objectives of the thesis described in Chapter 4, different numerical models of welded pipes containing a crack have been created. This chapter describes the basic geometrical and loading parameters of these models.

A crack in a polyolefin pipe in real service propagates usually more than fifty years. Studying the crack propagation and its description experimentally is a very time-consuming procedure, even when performing accelerated tests. The aims of the thesis refer to the welding connections of polyolefin pipes. These goals require comparing many different solutions and configurations for which experimental testing would be very difficult and expensive. Developing numerical models gives an advantage of studying the problems more efficiently, since also very long time processes can be simulated and analysed in shorter times and different time frames of the process. It was noticed, that for some conditions (small scale yielding and slow crack growth) which are valid for the studied problem, the Linear Elastic Fracture Mechanics (LEFM) can be used to solve a reliability of pipe systems. The presented numerical models are based on the methodology using the LEFM, describing creep crack growth in a polyolefin pipe in the basic as well as welded pipe material.

Different configurations which have been numerically studied are,

- butt welded pipes with removed weld bead from both outer and inner pipe surface, containing an axial or circumferential crack,
- Butt welded pipes where the weld bead was not removed (general case used in praxis nowadays), containing an axial or circumferential crack.
- implementation of inhomogeneous distribution of Young's modulus for different inhomogeneity ratio  $E_{max}/E_{min}$ , varying from 1 (homogeneous pipe) up to 1.5, into the previous models,
- butt welded pipes with non-optimal weld bead shapes considering different welding conditions,
- optimal weld bead shape with various weld bead notch radius, varying from 1.1mm to 1.5mm,

- electro-fusion welding joint containing a circumferential crack.

Electro-fusion welding is only marginally described in the end of the thesis, as it initially was not the subject nor a goal of this thesis. However the results for the stress intensity factors are compared to the butt welding joint, giving an outlook on the welding joint resistance to creep crack growth.

## 6.1 Description of the Pipe Geometry

For the presented study, the polyethylene pipe from production of PipeLife was chosen (PE-100 110 x 6.3 SDR 17.6).

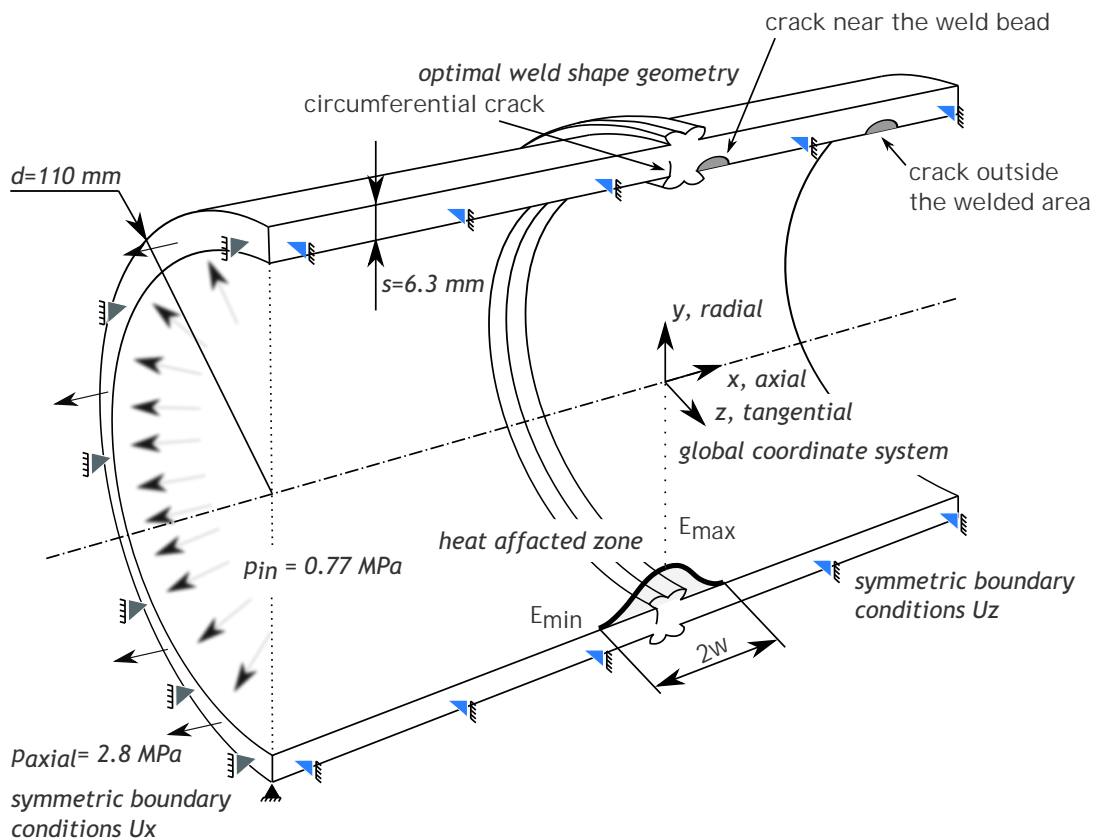


FIGURE 6.1: Geometry of butt welded pipes with different crack defects

Two different welding connections were studied - butt welding and electro-fusion welding. As for the butt welding, different weld bead shapes have been considered according to the experimental observations for different welding conditions (see Figure 9.1). Electro-fusion welding joint was not studied in much details, but the results are used to show how it differs to the butt welding joint in terms of lifetime safety and Slow Crack Growth (SCG). A butt welded pipe with two differently oriented cracks (axial or circumferential) and different crack initiation places is shown in Figure 6.1. Electro-fusion welding joint is shown in Figure 10.1 in Chapter 10, where it is described separately.

According to the presented geometry, different numerical models have been created as described at the beginning of this chapter. Numerical models were used to predict lifetime of the pipes for different assumptions and to make a conclusions on what effects are important to be included into the welded pipe lifetime calculations. The results give an idea on how the welding effects the lifetime and how it can be changed for better.

Dimensions of the pipe for numerical modelling are shown in Figure 6.1 ( $d = 110mm$ ,  $s = 6.3mm$ ). For the purposes of calculations the considered length of the pipe system was  $300mm$ . All the numerical models were developed and processed using the Finite Element Method (FEM), where the commercial package ANSYS has been used.

Typical experimental conditions for the polyolefin pipe testing assume hoop stress  $\sigma_{hoop} = 6MPa$ . The relation between hoop stress and internal pressure can be expressed as,

$$p_{in} = \sigma_{hoop} \frac{2s}{d - 2s}. \quad (6.1)$$

The applied internal pressure  $p_{in} = 0.77MPa$  guarantees the desirable tangential stress conditions. For all the numerical models, the pipe was assumed to stay at the room temperature when the Young's modulus of polyethylene for the basic material is  $E = 1750MPa$  and the Poisson's ratio is  $\mu = 0.35$ . Furthermore, testing of HDPE pipes considers another axial stress, just when the pipe system is closed. From the given values, the axial stress is  $p_{axial} = 2.8MPa$ . Numerical calculations were performed for both "open" and "closed" pipe systems, to see the outer limits on the stress intensity factors. From this point now on, referring to the open pipe system will be considered for a pipe without any outer axial pressure acting on. For the closed pipe system, additional axial stresses are considered having a magnitude of the same as the pipe system was closed.

## 6.2 Description of the Crack Front Shape

In 2D cases the crack is simply described just by one point - crack tip and the crack front is considered as a straight line. The crack must however be defined depending on the stress state, either in plane stress or plane strain conditions.

In 3D analyses the crack cannot be described simply just by one sharp point (crack tip), where the stress intensity factor is easily estimated. Instead there is a crack front having an arbitrary shape which can be represented by a general curve, depending on loading, boundary conditions or geometry. The crack usually propagates with a close-to semi-elliptical shape, and this case is also considered in the simulations presented in this thesis. Semi-elliptical shape can be observed by many experiments and two cases from different failed parts of polyolefin pipes are shown in the following figures (Figure 6.2 and Figure 6.3).

The semi-elliptical shape can be proved also by numerical calculations where it is considered that the crack shape obeys the Paris-Erdogan law [28]. The consequences are that the point of the crack front with a higher SIF would move faster than the others. For a very slow



FIGURE 6.2: Fracture surface in a PE-Pipe subjected to internal pressure only [35]

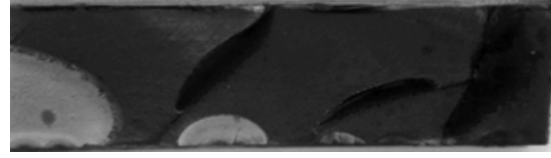


FIGURE 6.3: Axial semi-elliptical cracks in a pipe wall [66]

crack growth it can be assumed that the crack front stays in an equilibrium where the SIFs are relatively the same for each point of the crack front.

It is possible to estimate the SIF e.g. in 30 points along the crack front and change the aspect ratio of the semi-elliptical crack shape in order to find the real crack front shape according to the previous statement. However the extrapolation paths along the crack front should not be close to the free surface of the body. The reason for this is a presence of the vertex singularity [67], [68], [69] near the free surface that significantly changes the stress field in the vertex point at the free surface. At this point the SIF cannot be estimated correctly by classical approaches of LEFM. The process of the SIF assessment using the direct method on a symmetrical part of polyolefin pipes is described in Figure 6.4.

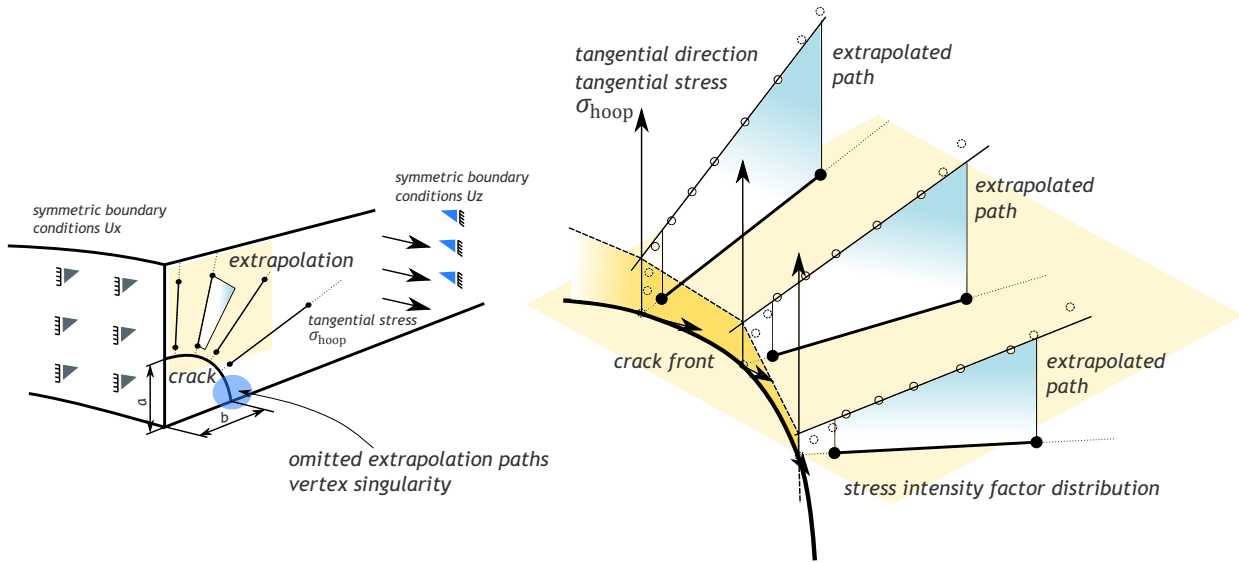


FIGURE 6.4: Application of the direct method to obtain the SIF for a semi-elliptical crack front

The direct method was explained in Chapter 3.2.2. Hutař et al. [3] published an approximate relation for the development of the semi-elliptical crack front in a homogeneous polymer pipe as follows,

$$b = a \left[ -0.1936 \left( \frac{a}{s} \right)^2 + 0.6628 \left( \frac{a}{s} \right) + 1.0919 \right]. \quad (6.2)$$

Notation of the semi-elliptical crack dimensions is shown in Figure 5.1. The semi-elliptical shape can be described by two parameters - length of major axis here denoted as  $2b$  and length of minor axis here denoted as  $a$  where this axis represents the crack length.

Obtaining the equation which would describe the semi-elliptical shape has to be based on iterative methods. The iterative process begins with an initial crack front shape which is chosen arbitrary but close to the expected crack front shape. Usually a semi-circular shape is chosen. This will ensure decrease in number of iterations. After one iteration is performed a SIF distribution along the crack front can be obtained using one of the methods for SIF estimation (the direct method in this case) in a few points of the crack front. According to this distribution the crack front will be changed in order to obtain a constant SIF distribution along the crack front within a reasonable precision.

Generally in our case, four to five iterations had to be done in order to get the desirable crack front shape just for one crack length. It can be deduced, that this is a very time consuming procedure. However, once the equation is found, it can be used for all other similar cases. The stress intensity factor for all the other cases (numerical models) in this thesis was estimated on 30 paths along the crack front using the direct method. A flow diagram of the procedure is given in Appendices.

In the cases, where the SIF distribution along the crack front was not constant (the crack shape would be more complicated than given semi-elliptical shape), due to more complex geometry, or material inhomogeneity, only one value in the deepest point of the crack was always taken for description of the crack.



# Chapter 7

## Optimal Welding Conditions

This chapter describes material properties and numerical models of butt welded pipes according to the optimal welding conditions outlined in ISO 21307 [1].

### 7.1 Optimal Welding Procedure of PE 100

Experimental data and material properties of butt welded regions shared in this thesis were measured in cooperation with the Montanuniversität Leoben, Martin Luther University and Polymer Competence Center Leoben. The polyethylene pipe from production of PipeLife was chosen (PE-100 110x6.3 SDR 17.6). The welding was performed using ROWELD P160B welding equipment. The welding regime was chosen depending on type of polymer material and the dimensions of welded pipe.

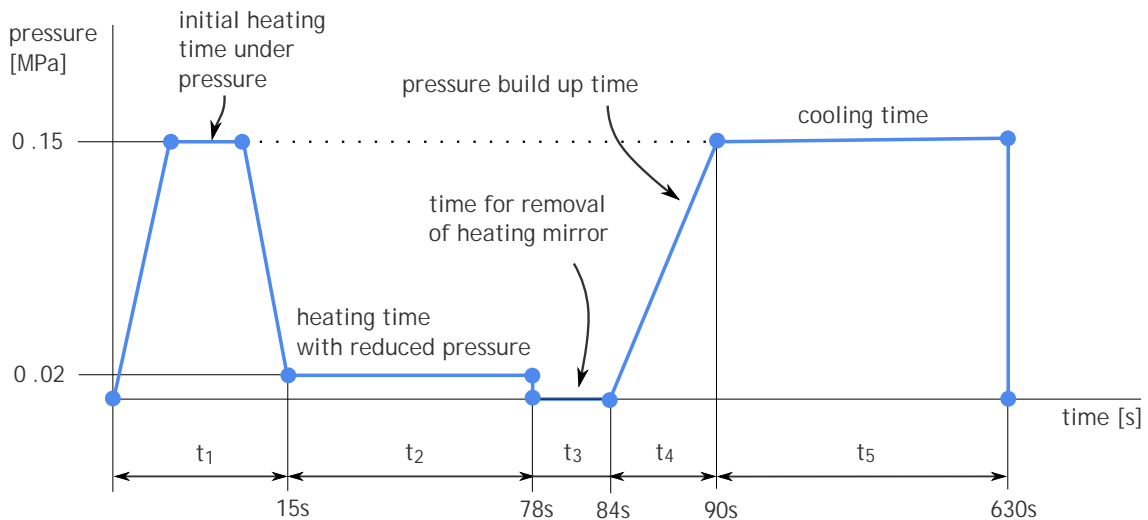


FIGURE 7.1: Optimal welding procedure according to the ISO 21307 [1]

Figure 7.1 illustrates the corresponding optimal welding procedure, which is composed of the following five time intervals,

1. alignment of the pipe joining surfaces  $t_1 = 15s$ ,
2. time for preheating of the joining surfaces  $t_2 = 63s$ ,
3. time of the removal of the heating plate  $t_3 = 6s$ ,
4. time to achieve joining pressure  $t_4 = 6s$ ,
5. cooling time of the weld at joining pressure  $t_5 = 9min$ .

After this procedure (optimal welding conditions for given pipe) was complete, samples from the experimental welded pipes were prepared and used for laboratory tests.

## 7.2 Material Inhomogeneity Implementation

The results of the micro-hardness tests show that a change of elastic material properties inside the polyethylene weld can be found [17]. This correlation was presented in Chapter 2.5. An experiment performed for polyethylene (PE-100 used in this study) (see Figure 7.2) and for polypropylene (see Figure 7.3) shows the distribution of the Young's modulus over the welded region. This distribution was normalized to the basic pipe material (Young's modulus of the basic non-welded material). The ratio  $E_{max}/E_{min}$  for polyethylene ( $E_{max}/E_{min} = 1.07$ ) and for polypropylene ( $E_{max}/E_{min} = 1.3$ ) was found. Indentation modulus is highest in the center of the weld joint (red area in Figure 2.9) and decreases with proximity to basic pipe material.

The material inhomogeneity presented in the weld can be modeled similarly to a Functionally Graded Material (FGM) [70], [71] and taken into account in subsequent numerical calculations.

Based on experimental experiences, the distribution of Young's modulus across the weld  $E(z)$  can be prescribed into the numerical model using a double power-law function as follows [72],

$$\begin{aligned} E(z) &= h_1(z)E_{max} + [1 - h_1(z)] E_{min} \quad \text{for } 0 < z < w/2, \\ E(z) &= h_2(z)2E_{max} + [1 - h_2(z)] E_{min} \quad \text{for } w/2 < z < w, \end{aligned} \quad (7.1)$$

where the functions  $h_{1,2}(z)$  are,

$$\begin{aligned} h_1(z) &= \frac{1}{2} \left( \frac{z}{w/2} \right)^p \quad \text{for } 0 < z < w/2, \\ h_2(z) &= 1 - \frac{1}{2} \left( \frac{w-z}{w/2} \right)^p \quad \text{for } w/2 < z < w. \end{aligned}$$

The exponent  $p$  describes the change of material properties (here  $p = 2$ ), and  $w$  represents the half-width of the weld (here  $w = 7mm$ ). Using Equation 7.1, the change of Young's modulus  $E(z)$  can be easily parametrized when the ratio  $E_{max}/E_{min}$  is known. The process can therefore be used for different materials.



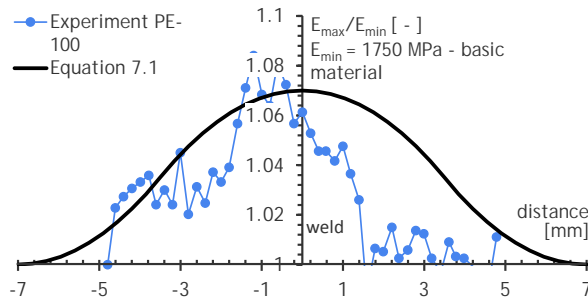


FIGURE 7.2: Normalized Young's modulus from micro indentation tests for the optimal welding conditions of PE

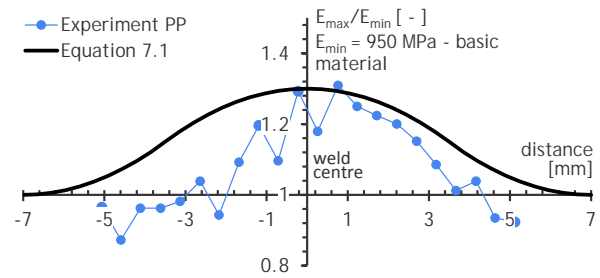


FIGURE 7.3: Normalized Young's modulus from micro indentation tests for the optimal welding conditions of PP

The double power-law function (Equation 7.1) was implemented in the numerical models using a temperature change. This function was discretized into twenty-one values for a symmetric part, which were then linearly interpolated. Figure 7.4 presents the corresponding distribution of Young's modulus along the weld.

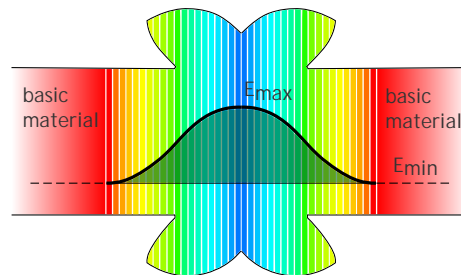


FIGURE 7.4: Implementation of material inhomogeneity into the numerical model

Within the commercial package ANSYS, the temperature is always linked with a material property - Young's modulus value. Since the Young's modulus cannot be prescribed to individual elements, the temperature is used to do so. In the structural analyses, the temperature does not enter the calculations and therefore the values are not important, rendering the temperature values unimportant. However, this approach does not require creating special volumes or areas which would have to be meshed with different values of elastic constants. Instead, different elastic constants are ascribed to different elements in one volume. The pipe geometry is thus much simpler, especially for crack propagation simulations. The crack tip does not have to cross different areas, and the simulation can be easily automated. An APDL code is given in Appendices.

### 7.3 Different Locations of Crack Initiation

Cracks usually initiate in places with high amount of stress, such as in weld bead notches and locations with strong material inhomogeneity. As the first step of the numerical modelling, a stress distribution in the butt welded pipes was estimated based on 2D axisymmetrical models, without implementing a crack. The stress state corresponding to the typical inner

pressure test of polyolefin pipes is shown in Figure 6.1 where the boundary conditions are drawn and the pipe system is closed.

The deformed shapes of pipes with and without the weld bead are shown in Figure 7.5. The deformation is scaled by a factor of six. The weld bead and the material inhomogeneity make the area near the weld stiffer as seen from the deformation and do not allow this area to undergo high radial displacements.

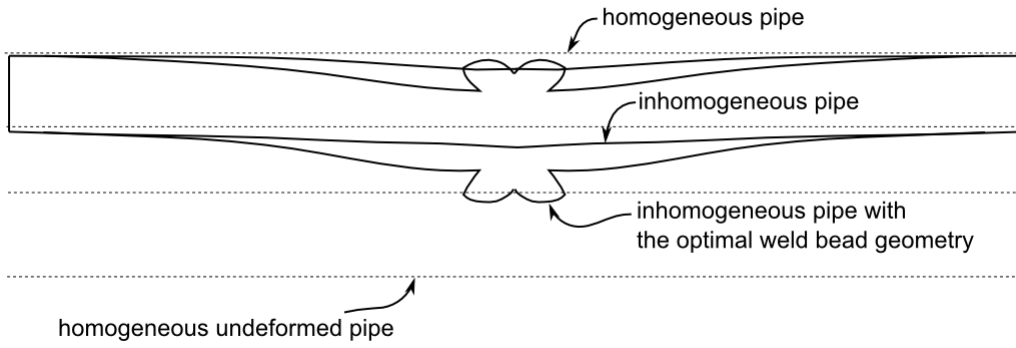


FIGURE 7.5: Deformation of welded pipes with different weld geometry (magnified six times)

A typical initiation place for axial or circumferential cracks in the case of pipe with the weld bead is near the weld bead notches as shown in Figure 7.6 and Figure 7.7. To obtain a better image of the resulting stress field, the welded areas were calculated with the highest ratio of Young's modulus  $E_{max}/E_{min} = 1.5$ . While stress distribution is not significantly altered by changes in inhomogeneity, the magnitude of the resulted stresses is greatly affected.

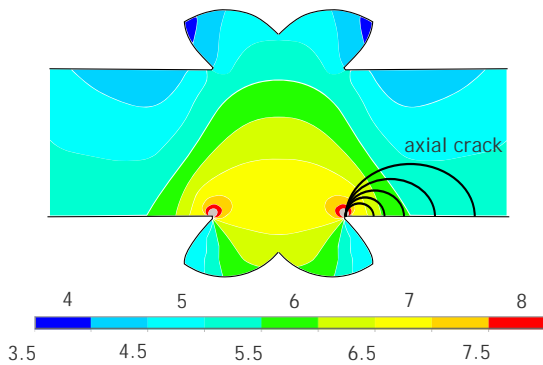


FIGURE 7.6: Axial crack initiation (tangential stress)

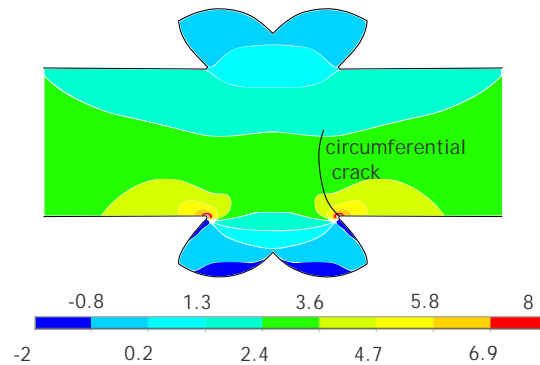


FIGURE 7.7: Circumferential crack initiation (axial stress)

The axial crack is governed by hoop (tangential) stress, which is strongly localized in the area near the weld bead. The magnitude of the stress is largely dependent on the weld bead geometry and the notch radius. The crack initiation is therefore estimated to appear near the stress concentrators (indicated by the red color in the figures). Due to high stiffness in the region of the weld, the axial crack propagation is assumed to continue in the weld-affected area as shown in Figure 7.6.

The circumferential crack is governed by axial stress. It initiates near the weld bead notches, and propagates as shown in Figure 7.7.

In the case of a removed weld bead, stress states for welded pipes are as illustrated in Figure 7.8 and Figure 7.9. There are no weld bead notches in the weld, but the material inhomogeneity is a major influence on stress distribution and its magnitude. Due to inhomogeneity in material properties, the stress is concentrated in the center of the weld, where a possible crack initiation area is located just there. Axial crack propagation governed by hoop stress is given in Figure 7.8. As for the circumferential crack, the following two cases have been considered - the crack initiates either in the middle of the weld (1) or in the border of the weld (2) from the position as it was in the previous case, when the weld bead notch was present, see Figure 7.9.

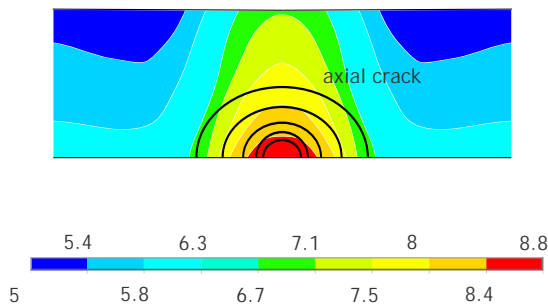


FIGURE 7.8: Axial crack initiation (tangential stress)

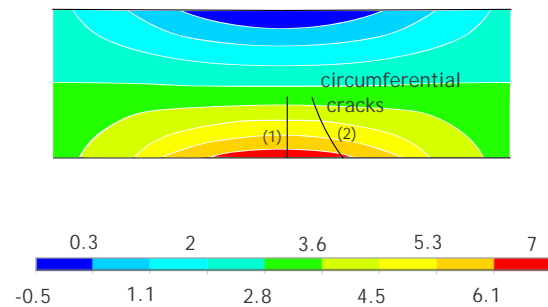


FIGURE 7.9: Circumferential crack initiation (axial stress)

All four cases were numerically studied and compared using different inhomogeneity ratios. The evaluation of the stress intensity factor is given in the following sections. The numerical models for welded pipes with removed weld beads are simpler and therefore discussed first. End of the following section deals with more complicated weld bead geometry.

## 7.4 Stress Intensity Factor Assessment

The Stress Intensity Factor (SIF) is the most important parameter of the Linear Elastic Fracture Mechanics (LEFM), and it will be used in Chapter 11 to assess the time of Slow Crack Growth (SCG). Describing crack growth kinetics it can be used to compare safety of a structure (welded polyolefin pipes in this case) and its resistance to unstable crack growth. Different methods for assessing the SIF were described in detail in Chapter 3.2.2. Assessment of the SIF in this chapter will be first shown for welded pipes with a crack where the weld bead has been removed. Then, the assessment for pipes where the weld bead has not been removed is presented. The results will be used to describe the tendency of crack growth to become unstable, and an important question about whether or not the weld bead should be removed will be answered.

### 7.4.1 Weld Bead Removed - Axial Crack Propagation

For the pipe with an axial crack, a 3D finite element numerical model had to be created. Geometry of the model is as described in Figure 6.1, excluding the weld bead. The presence of symmetry also gives the advantage of requiring a model for only a quarter of the welded pipes. The mesh with a mesh refinement near the crack is shown in Figure 7.10.

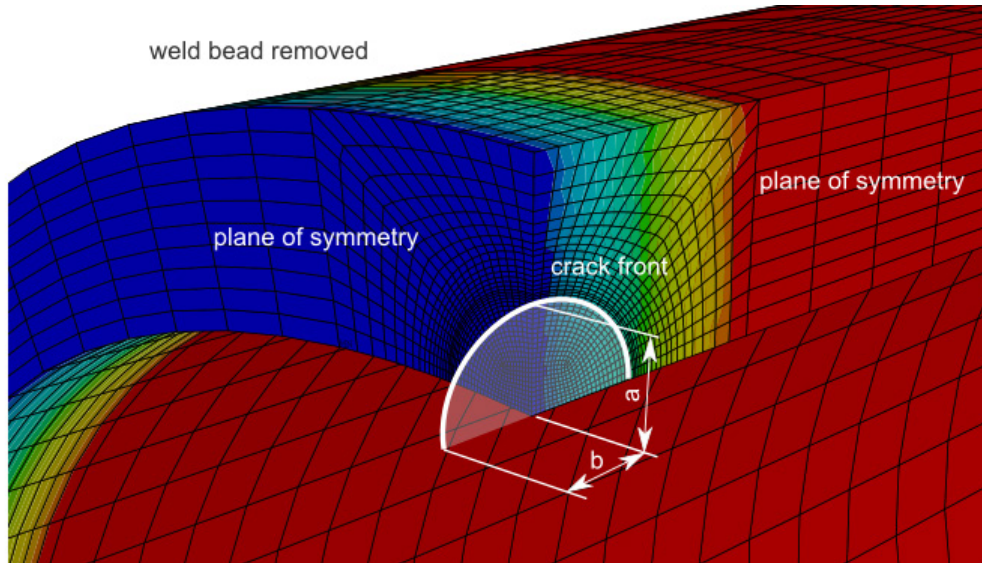


FIGURE 7.10: Finite element mesh near the semi-elliptical axial crack

For calculation time to be efficient, the quadratic elements (SOLID186) were used only in the area near the weld (squared volume containing the crack in Figure 7.10). All the elements outside that area were linear (SOLID45). The number of elements used was approximately 150 000, which is sufficient for making a good description of the stress field of pressurized pipe with a crack where the mesh is refined near the crack front. According to analytical solutions based on the shell theory, the mesh density outside the crack region was also calculated to be sufficient. Mesh density near the crack front and assessed stress intensity factor precision was also checked with the semi-analytical solutions given in Chapter 5. In addition, the results of the homogeneous pipe were compared to relevant literature [3]. At the end of this chapter, the comparisons are given, and both their precision and relevance are verified.

Boundary conditions used in the numerical model correspond to the standardized testing of closed polyolefin pipe systems. The pipe was assigned an internal pressure with corresponding hoop stress  $\sigma_{hoop} = 6MPa$ . The welded areas were modeled by implementing the change of Young's modulus in the double power law function (Equation 7.1), as described in Chapter 7.2.

The crack propagation was simulated using an initial crack length of  $0.1mm$  which grew to  $4mm$  over the course of the numerical calculations. The crack shape was assumed to be semi-elliptical and governed by Equation 6.2, as proposed in [3].

For different ratios of Young's modulus, varying from 1 (homogeneous pipe) to 1.5 (highly inhomogeneous weld), the stress intensity factors data were calculated and graphed (see

Figure 7.11). The influence of the inhomogeneity can be seen in Figure 7.11. The direct method was used for the stress intensity factor estimation.

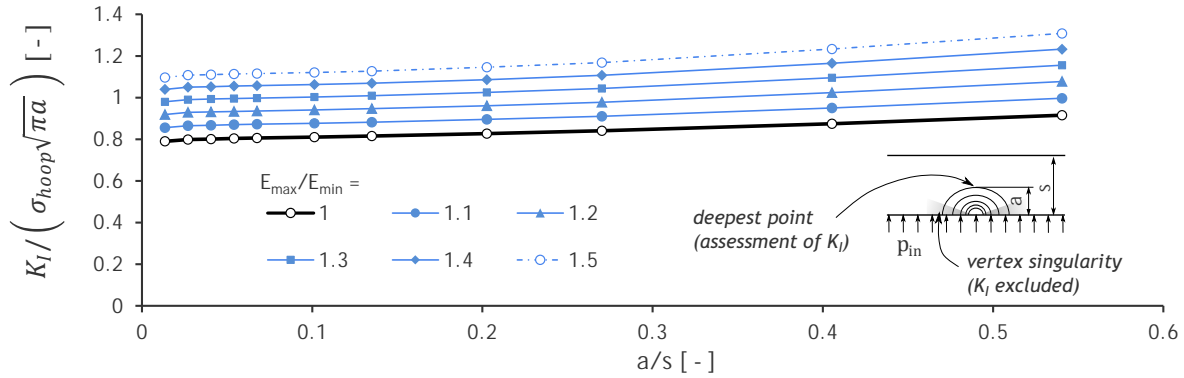


FIGURE 7.11: Normalized values of the SIFs for axial cracks within different ratios  $E_{max}/E_{min}$

In the case of a homogeneous connection, the stress intensity factor values are constant along the semi-elliptical crack front. However, due to the vertex singularity [67], the values lose their meaning when they are measured too close to the free surface. Propagation into a semi-elliptical shape is the natural result under normal conditions. However inhomogeneity or a more complex geometry will cause the crack front to take a rather general shape. Since all numerical models with the axial crack were forced to produce the semi-elliptical shape, and only one value of the stress intensity factor has to be considered, taking the highest value from the deepest point of the crack is the most relevant choice.

Since the stress intensity factor for mode I is usually expressed as a function of following [27],  $K_I = \sigma_{hoop} \sqrt{\pi a} Y(a/s)$ , the values were normalized with respect to hoop stress ( $\sigma_{hoop}$ ) and length of crack  $a$ . The black bold line represents the stress intensity factor related to the homogeneous pipe ( $E_{max}/E_{min} = 1$ ). This was taken as a reference case to which all other solutions could be compared.

From these results, it can be concluded that presence of the inhomogeneity increases the value of the stress intensity factor and depends approximately linearly on the ratio of Young's moduli. The following formula is therefore verified,

$$K_I \approx E_{max}/E_{min}. \quad (7.2)$$

#### 7.4.2 Weld Bead Removed - Circumferential Crack Propagation

For the pipe with a circumferential crack, an axisymmetry can be used to make a two dimensional model (see Figure 7.12). It is important to note that when using the axisymmetry, it was assumed that the crack front shape is circular with the same crack length for all points around the pipe.

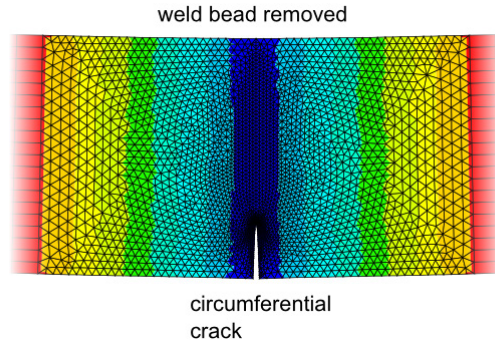
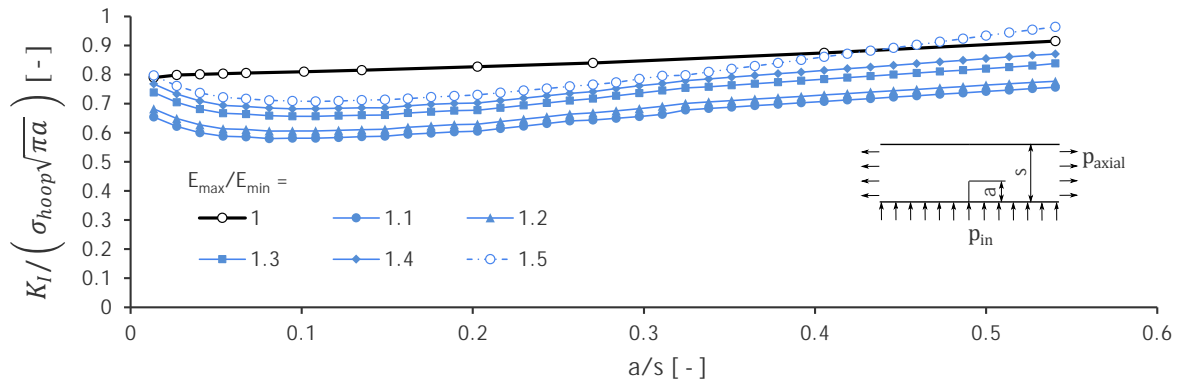


FIGURE 7.12: Finite element mesh near the circumferential crack

The mesh density was refined near the crack tip, as seen in Figure 7.12. Quadratic axisymmetric elements (denoted PLANE183 in ANSYS) were used near the welded area. To decrease the computational time, linear axisymmetric elements (denoted PLANE42) were used outside the welded area.

Due to the symmetry, the crack propagation is straight. An algorithm proposed in the author's bachelor's thesis [4] was used to simulate the crack propagation. The precision of the algorithm with respect to the stress intensity factor is described in the bachelor thesis.

The initial crack length was assigned to be  $0.1\text{mm}$ , the same as in the case with the axial crack. The location of crack initiation is shown in Figure 7.9. The corresponding SIF graph considering circumferential crack is shown in Figure 7.13.

FIGURE 7.13: Normalized SIF values for circumferential cracks for different ratios  $E_{max}/E_{min}$ 

A similar increase in the stress intensity was observed for both the axial crack case (Figure 7.11) and the circumferential case (Figure 7.13). The distance between the middle of the crack initiation and the border of the welded zone (approximately  $2.8\text{mm}$  according to the optimal weld bead geometry) was found to have a negligible effect on the stress intensity. It's important to emphasize that the boundary conditions used here (closed pipe system) induce high axial stresses in comparison to an open pipe system. Therefore, in practical applications where a relatively long pipe system is used, decreased stress intensity due to decreased axial stress can be expected, making these results quite conservative.



Chapter 7.5 presents an analysis of these results, comparing them with the corresponding results for the homogeneous pipe cases with removed weld bead.

### 7.4.3 Weld Bead Kept - Axial Crack Propagation

Assuming an optimal weld shape, the numerical model estimating stress intensity in the case of an axial crack is shown in Figure 7.14. In this case, only one plane of symmetry can be found.

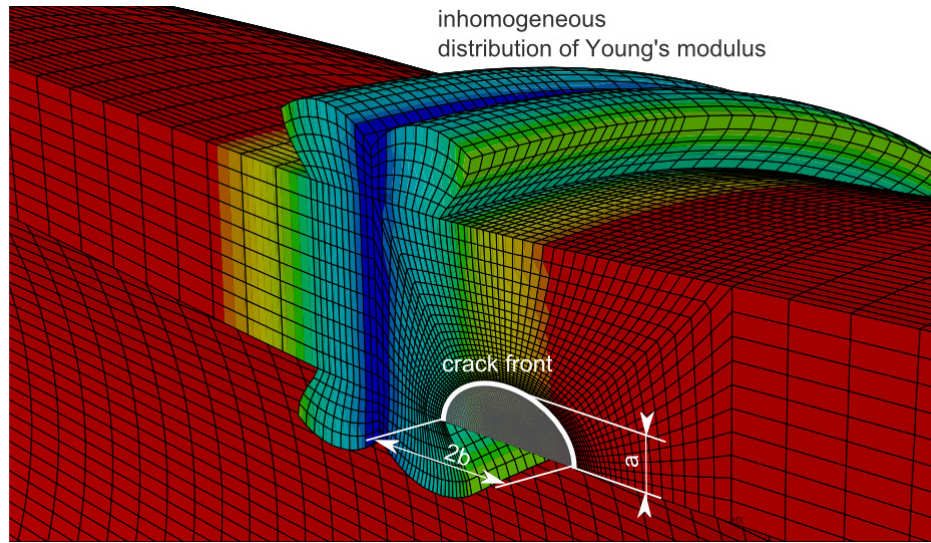


FIGURE 7.14: Finite element mesh near the semi-elliptical axial crack

An example of crack initiation and how it may propagate is shown in Figure 6.2. A simulation of the crack propagation was run in very much the very same way as it was run for the pipe without the weld bead. The initial crack length started with  $0.1\text{mm}$  and grew up to  $4\text{mm}$ . The axial crack had the same shape as described by equation Equation 6.2, proposed in [3]. The results in Figure 7.15 show that keeping the weld bead has a positive effect on decreasing the stress intensity factor. However, for small cracks when  $a/s < 0.1$ , the stress intensity factor is higher (and similar to the intensity for axial cracks in homogeneous pipe), due to the stress concentration at the weld bead notch. For longer cracks  $a/s > 0.1$ , a higher stiffness of the weld bead reduces the stress intensity factor, and independently with respect to the ratio  $E_{max}/E_{min}$ . The  $K_I$  values are smaller than for axial crack in the basic material.

### 7.4.4 Weld Bead Kept - Circumferential Crack Propagation

The propagation of the circumferential crack was simulated by the Maximal Tangential Stress (MTS) criterion. The stress intensity factors were estimated from the nodal displacements near the crack tip for both the first ( $K_I$ ) and the second ( $K_{II}$ ) mode of loading. Figure 7.16 illustrates the numerical model.

The numerical calculations were done in a similar way as in the axisymmetric model, but without the weld bead geometry. The results are plotted in Figure 7.17. In this case, the

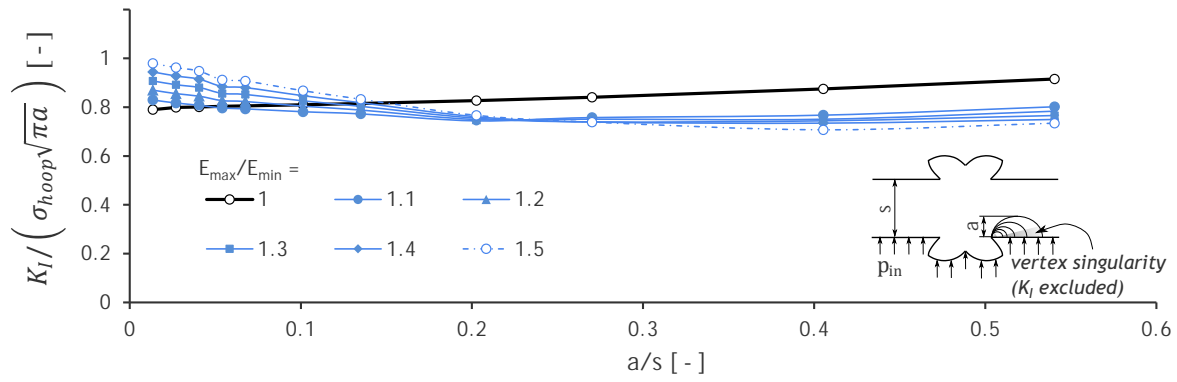
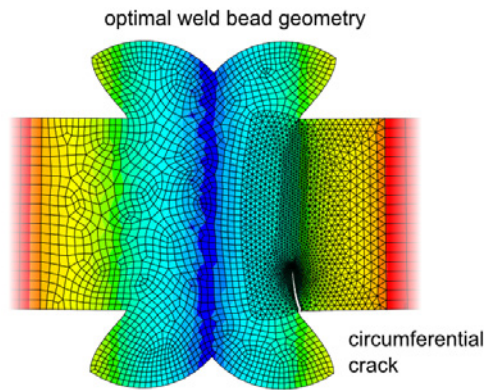
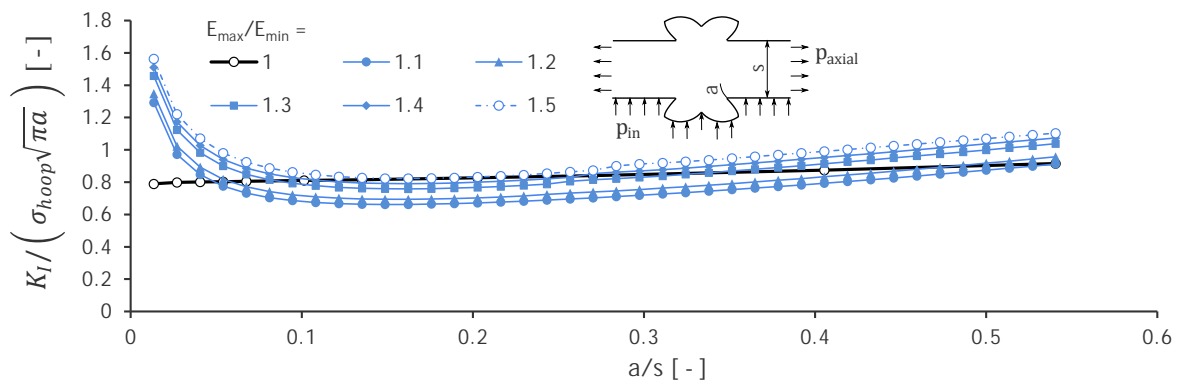
FIGURE 7.15: Normalized SIF values of axial cracks for different ratios  $E_{max}/E_{min}$ 

FIGURE 7.16: Finite element mesh near the circumferential crack

stress intensity factors of small cracks ( $a/s < 0.1$ ) are determined by the stress concentration at the weld bead notch. In case of longer cracks, the  $K_I$  is comparable to the stress intensity factor value determined for an axial crack in homogeneous pipe.

FIGURE 7.17: Normalized values of the SIFs for axial cracks for different ratios  $E_{max}/E_{min}$ 

The influence of the material inhomogeneity is still visible but negligible in comparison to the influence of the weld bead notch and its geometric concentrator.



## 7.5 Accuracy of the Obtained Results

To validate the mesh density and accuracy of the numerical results, this chapter compares the results with analytical solutions or some already published results. More complex geometries solved later (weld bead geometry, inhomogeneous distribution) are meshed with the same mesh refinement near the crack front (see Figure 7.10, Figure 7.12, Figure 7.14, Figure 7.16). Precision of the circumferential crack propagation algorithm and the stress intensity factor assessment is given in author bachelor's thesis [4].

### 7.5.1 Accuracy for Axial Cracks

The stress intensity factor for an axial crack in homogeneous pipe without any weld bead geometry was measured using Equation 5.7 presented in Chapter 5. Numerical results for the axial crack in homogeneous pipe were presented by a black bold line in all the previous graphs. These values were taken as reference values to which all other cases could be compared.

The results for the homogeneous pipe (black bold line) cases are in agreement with the stress intensity factors published by Hutař et al. [3], where only the homogeneous pipe without a weld bead and without material inhomogeneity was studied. The proposed function in [3] is,

$$K_I = \frac{p_{ind}}{s} \sqrt{\pi a} Y \left( \frac{a}{s} \right), \quad (7.3)$$

where

$$Y \left( \frac{a}{s} \right) = 0.3417 + 0.0588 \left( \frac{a}{s} \right) - 0.0319 \left( \frac{a}{s} \right)^2 + 0.1409 \left( \frac{a}{s} \right)^3.$$

Another possible analysis is to compare the solution with the semi-analytical solution given in Chapter 5, in which the results of Raju and Newman [63] for a semi-elliptical crack are applied. Their results were also based on finite element calculations, but in a plate (not a pipe) of finite dimensions. However, their results could be compared to simulations of large diameter pipes with a thin pipe wall. Some of the restrictions are described in Chapter 5.

The three data sets (thesis numerical calculations, Equation 7.4, and the semi-analytical solution Equation 5.7) are compared in the graph in Figure 7.18.

The results are almost exactly the same for all the three cases, especially when the crack is small. Equation 5.7 obtained a lower SIF because the equation assumes a semi-circular crack. As explained in Chapter 6.2, the crack front changes from being semi-circular to being semi-elliptical. However, this change is not strong. The more the crack front changes, and the higher the ratio  $a/b$  gets, the higher the SIF will be. This follows from the solution of an elliptic integral of the second kind (see Equation 5.2). The semi-analytical solution should therefore lead to higher numerically obtained SIF values, which would be even closer to the numerically calculated results for the first two cases.

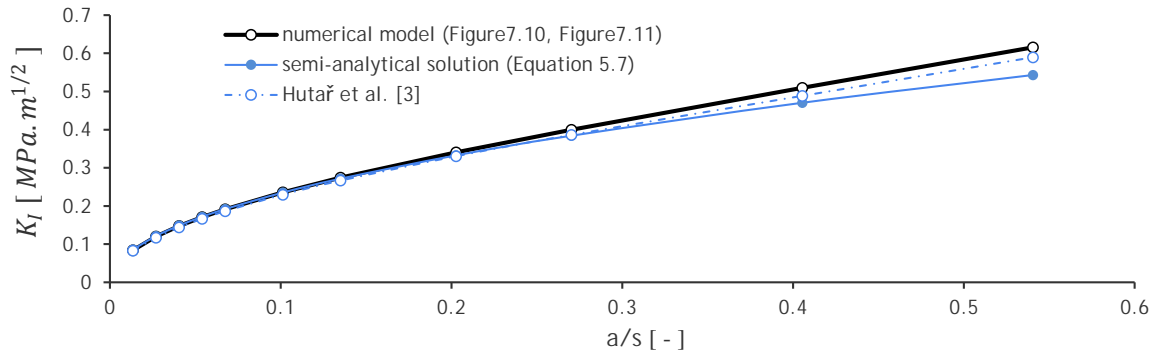


FIGURE 7.18: Different approaches to measuring the SIF for axial crack in a homogeneous pipe

### 7.5.2 Accuracy for Circumferential Cracks

The semi-analytical solution for circumferential cracks was presented in Equation 5.10. The solution is valid only for a crack in a homogeneous pipe without a weld bead. The numerical model results and the semi-analytical solutions are compared in Figure 7.19.

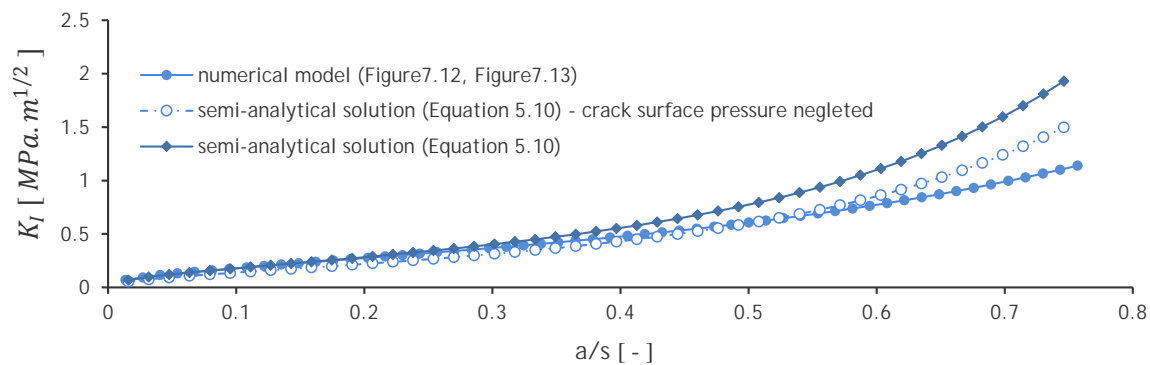


FIGURE 7.19: Different approaches to measuring the SIF for circumferential crack in a homogeneous pipe

For small cracks, all three data sets are almost identical. As presented in Chapter 5.2, the function for the single edge notched plate loses its accuracy when the ratio  $a/s$  exceeds 0.6. This may be the reason for the deviation from the numerical calculations. In addition, as mentioned in the previous chapters, the algorithm for the circumferential crack propagation did not take the pressure acting on crack surfaces into account. The algorithm was simplified since the pressure on the crack surface is negligible for small cracks. In Figure 7.19. In Chapter 11 the pipe lifespan prediction results show that small crack lengths correspond to the majority of the propagation time, and all curves for longer cracks yield roughly the same results.

Due to having similar discretization and SIF assessment, the results of other numerical models presented in the thesis (for which analytical solutions were not possible) are relevant for comparison.

## 7.6 Crack Trajectories in Optimal Butt Welded Pipes

This chapter shows crack propagation of the circumferential cracks near the butt welding joint. The trajectory of the axial crack is always perpendicular to the tangential stress, due to symmetry and the semi-elliptical shape change described by Equation 6.2 in Chapter 6.2. Assumptions on the axial crack propagation are given in Figure 6.2 and Figure 7.8.

The circumferential crack propagation for more complex geometries was performed based on the maximal tangential criterion discussed in Chapter 3.2.3.

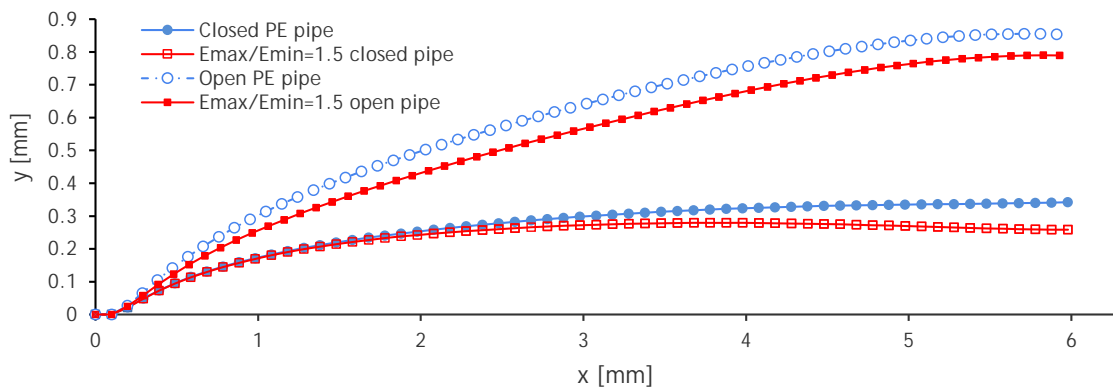


FIGURE 7.20: Circumferential crack trajectories for different welding conditions

When the weld bead is removed, the circumferential crack propagates from the place with the highest stress concentration, the middle of the inhomogeneous distribution. Since the model is now symmetric the crack propagates straight without any change in the direction. The stress intensity factor of the second loading mode is very small, approaching zero.

The circumferential cracks near a weld bead geometry propagate from the area of highest stress concentration, the weld bead notch (see Figure 6.3). As the crack propagates, it curves into the welded region and later it is attracted by the stress concentrator on the outer side of the pipe wall. Crack propagation trajectory for different cases in PE pipe is given in Figure 7.20.

For the closed pipe system, the high axial stress increases the  $K_I/K_{II}$  value, which is responsible for smaller crack curvature. The  $K_I/K_{II}$  value for the open pipe system is smaller and the crack is curved more into the region of higher inhomogeneity. The graph shows also the influence of inhomogeneity on the crack trajectory. The higher the inhomogeneity, the less the crack curves.



# Chapter 8

## Comparison of the Optimal Butt Welding Pipe Failure Modes

Previous chapters were dealing with different numerical models considering different ratio of Young's modulus (thus assuming different polyolefins), different geometry or a different type of crack - axial or radial. In the following, all these models are gathered into two graphs just for one material - polyethylene (PE) where the ratio of Young's moduli is  $E_{max}/E_{min} = 1.1$ . The graphs are seen in Figure 8.1 and Figure 8.2 and the homogeneous pipe's data are added as the black bold line. The same trend would be plot for any other ratio of  $E_{max}/E_{min}$  as seen from the graphs presented in previous chapters.

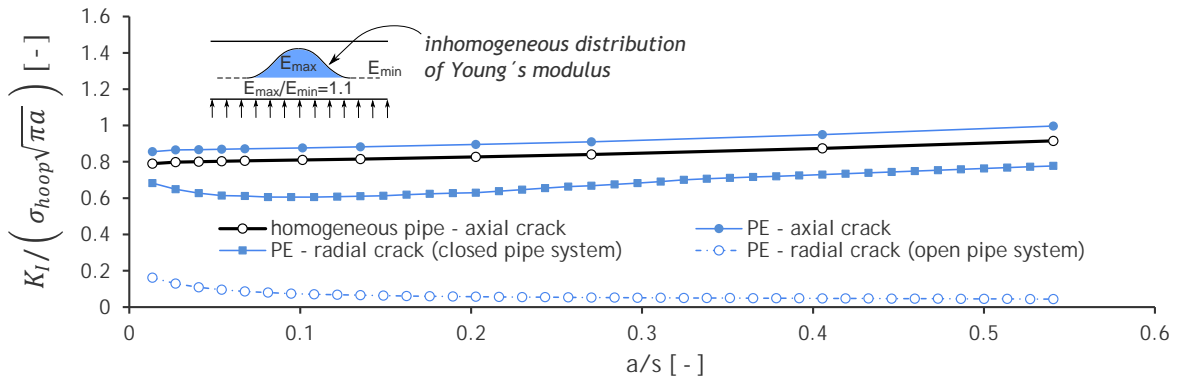


FIGURE 8.1: Normalized values of the SIF for axial cracks for different ratios  $E_{max}/E_{min}$

The graphs here describe the weld either with or without the weld bead as shown on the corresponding pictures. The boundary conditions corresponding to the testing of pipes where the system is closed are denoted as "closed pipe system", whereas the boundary conditions where no axial stress is added are denoted as "open pipe system" where only the inner wall pressure is acting on. Boundary conditions of the pipe system used in praxis are somewhere in between. The system is usually not closed because of the flowing medium, but additional axial stresses should be considered as well. It is therefore recommended to analyse the data with respect to different boundary conditions.

Analysing the graphs the following conclusions can be drawn.

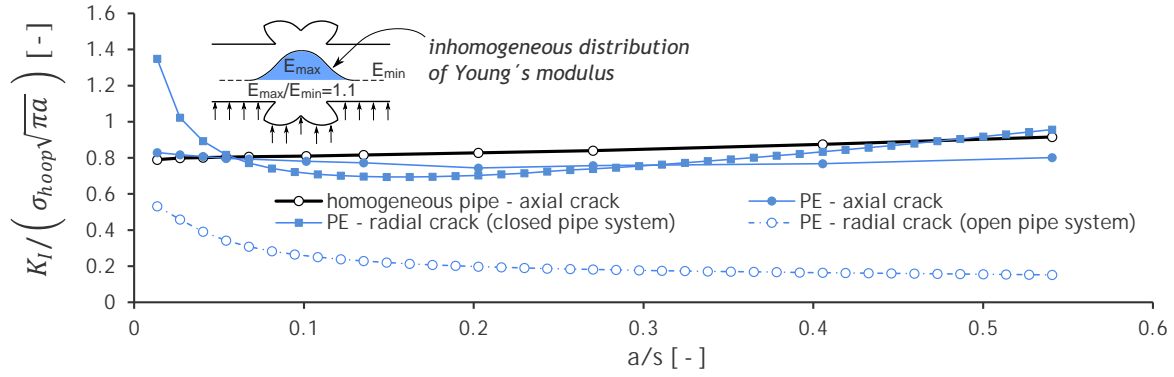


FIGURE 8.2: Normalized values of the SIF for axial cracks for different ratios  $E_{max}/E_{min}$

In case of a pipe without the weld bead the circumferential crack signifies no danger because in the whole range of  $a/s$  the stress intensity factor is smaller than the stress intensity factor of the axial crack in a homogeneous material. Therefore, after removing of the weld bead the dangerous configuration is the axial crack initiated in the middle of the weld (at the inner pipe wall) and propagating inside the welded region. Additionally, this area is a weak point of the structure, due to a decrease in resistance against slow crack growth (demonstrated in Chapter 2.3) and possible defect existence on the welded surfaces. An increase of the stress intensity factor is dependent on the ratio  $E_{max}/E_{min}$ . In the case of polyethylene weld the stress intensity factor is 10% higher than for the basic pipe material. In the case of polypropylene the difference in the  $K$  can reach 30%, which can significantly decrease final residual lifetime of the pipe.

An advantage of the weld with remained weld bead is that the area of the worst material resistance against the slow crack growth (middle of the weld) is covered by additional material and crack initiation in this area is impossible due to compressive stresses in the weld bead on the inner pipe surface, see Figure 7.7. A disadvantage is the presence of the stress concentration around the weld bead notch. In this area both the axial or circumferential cracks may initiate. In the case of axial crack the stress intensity factor is quite similar to the stress intensity factor in the homogenous material. Also the material properties in this area would be comparable to the basic pipe material, which can be documented by similar crystallinity in this area as well as by the values of indentation modulus (see Chapter 2.3).

Circumferential cracks in the weld are strongly affected by the stress concentration produced by the weld bead notches especially when it comes to small cracks where  $a/s < 0.1$ . The value of the stress intensity factor is then significantly higher than for the axial crack in the homogenous case. But, the stress intensity factor for presented "closed pipe system" is a conservative overestimation of the real values, because the axial stress in the real pipe system is probably lower than applied when pipe testing. Growing the circumferential crack is not perfectly circumferential especially in case of small cracks and stress concentration in the notch tip is partially reduced by plastification of the material in the notch.

# Chapter 9

## Non-Optimal Welding Conditions

Until now, only the optimal welding conditions have been discussed. This chapter gives a short outlook onto the non-optimal welding conditions to show how they could be changed in order to optimize the welding joint for a better fracture resistance. Two different non-optimal weld bead shapes have been studied in this thesis. These are illustrated in Figure 9.1 on the right.

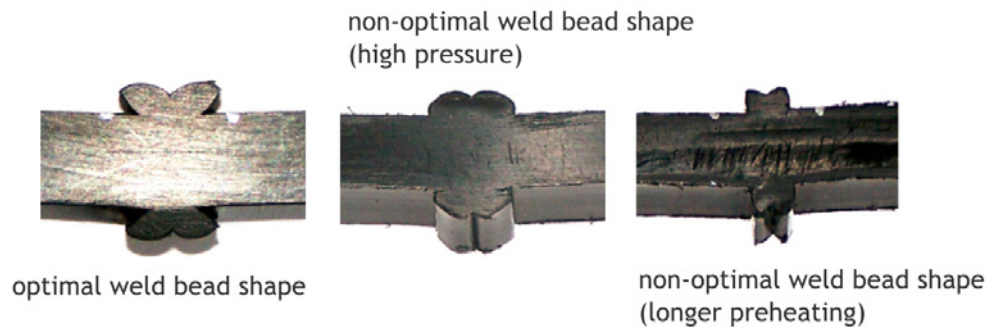


FIGURE 9.1: Different weld bead shapes for optimal and non-optimal welding conditions

The weld bead illustrated on the left represents the optimal weld bead shape. The welding conditions for this case were discussed in Chapter 7.1 and the welding process was described in Figure 7.1. The two studied non-optimal weld bead shapes are produced when,

### **high joining pressure**

joining pressure was increased from  $0.15MPa$  (optimal welding conditions) up to  $0.75MPa$ ,

### **longer time for preheating**

preheating of the joining surfaces was increased from  $t_2 = 63s$  to  $t_2 = 126s$ .

For numerical modelling the geometry of the pipe is the same as heretofore used (see Figure 6.1).

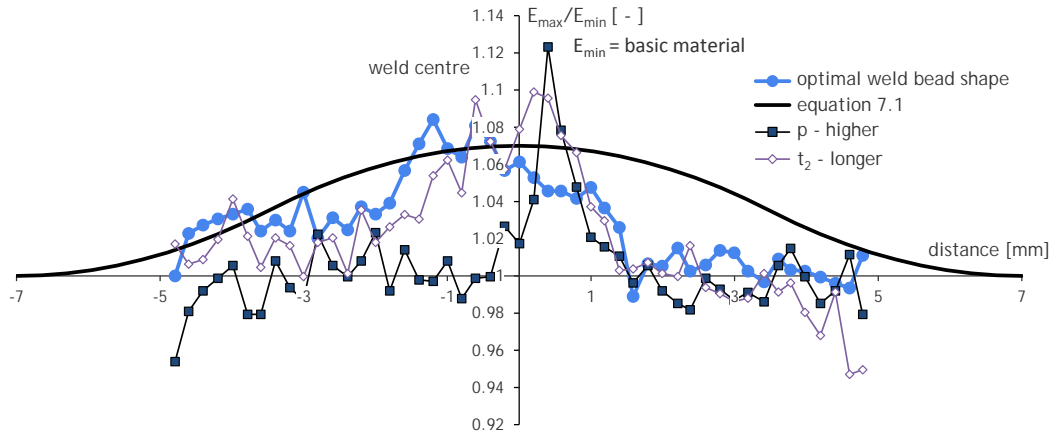


FIGURE 9.2: Normalized Young's modulus from micro indentation tests for different welding conditions

Figure 9.2 illustrates the inhomogeneous distribution of Young's modulus for the three studied welding conditions. In all cases the inhomogeneity is highest in the center of the weld and decreases with proximity to basic material. The same function (Equation 7.1) was used for the inhomogeneous description for all the three cases (black bold line in the figure).

It was shown that the inhomogeneity increases the Stress Intensity Factor (SIF) almost linearly with increasing the ratio  $E_{max}/E_{min}$ , either the axial or the circumferential crack. This is valid also for different weld bead shapes.

The following calculations were performed only on axisymmetrical models with circumferential cracks. The methodology of obtaining the SIF and the numerical model procedures were described in Chapter 6. This chapter therefore describes only the obtained results as the used methods remain the same.

## 9.1 Influence of Weld Bead Shape

Influence of different weld bead shapes is shown in Figure 9.3, expressed in terms of the stress intensity factor. Comparing the values of the SIF for different geometries (see Figure 9.3) suggests that the non-optimal shape caused by high pressure represents the worst case. The difference is highest mainly for small cracks ( $a/s < 0.2$ ). For longer cracks the stress intensity factors are approaching the same value and the shape of the weld bead loses its meaning there. However, the most of the time of crack propagation is concentrated in small cracks and the weld bead shape is important. Especially the volume seems to be the parameter influencing the stress intensity factor rather than the shape of the weld bead.

The reason for higher SIF in case of having the weld bead produced by higher pressure can be explained by looking at the deformation of the pipe in Figure 9.4. The pipe system is considered to be closed and pressurized. The stiffer the welded area is the higher the deformation near the weld bead appears. This deformation adds bending stresses to the axial stresses induced by the inner pressure in a closed pipe system. The bending is caused



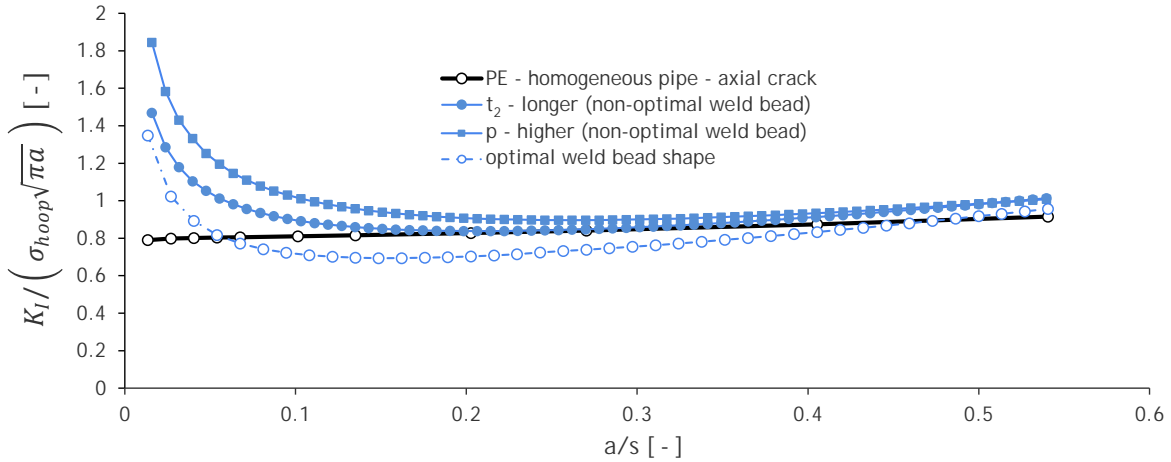


FIGURE 9.3: Normalized stress intensity factors for different weld bead shapes

by the inhomogeneous distribution of Young's modulus and by the amount of material in the welded region. Deformed shapes for different weld bead shapes are magnified with a factor of 100 and compared in Figure 9.4.

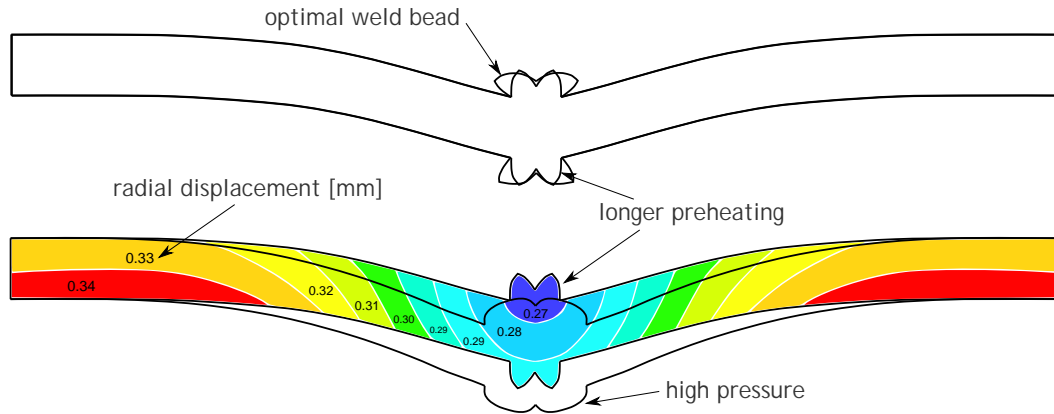


FIGURE 9.4: Deformation of the pipe wall for different weld bead shapes

The crack initiates usually very close to the stiffer welded area which is due to higher bending stresses the reason for having higher values of the SIF. It can be concluded that having more material in the welded region or higher inhomogeneity leads due to deformation to higher stress intensity factor values. This is, however, valid only for the circumferential crack and the opposite effect was observed when having an axial crack. The amount of material can be thus optimized to ensure good properties for both types of cracks. From all of the three studied weld bead shapes the optimal one is the best case in terms of service lifetime.

## 9.2 Influence of Weld Bead Radius

The influence of the weld bead radius was studied on the optimal weld bead shape. The optimal weld bead shape geometry with varying radius is shown in Figure 9.5.

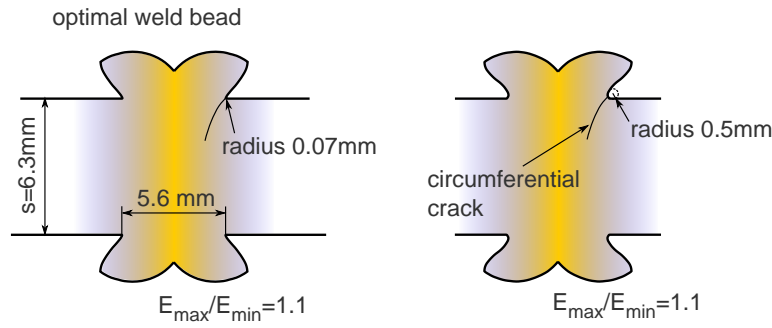


FIGURE 9.5: Weld bead radius geometry

Various radii were considered from the interval from  $0.07\text{mm}$  to  $0.5\text{mm}$ . Smaller radius may influence crack initiation time to shorter times but in overall it does not influence the further crack propagation since the change in the stress concentration is just local and very small. This insignificant change of the SIF is shown in Figure 9.6. The creep crack growth is influenced much more by the inhomogeneity of the welded region or by the weld bead shape as shown in the previous chapter.

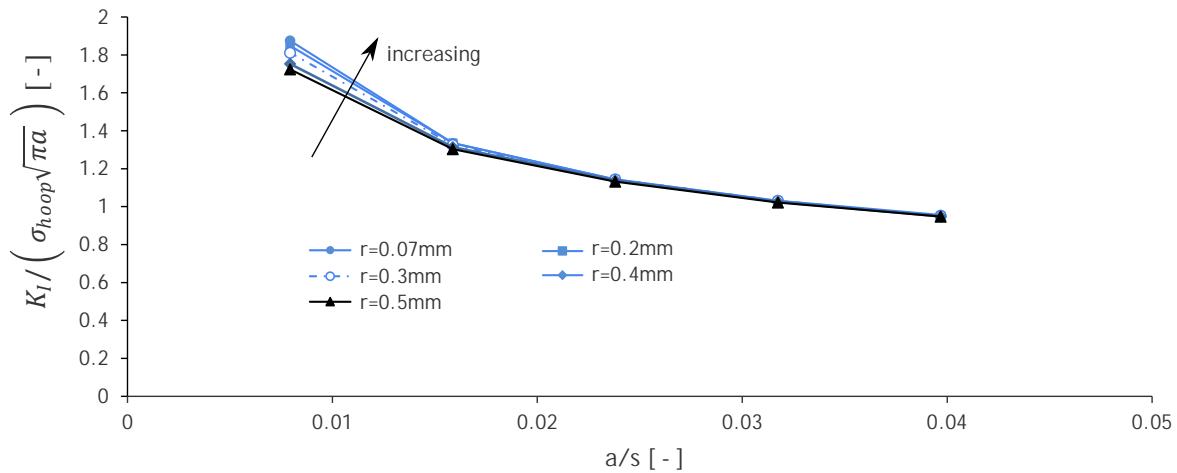


FIGURE 9.6: Normalized stress intensity factor values for different weld bead notch radius

### 9.3 Crack Trajectories for Various Welding Conditions

Crack trajectories for different welding conditions are illustrated in Figure 9.7. Circumferential cracks initiate near the weld bead notches and continue to propagate through the pipe wall. From the crack trajectories it can be seen that the crack is influenced by the stress concentrations of the weld bead notch and later the trajectory is curved back attracted by the stress concentration of the opposite weld bead notch. Trajectories for different weld bead shapes are given in Figure 9.7, where the y-axis is scaled to see the curvature of the crack path. The curvature is highest for the optimal weld bead shape but as seen in the small figure in the graph this change is hardly recognizable using the true scale. All the

results correspond to HDPE pipe with the ratio of Young's modulus in the welded area  $E_{max}/E_{min} = 1.1$ .

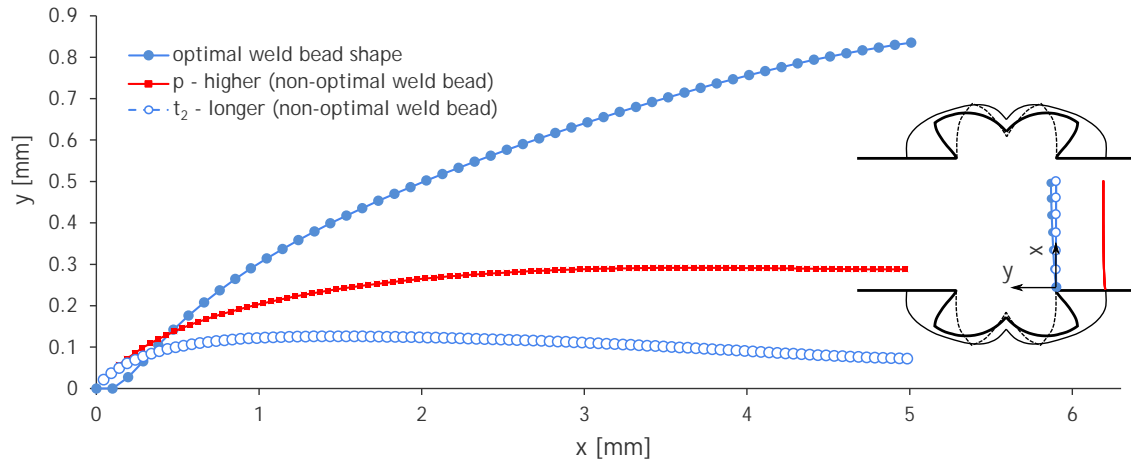


FIGURE 9.7: Circumferential crack trajectories for different weld bead shapes

The origin of the coordinate system is in the place from which the crack started to propagate. The x-axis is related to the radial direction and the y-axis to the axial direction as seen in the figure.



## Chapter 10

# Crack Propagation in Electro-Fusion Welded Pipes

Electro-Fusion welding is another welding technology for connecting of two polyolefin pipes. The technological process was briefly described in Chapter 2.4.2.

A simple drawing of the electro-fusion welding joint in compare to the butt welding joint is shown in Figure 10.1.

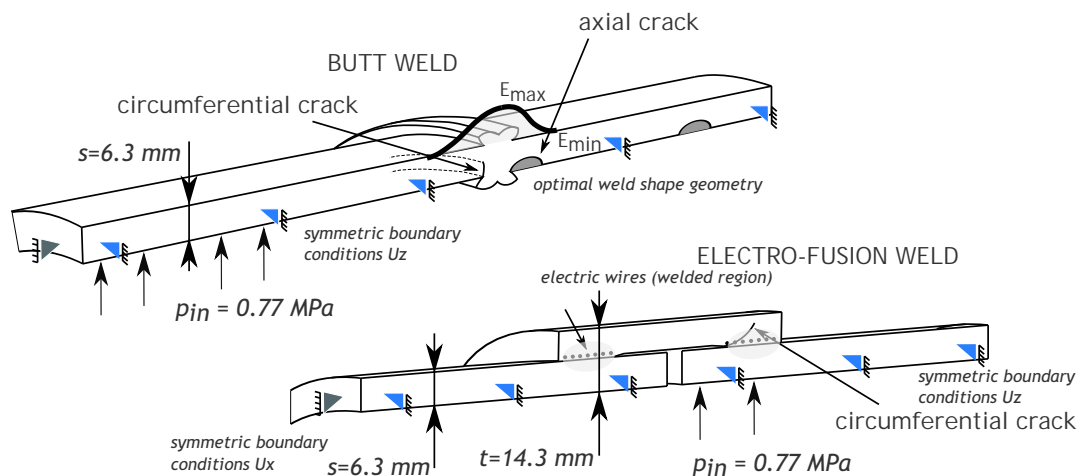


FIGURE 10.1: Geometry of welded pipes showing the butt or electro-fusion welding connection

The butt welding joint and the electro-fusion welding joint are visibly different. While there is only one connection in the butt welded pipes, there are two connections in the electro-fusion welded pipes (see also Figure 2.8). The welding technology and the process of connection was described for both of the connections in Chapter 2.4.

If these two welding joints are to be compared, the very same pipe (PE-100 110 x 6.3 SDR 17.6, see Figure 6.1) geometry has to be studied here, just the connection is different. The circumferential crack usually propagates from the sharp notch at the edge of the welded region, as sketched in Figure 10.1.

## 10.1 Numerical Model

Deformation of the pressurized pipe according to the boundary conditions (see Figure 10.1 and Figure 6.1) is shown in Figure 10.2.

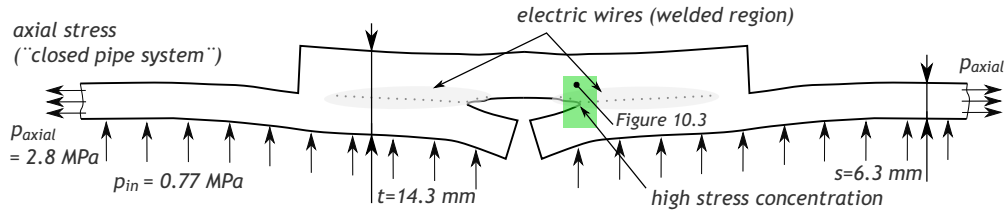


FIGURE 10.2: Deformation of pressurized electro-fusion welded pipes (deformation is scaled with factor of 100)

The welding connection is stiffer than the rest of the pipe system, but there is a visible sharp notch near the welded region. To simulate a circumferential crack propagation the axisymmetry is used, and only a 2D model is created, similarly to the previous.

Mesh density with the mesh refinement near the critical places is shown in Figure 10.3. (The figure is turned 90° from the previous figure.)

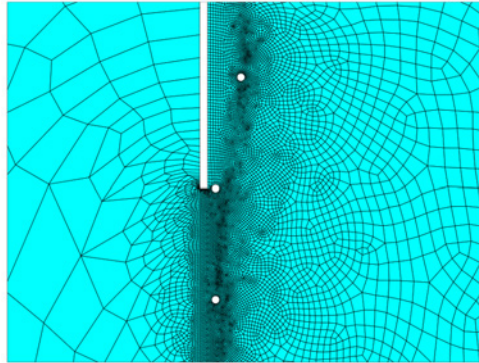


FIGURE 10.3: Mesh refinement near the welded and non welded region (holes represent the electric coil)

An initial stress concentrator from which a circumferential crack propagates is created by the sharp notch at the end of the weld, and also near the places of the electric coil. The coil was not considered in the simulations. Instead, only small holes were created. By this assumption the coil is not in contact with the material. The holes are too small to have any stronger effect on further crack propagation and only crack initiation can be influenced.

As the basic pipe material properties for the numerical model the polyethylene was taken. The Young's modulus of the material is approximately  $E_{min} = 1750 \text{ MPa}$ . The Poisson ratio was considered  $\mu = 0.3$ . The change of inhomogeneous distribution of Young's modulus near the welding joint influenced by the welding process was not taken into account and the same Young's modulus has been applied for all parts of the assembly.

In ANSYS, the 2D axisymmetric element denoted as PLANE182 and PLANE183 were chosen to discretize the domain. The first one is a linear element and was used in the area further

from the stress concentrations in order to reduce the calculation times. The latter one is a quadratic element used near the stress concentrations and near the crack tip where high gradients of stresses appear.

## 10.2 Crack Propagation

The circumferential crack propagation with the initial place from which the crack started to propagate is shown in Figure 10.4.

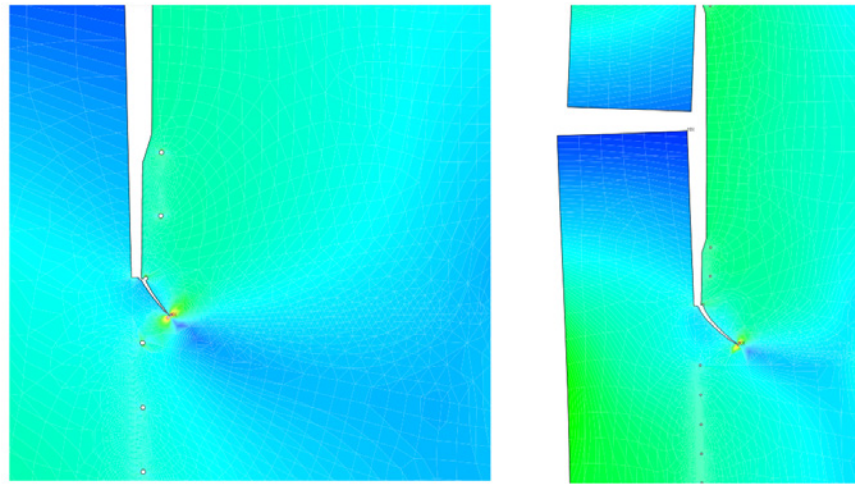


FIGURE 10.4: Crack propagation from the sharp notch crossing the nearest hole (on the left  $a = 1.5\text{mm}$ , on the right  $a = 3\text{mm}$ ), von-Mises stress distribution

The deformation on the figure is 10 times magnified. As the crack propagates from the first hole, it does not seem to be influenced by the second one, and from the very beginning it turns into the radial direction in which is driven by the high axial stresses. The same situation arises for an open pipe system, but the curvature is milder. Crack propagation was simulated by the MTS criterion implemented in an APDL macro proposed in author's bachelor thesis [4]. Important results on the Stress Intensity Factors (SIF) are graphed in the following chapter.

## 10.3 Comparison of the Electro-Fusion and Butt Welding Joint Failure Modes

Resistance to crack propagation is given in terms of the stress intensity factors. The calculated stress intensity factors for open and closed pipe system in compare to the butt welding results are shown in Figure 10.5.

The SIF is plotted as a function of crack length  $a$ , because the ratio  $a/s$  is not appropriate here. The reason for this is that in the electro-fusion welding joint the crack changes its direction from axial to radial.

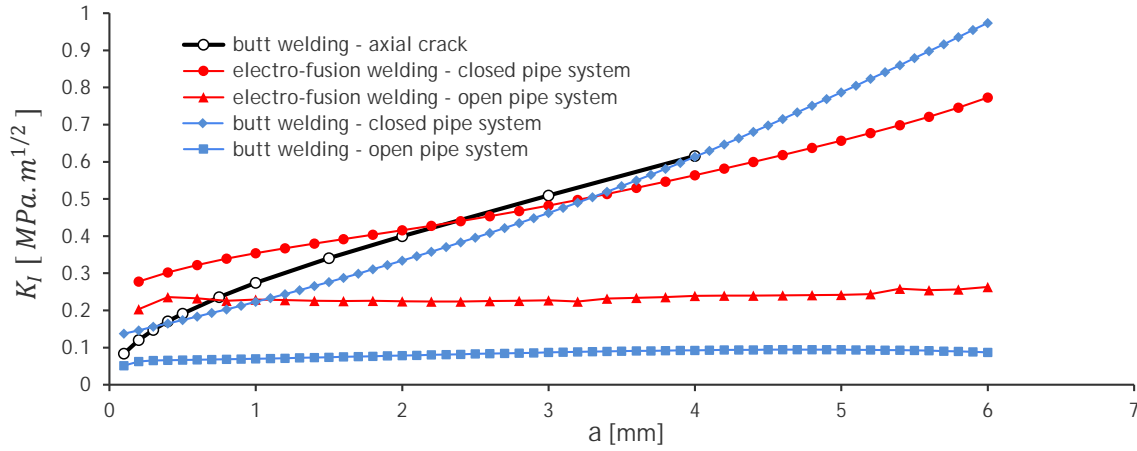


FIGURE 10.5: Stress intensity factors for the circumferential cracks for different welds

High SIF values for small cracks rapidly decrease pipe's lifespan. These values should be as low as possible. For the electro-fusion welding joint the values of the SIF are almost twice that high than for the butt welding joint from which it can be concluded that the electro-fusion welding joint resistance to slow crack growth (because of its geometry configuration) is much lower. According to these results, the lifetime of the joint is calculated in the following chapter.

The following figure illustrates the difference between the two welding connections and crack propagation for the same pipe.

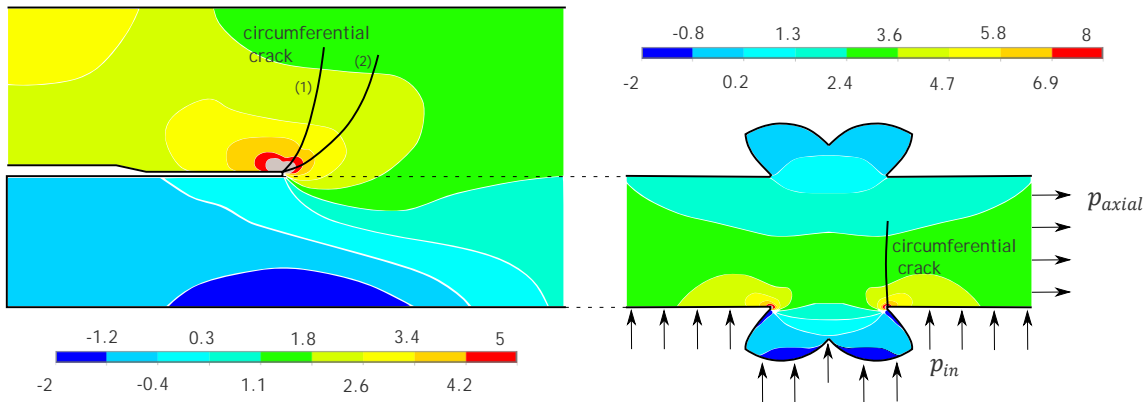


FIGURE 10.6: Crack propagation in electro-fusion and butt welding joint (plotted  $\sigma_{axial}$  stress)

In the electro-fusion welding joint the crack trajectory (1) is when the pipe system is closed and the trajectory (2) when the pipe system is open.



# Chapter 11

## Lifetime Prediction of PE 100

The final chapter of the thesis discusses the problematic of the polyethylene pipe lifetime prediction. The first part of the chapter is devoted to the material properties of PE 100 measured with the cooperation of the Martin-Luther University, Montanuniversität Leoben and Polymer Institute Brno. These material properties of the welding joint should be taken into account when assessing lifetime prediction, especially with respect in what region of the pipe the crack propagates.

The second part of the chapter is devoted to the lifetime prediction of PE 100 110x6.3 SDR 17.6 using the results of the presented numerical models based on the Linear Elastic Fracture Mechanics (LEFM) methodology.

### 11.1 Material Properties of PE 100

#### 11.1.1 PE 100 Short Term Properties

Short term experiments performed at the Martin-Luther University for polyethylene pipe material (PE 100) are given in this chapter. The results compare the basic pipe material and the welded material.

Crack resistance ( $R$ ) curves for polyethylene PE 100 were determined in form of J-integral versus stable crack growth  $\Delta a$ , using a universal testing machine (Zwick Z020) at a crosshead speed of  $10\text{mm}/\text{min}$  at the room temperature. As a result of higher degree of crystallinity inside the welding joint (see Figure 2.9), both the resistance against stable crack initiation ( $J_{0,2}$ ) and resistance to stable crack propagation ( $T_j$ ) are higher inside the welding joint than in the basic material. This is shown in Figure 11.1.

However, these short-term tests do not correctly describe long term properties of material in actual applications. The reason is that polyolefin pipes do not undergo so high deformation rates in real service when failing due to the slow crack growth. Therefore long-term tests have been performed to differentiate between good and bad welds. These are described in the sections below.

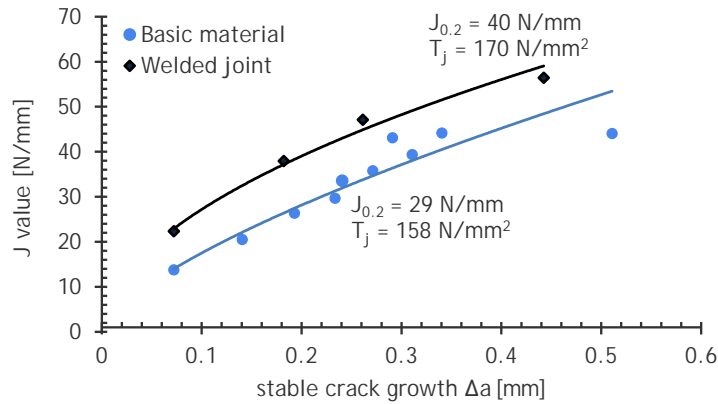


FIGURE 11.1: Resistance against stable crack initiation ( $J_{0,2}$ ) and stable crack propagation ( $T_j$ ) in the basic and welded material [17]

### 11.1.2 PE 100 Long Term Properties

Long term properties of welded pipes are in a better way described by Pennsylvania Notch Tensile (PENT) Test or Cracked Round Bar (CRB) tests. Both of these tests were described in Chapter 5.7. As the short term tests on one side show that the weld itself has better mechanical properties, the long term test on the other side result just in the opposite.

To properly describe the long term properties, the fatigue tests using CRB specimens directly lathed from the pipe wall were performed. The testing conditions were applied (frequency of  $10\text{Hz}$ , R-ratio of 0.1, temperature  $23^\circ\text{C}$ ). Specimens were circumferentially notched with a fresh razor blade in welded area. Comparison between the optimal weld and the basic material is shown in Figure 11.2.

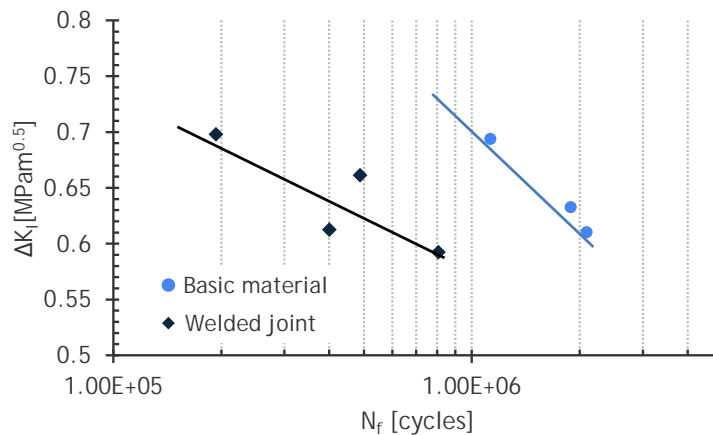


FIGURE 11.2: Number of cycles until failure of PE 100 pipe welds and pipe material as a function of the maximum applied  $K_I$  (according to DVS 2207-1) [73]

It can be seen that the pipe material itself shows significantly better resistance against fatigue loading than the welded area [74].

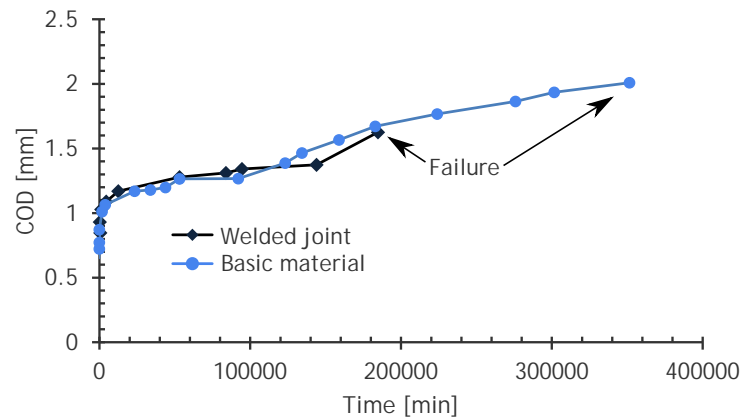


FIGURE 11.3: Evolution of the COD measured by PENT test (Polymer Institute Brno)

The results of the CRB test were confirmed by a PENT test. Specimens were also prepared directly from the welded pipe wall as described in the paper [75]. The notch was made by pressing a fresh razor blade into the specimen at a constant speed of  $330\mu\text{m}/\text{min}$ . The kinetics of the failure process is observed under a constant nominal stress of  $2.4\text{MPa}$  and temperature of  $80^\circ\text{C}$ . In general the stress for brittle failure caused by slow crack growth should be less than one-half of the yield point at the particular testing temperature. The Crack Opening Displacement (COD) was measured with an optical microscope with the resolution about  $2\mu\text{m}$ . The evolution of the COD for welded and non-welded specimen is shown in Figure 11.3

The basic pipe material according to these results has also a better resistance against the creep crack growth propagation than the welded material itself. These experimental results are also in a good agreement with the results published by [76] for the high density polyethylene (P6B00BL).

**Generally, based on the experimental observations (see Figure 11.2 and Figure 11.3) it can be concluded that the slow crack growth resistance of the polyethylene weld (PE 100) is due to the microstructural changes (see Figure 2.9) lower in the welded area in compare with the basic material.**

This is very important when assessing lifetime of a pipe system. Crack propagation near the welded region will be effected by lower resistance to creep crack growth consequently leading to a decrease in pipe's lifetime. It is therefore important to distinguish between crack propagation in the basic and welded material when calculating the lifetime.

## 11.2 Lifetime Prediction Based on the Numerical Models

This section is discussing a methodology for polyolefin pipe lifetime prediction based on the concepts of the Linear Elastic Fracture Mechanics (LEFM). This methodology was extensively studied for instance by [77], [3].

The region of the stable slow crack growth can be described by a similar law as originally proposed by Paris and Erdogan [28], in which the crack growth rate (crack kinetics)  $da/dt$  is the function of stress intensity factor  $K_I$  and material specific constants,  $C$  and  $m$ ,

$$\frac{da}{dt} = C (K_I)^m. \quad (11.1)$$

In the laboratory tests, suitable specimens with well-defined stress configurations are used for an empirical determination of crack kinetic laws. Once the crack kinetics for one geometric structure is known, the  $K_I$ -concept allows a transfer to any other component (e.g. pipe) as long as all the geometrical and loading parameters are known. The time for a crack to growth through the component can be calculated by transforming Equation 11.1, so that the time for creep crack growth  $t_{SCG}$  from an initial defect size  $a_0$  to the failure crack size of  $a_f$  is a function of the component-specific function of  $K_I$  and material parameters  $C$  and  $m$  (Equation 11.1).

In practical applications the crack also requires some incubation time for the initiation of SCG so that the total failure time is the sum of this initiation time  $t_0$  and  $t_{SCG}$ . However, the mechanisms of the crack initiation are difficult to predict and not yet fully understood so that engineering fracture mechanics lifetime assessments are based on predictions of  $t_{SCG}$  which moreover lead to conservative results as they only take immediately growing cracks into account,

$$t_{SCG} = \int_{a_0}^{a_f} \frac{da}{A [K_I(p_{in}, d, s, a)]^m}. \quad (11.2)$$

The resulting lifetime assessment is performed on a polymer pipe from PE-100 ( $d = 110mm$ , SDR 17.6) loaded by hoop stress  $6 - 10MPa$  with an initial defect in the range between  $100\mu m - 400\mu m$ . Initial defect was chosen based on recommendations in literature [24], [78],[79], [80], [20], where typical defects found in the inner surface of the polyolefin pipes were evaluated. In case of the polymer weld, due to the weld bead development a typical defect size increases and values higher to  $400\mu m$  would be relevant.

Material properties of the crack kinetics of PE 100 were estimated experimentally by Frank et al. [80] ( $C = 8.5 \cdot 10^{-7}$  and  $m = 6.8$ ).

The following sections discuss the lifetime predictions and the results in more detail for all the studied connections. Material properties of welded region described in the previous chapter should be taken into account with respect to the region in which the crack propagates. All the presented results will be given for polyethylene but of course any other material (with different  $E_{max}/E_{min}$ ) ratio could be chosen as well.

### 11.2.1 Time to Failure of Butt Welded Pipes (Optimal Welding Conditions)

Optimal welding conditions were detailed in Chapter 7. The lifetime prediction is estimated for polyethylene, based on the stress intensity factor results given in Figure 8.1 and Figure 8.2. The results shown in " $\sigma_{hoop}$  vs. time" diagrams (see Figure 2.12) for two different initial crack sizes are presented in Figure 11.4, Figure 11.5 considering the initial defect size of  $a_0 = 0.1mm$  and in Figure 11.6, Figure 11.7 considering the initial crack size of  $a_0 = 0.4mm$ . The graphs on the left side are comparing the axial cracks, whereas the graphs on the right side the circumferential cracks. Experimental data are given for the stage A (ductile failure, see Figure 2.12), where the time to failure is still possible to measure in a reasonable time frame.

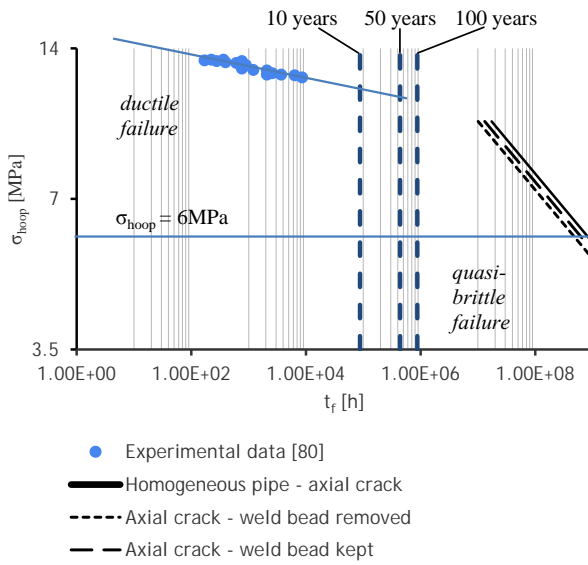


FIGURE 11.4: Time to failure diagram of PE 100 from numerical simulations (axial crack with  $a_0 = 0.1mm$ )

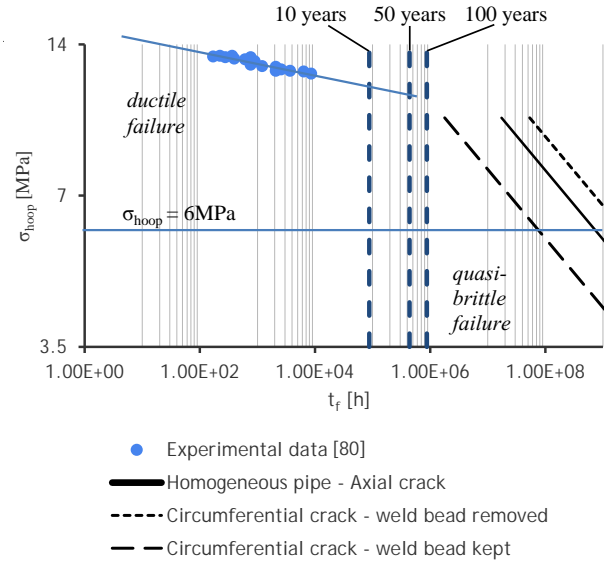


FIGURE 11.5: Time to failure diagram of PE 100 from numerical simulations (circumferential crack with  $a_0 = 0.1mm$ )

It is shown that the resulting lifetime is strongly sensitive to the initial defect size ( $a_0$ ) and a small increase in the defect size dramatically decreases the lifetime of the structure, see the difference in Figure 11.4, Figure 11.5 and Figure 11.6, Figure 11.7.

The existence of axial cracks in the welded area slightly reduces the lifetime, due to small ratio  $E_{max}/E_{min}$ , see Figure 11.4. For higher ratio (different material, for instance polypropylene), the lifetime reduction would be higher. As seen in the figures, removing of the weld bead has a negative effect on the lifetime and this effect is further enhanced by lower resistance to creep crack growth in the welded region, as pointed out in the previous chapter.

Circumferential crack propagating from the weld bead notch significantly reduce  $t_{SCG}$  (residual lifetime), but still the final lifetime is higher than 100 years, see Figure 11.5. In the case of circumferential crack, keeping of the weld bead has a negative impact on the lifetime. However, in real service when the pipe system is not fully closed (lower axial stresses can be expected) the stress intensity factors are too low in compare to the axial cracks, that it is not

probable for the circumferential crack to propagate. Instead an axial crack would initiate either in the basic pipe material in a non-welded region if the weld bead is not removed or in the welded region if the weld bead is removed.

A very similar situation is plot in Figure 11.6, Figure 11.7, where now the initial defect is taken as  $a_0 = 0.4mm$ .

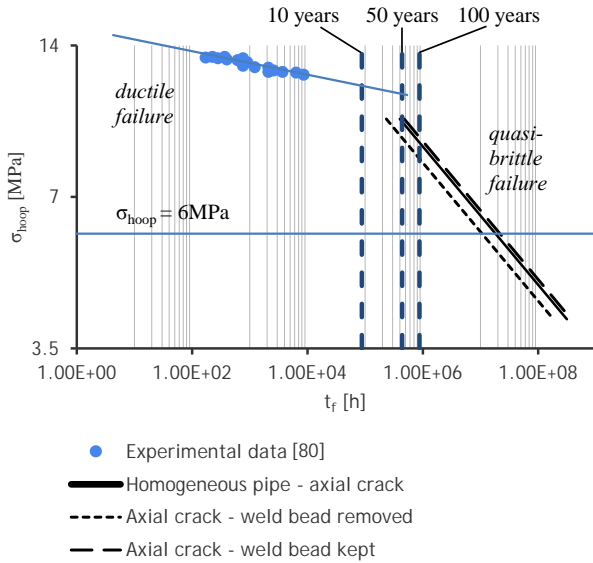


FIGURE 11.6: Time to failure diagram of PE 100 from numerical simulations (axial crack with  $a_0 = 0.4mm$ )

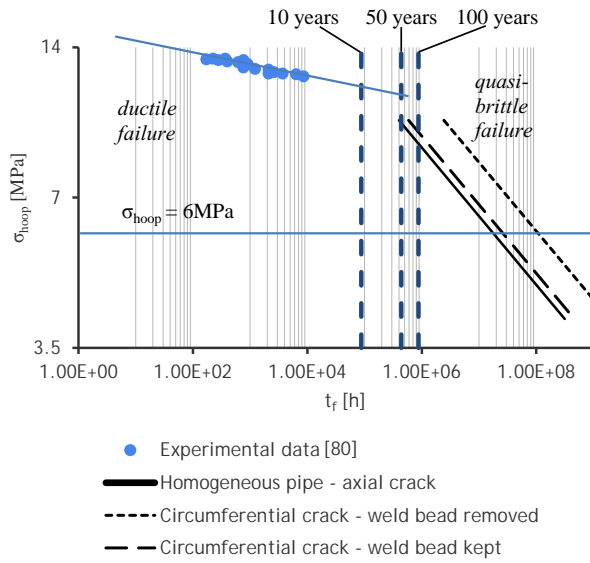


FIGURE 11.7: Time to failure diagram of PE 100 from numerical simulations (circumferential crack with  $a_0 = 0.4mm$ )

As seen the initial defect consideration is very important and changes the lifetime rapidly, (all lines are shifted to the left). Lifetime of the homogeneous pipe in this case is realistic and corresponds well with simulations of the lifetime predictions published in [80], [3], [81]. The effect of the weld bead has a positive contribution on pipe's lifespan in both modes of failure, regardless on crack orientation (axial or circumferential).

In the case of pipe without the weld bead, the axial crack initiated in the center of the weld slightly reduces the lifetime of the pipe and propagation of the circumferential crack is from the mechanics point of view improbable. It should be noted that resistance of polyolefin material in the center of the weld is significantly reduced (see the previous chapter), which is not considered in the residual lifetime estimation shown in Figure 11.6, Figure 11.7. Therefore, reduction of the lifetime due to crack propagation in the center of the weld can be much higher.

Results obtained for PE 100 welded pipes indicate that remaining of the weld bead induces a stress concentration in the weld bead notch but a possible crack (axial crack) propagates far from the weld bead center and predicted lifetime of the pipe is comparable with non-welded pipe. Material properties of non-welded region are not reduced and the presented results in this case are much closer to reality. Contrary to that, in the case of welded pipe without the weld bead a crack can initiate in the center of the weld, where resistance of the material against slow crack growth is significantly reduced and possible macroscopic defects after the welding procedure are present. Calculated lifetime in this case is also the lowest from all of

the studied cases. Therefore generally, it can be concluded that removing of weld beads can be seen critical with respect to decreasing lifetime expectations.

### 11.2.2 Time to Failure of Butt Welded Pipes (Non-Optimal Welding Conditions)

As it was shown in Chapter 9, the optimal weld bead shape has the best resistivity against the slow crack growth due to its geometrical configuration, which decreases the stress intensity factor values, especially for small cracks. As seen in the previous chapter, the initial crack size is very important and a significant part of the crack propagation time is characterized by small cracks. The reason for lower stress intensity factors of the optimal weld bead shape was explained on the deformation, (see Figure 9.4) in Chapter 9.

Lifetime prediction and its results for the optimal welding conditions were described in the previous chapter. In case of non-optimal welding conditions a significant decrease of lifetime is visible in the case of circumferential crack for both non-optimal studied cases (higher time of preheating and higher pressure).

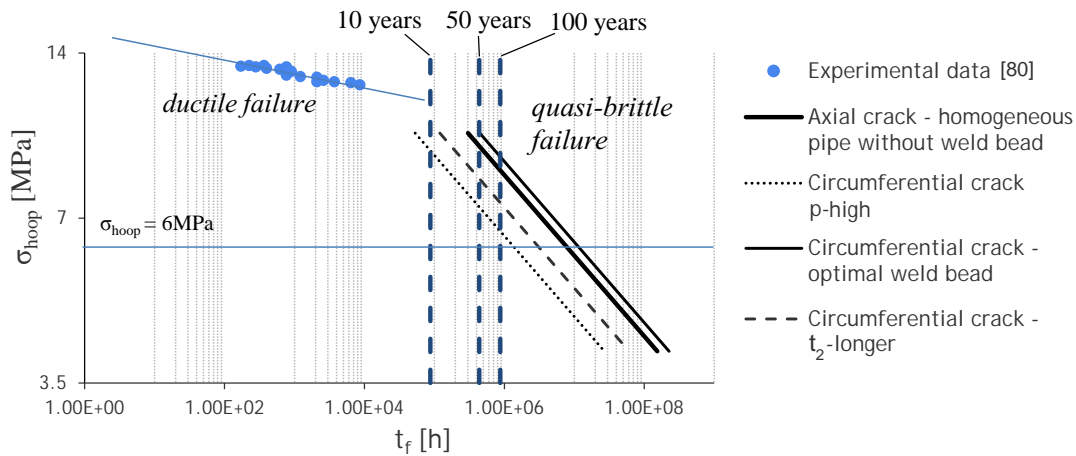


FIGURE 11.8: Hoop stress vs. time to failure diagram for different welding conditions considering the initial crack length of  $0.4\text{mm}$

The presented results are conservative and a higher reduction of lifetime can be further expected since the crack propagates in welded region where the resistance to creep crack growth is decreased.

Non-optimal welding conditions are not recommended and from all the three studied cases the optimal welding conditions are the best. However, welding conditions can still be optimized in order to find a better weld bead shape which would decrease the SIF even more. This can be considered for future related research.

### 11.2.3 Time to Failure of Electro-Fusion Welded Pipes

The last section of this chapter describes the electro-fusion welding joint lifetime prediction in compare to the butt welding joint. The results are graphed in the following figure.

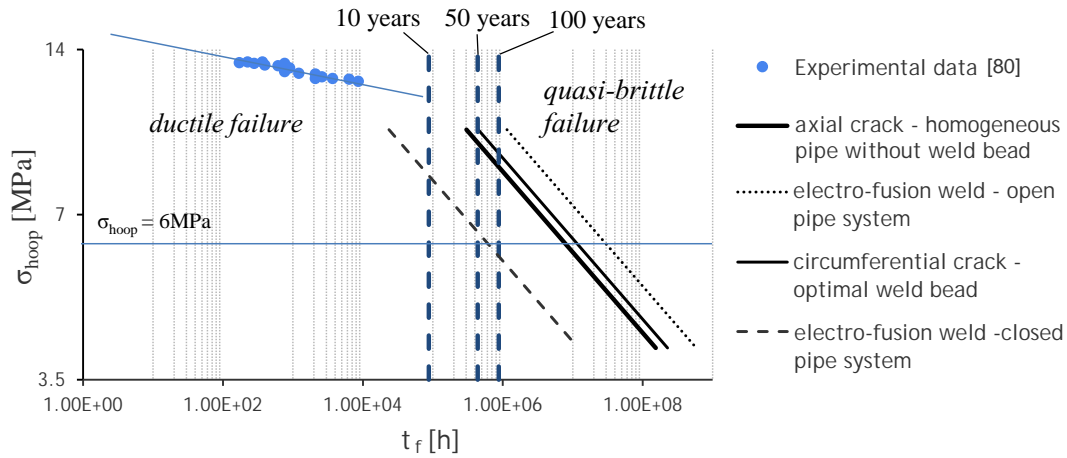


FIGURE 11.9: Hoop stress vs. time to failure diagram for the electro-fusion welding joint considering the initial crack length of  $0.4mm$

There are visible limits in Figure 11.9 in lifetime for the open and closed pipe system with the electro-fusion joint. As the stress intensity factor distribution indicated, the lifetime for the closed pipe system is decreased in compare with the butt welding joint. Electro-Fusion joint seems to be inefficient in terms of slow crack growth. Further optimization can be, however, studied. Changing the dimensions and shape of the electro-fusion joint can decrease the SIF eventually increasing the resistance of the joint to slow crack growth.



# Chapter 12

## Conclusion

The main aim of the thesis was to describe fracture behavior of welded polyolefin pipes. For this purpose, various numerical models have been successfully created. These models were used to simulate pipe crack propagation for two different crack orientations: axial crack (3D case) and circumferential crack (2D case). Crack propagation in each case was simulated separately for both welded and non-welded pipe material.

This thesis also describes a methodology for assessing the lifespan of welded polyolefin pipes. The presented results and recommendations complement existing procedures based on the concepts of Linear Elastic Fracture Mechanics (LEFM). Specifically, the numerical models simulated changes in polyolefin properties by considering the effect of Young's modulus (which describes the inhomogeneity near the welded region).

Prediction of pipe lifespan and subsequent assessments were done mainly for polyethylene (PE). However, as seen in the analysis of the stress intensity factor, the same conclusions could be drawn for any other material.

Different numerical models were designed to describe crack propagation in both optimal and non-optimal welding joints. Numerical models of crack propagation in homogeneous pipes were compared to the analytical solutions or other published results, and the mesh refinement near the crack front was confirmed to be sufficient with respect to the corresponding stress intensity assessment. Initial comparisons assisted in the debugging of algorithms later used for more complex geometries, such as inhomogeneous distributions and different weld bead geometries, as well as for the electro-fusion welding joint description.

Presented results include the quasi-brittle failure mechanism, in which a slow creep crack growth is observed to cause the failure. In the case of the axial crack, the crack front has a semi-elliptical shape and propagation stems from the meridian. The change of the crack front was estimated for a homogeneous pipe based on the constant Stress Intensity Factor (SIF) distribution along the crack front. The SIF was estimated using the direct method. This crack front shape was then used for all other 3D cases with the axial crack. In the case of the circumferential crack, propagation occurs in the radial and axial direction. These crack propagations were simulated by combining the Maximal Tangential Stress (MTS) criterion with an algorithm proposed in author bachelor's thesis [4], improving upon the existing

method for solving axisymmetric problems. The SIF in this case was estimated based on the nodal displacements near the crack tip.

The following conclusions summarize the results of the numerical models for inhomogeneous butt welded pipes:

- The stress intensity factor increases in the presence of material inhomogeneity, regardless of crack orientation (axial or circumferential), and correlates approximately linearly with the ratio  $E_{max}/E_{min}$ .
- The weld bead makes the welded area stiffer and increases the probability of initiating a circumferential crack, especially when the pipe system is fully closed. Otherwise, it is more likely that an axial crack propagates in a non-welded area.
- If the weld bead is removed, the axial crack propagates in the middle of the weld and the resulting stress intensity factor is higher (leading to decreased residual lifespan) than for the corresponding non-welded pipe.

From the perspective of fracture mechanics, numerical results show that keeping the weld bead increases the lifespan of welded pipes.

Conclusions regarding the different welding conditions are summarized as follows:

- The optimal weld bead shape has the best geometry in terms of pipe's lifetime.
- The weld bead notch radius has no effect on crack propagation other than its influence on initiation time.

Lifespan estimates for welded pipes were calculated using an equation analogous to the Paris-Erdogan equation, applying the material properties published in [80]. The lifespan of the pipes is influenced mainly by small cracks. It was shown that the lifespan predictions are conservative and highly dependant on the choice of the initial crack length. Stress intensity factors for  $a/s < 0.1$  were significant. According to some recommendations, the experimental initial crack length of  $0.4mm$  was selected.

The following are the most important experimental results regarding pipe lifespan:

- The slow crack growth is accelerated by the welding process for both the axial and circumferential cracks.
- Considering an initial crack of  $0.4mm$ , the pipe lifespan is significantly reduced if the weld bead is removed and the axial crack is initiated in the homogeneous area.
- If the weld bead is kept, then the lifespan of a butt welded pipe with a circumferential crack is comparable to the lifespan of a homogeneous pipe with an axial crack. Circumferential cracks are therefore not dangerous in butt welded pipes, especially if the system is not fully closed.

Finally, the electro-fusion welding joint was also compared to the butt welded pipes. Results show that the electro-fusion welded pipes have a lower resistance to circumferential crack propagation, due to their joint geometrical configuration.

All objectives of the diploma thesis have been met. The thesis results were also presented at three conferences (Engineering Mechanics 2014, Computational Mechanics 2014, and Applied Mechanics 2015), and have been submitted for publication in *Materials & Design*. An additional related research paper including the thesis results has been sent to the Springer book entitled *Deformation and Fracture Behavior of Polymer Materials*.

The thesis results can be used for estimating the lifespan of welded pipe systems, predicting creep crack growth, and optimizing conditions for butt welding or electro-fusion welding. Minimizing the SIF leads to higher life expectancy. However, the long-term behavior of material properties of the welded region must be considered. Geometrical configuration plays an important role in determining the stress intensity factor, and this is one possible direction for future related research.



# Chapter 13

## Author's Contributions

Results of the thesis were presented at the following conferences:

- *Engineering Mechanics 2014*, J. Mikula, M. Ševčík, P. Hutař, and L. Náhlík, "Fracture Mechanics Assessment of Cracked Welded Polyolefin Pipes", May 2014
- *Computational Mechanics 2014*, J. Mikula, P. Hutař, M. Ševčík, and L. Nahlik, "Crack Propagation in Welded Polyolefin Pipes", November 2014 - Czech Society for Mechanics Award for the best presented paper
- *Applied Mechanics 2015*, J. Mikula, P. Hutař, M. Ševčík, and L. Náhlík, "Crack Propagation in an Electro-Fusion and Butt Welding Joint", April 2015

Papers submitted for publication:

- J. Mikula, P. Hutař, E. Nezbedová, R. Lach, F. Arbeiter, M. Ševčík, G. Pinter, W. Grellmann, and L. Nahlik, "On Welded Polyolefin Pipes from Perspective of Fracture Mechanics", paper submitted to the *Materials and Design* journal
- J. Mikula, P. Hutař, M. Ševčík, E. Nezbedová, R. Lach, W. Grellmann, and L. Náhlík, "Influence of Different Welding Conditions of Polyolefin pipes on Creep Crack Growth", paper submitted to Springer book entitled "Deformation and Fracture Behaviour of Polymer Materials"



# Bibliography

- [1] ISO 21307, “Plastics pipes and fittings – Butt fusion jointing procedures for polyethylene (PE) pipes and fittings used in the construction of gas and water distribution systems.” International Organization for Standardization, 2011.
- [2] EN ISO 9080, “Plastics piping and ducting systems – determination of the long-term hydrostatic strength of thermoplastics materials in pipe form by extrapolation.” International Organization for Standardization, 2012.
- [3] P. Hutař, M. Ševčík, L. Náhlík, G. Pinter, A. Frank, and I. Mitev, “A numerical methodology for lifetime estimation of HDPE pressure pipes,” *Engineering Fracture Mechanics*, vol. 78, no. 17, pp. 3049–3058, 2011. [Online]. Available: <http://www.sciencedirect.com/science/article/pii/S001379441100347X>
- [4] J. Mikula, “Numerical modeling of crack propagation under conditions of LEFM,” 2012, Bachelor’s thesis, Institute of Solid Mechanics, Mechatronics and Biomechanics, Faculty of Mechanical Engineering, Brno University of Technology, Supervisor: Martin Ševčík. [Online]. Available: <https://www.vutbr.cz/www`base/zav`prace`soubor`verejne.php?file`id=53053>
- [5] H. Lester, “History and physical chemistry of HDPE,” *Plastics Pipe Institute*, 2010. [Online]. Available: <http://www.plasticpipe.org/pdf/chapter-1`history`physical`chemistry`hdpe.pdf>
- [6] L. E. Janson, “Pipes for water supply and sawage disposal,” *Stockholm: Magnestams Reklam/ Christensons Grafika AB*, 1989.
- [7] ASTM D3350, “Standard specification for polyethylene plastics pipe and fittings materials.” ASTM International, 2014. [Online]. Available: <http://www.astm.org/Standards/D3350.htm>
- [8] P.E.S Co., “Welding & installing,” 2009. [Online]. Available: <http://www.pespipe.com/services/welding-installing.htm>
- [9] DVS 2207-1, “Schweißen von thermoplastischen kunststoffen – Heizelementschweißen von rohren, rohrleitungsteilen und tafeln aus PE,” 2014.
- [10] Polyweld Tech Academy, “Electrofusion welding,” 2015. [Online]. Available: <http://www.polyweldtech.com.au/training/electrofusion-welding/#prettyPhoto>

- [11] S. Jose, A. Aprem, B. Francis, M. Chandy, P. Werner, V. Alstaedt, and S. Thomas, "Phase morphology, crystallisation behaviour and mechanical properties of isotactic polypropylene/high density polyethylene blends," *European Polymer Journal*, vol. 40, no. 9, pp. 2105–2115, 2004. [Online]. Available: <http://www.sciencedirect.com/science/article/pii/S0014305704000862>
- [12] N. Sun, M. Wenzel, and A. Adams, "Morphology of high-density polyethylene pipes stored under hydrostatic pressure at elevated temperature," *Polymer*, vol. 55, no. 16, pp. 3792–3800, 2014. [Online]. Available: <http://www.sciencedirect.com/science/article/pii/S0032386114004443>
- [13] L. Hubert, L. David, R. Sgula, G. Vigier, C. Degoulet, and Y. Germain, "Physical and mechanical properties of polyethylene for pipes in relation to molecular architecture. i. microstructure and crystallisation kinetics," *Polymer*, vol. 42, no. 20, pp. 8425–8434, 2001. [Online]. Available: <http://www.sciencedirect.com/science/article/pii/S0032386101003512>
- [14] X. Sun, H. Shen, B. Xie, W. Yang, and M. Yang, "Fracture behavior of bimodal polyethylene: Effect of molecular weight distribution characteristics," *Polymer*, vol. 52, no. 2, pp. 564–570, 2011. [Online]. Available: <http://www.sciencedirect.com/science/article/pii/S0032386110010633>
- [15] K. Leskovics, M. Kollár, and P. Bárczy, "A study of structure and mechanical properties of welded joints in polyethylene pipes," *Materials Science and Engineering: A*, vol. 419, no. 12, pp. 138–143, 2006. [Online]. Available: <http://www.sciencedirect.com/science/article/pii/S092150930501467X>
- [16] C. Biergel, W. Grellmann, T. Fahnert, and R. Lach, "Material parameters for the evaluation of PA welds using laser extensometry," *Polymer Testing*, vol. 25, no. 8, pp. 1024–1037, 2006. [Online]. Available: <http://www.sciencedirect.com/science/article/pii/S0142941806001334>
- [17] P. Veselý, I. Kotter, R. Lach, E. Nezbedová, Z. Knésl, P. Hutař, and W. Grellmann, "Prüfmethode zur analyse des lokalen mechanischen verhaltens von schweißnähten in polyethylen-kunststoffrohren," *Borsutzki M, Geisler S (Eds.). Fortschritte der Kennwertermittlung für Forschung und Praxis (Proceedings Werkstoffprüfung 2009*, pp. 371–376, 2009.
- [18] H. Brömstrup, *PE 100 Pipe Systems*. Vulkan-Verlag, 2009, ISBN 978-3-8027-2759-7.
- [19] X. Lu and N. Brown, "A test for slow crack growth failure in polyethylene under a constant load," *Polymer Testing*, vol. 11, no. 4, pp. 309–319, 1992. [Online]. Available: <http://www.sciencedirect.com/science/article/pii/0142941892900257>
- [20] M. Barker, J. Bowman, and M. Bevis, "The performance and causes of failure of polyethylene pipes subjected to constant and fluctuating internal pressure loadings," *Journal of Materials Science*, vol. 18, no. 4, pp. 1095–1118, 1983. [Online]. Available: <http://dx.doi.org/10.1007/BF00551979>



- [21] R. Lang, A. Stern, and G. Doerner, "Applicability and limitations of current lifetime prediction models for thermoplastics pipes under internal pressure," *Die angewandte makromolekulare Chemie*, vol. 247, no. 1, pp. 131 – 145, 1997.
- [22] K. Sehanobish, A. Moet, A. Chudnovsky, and P. P. Petro, "Fractographic analysis of field failure in polyethylene pipe," *Journal of Materials Science Letters*, vol. 4, no. 7, pp. 890 – 894, 1985.
- [23] B.-H. Choi, A. Chudnovsky, R. Paradkar, W. Michie, Z. Zhou, and P.-M. Cham, "Experimental and theoretical investigation of stress corrosion crack (scc) growth of polyethylene pipes," *Polymer Degradation and Stability*, vol. 94, no. 5, pp. 859–867, 2009. [Online]. Available: <http://www.sciencedirect.com/science/article/pii/S0141391009000226>
- [24] H. Hamouda, M. Simoes-betbeder, F. Grillon, P. Blouet, N. Billon, and R. Piques, "Creep damage mechanisms in polyethylene gas pipes," *Polymer*, vol. 42, no. 12, pp. 5425–5437, 2001. [Online]. Available: <http://www.sciencedirect.com/science/article/pii/S0032386100004900>
- [25] H. B. H. Hamouda, L. Laiarinandrasana, and R. Piques, "Fracture mechanics global approach concepts applied to creep slow crack growth in a medium density polyethylene (mdpe)," *Engineering Fracture Mechanics*, vol. 74, no. 14, pp. 2187–2204, 2007. [Online]. Available: <http://www.sciencedirect.com/science/article/pii/S0013794406004085>
- [26] L. Andena, M. Rink, R. Frassine, and R. Corrieri, "A fracture mechanics approach for the prediction of the failure time of polybutene pipes," *Engineering Fracture Mechanics*, vol. 76, no. 18, pp. 2666–2677, 2009, fracture of Polymers, Composites and Adhesives 5th ESIS TC4 Conference. [Online]. Available: <http://www.sciencedirect.com/science/article/pii/S0013794409003099>
- [27] M. Chan and J. Williams, "Slow stable crack growth in high density polyethylenes," *Polymer*, vol. 24, no. 2, pp. 234–244, 1983. [Online]. Available: <http://www.sciencedirect.com/science/article/pii/0032386183901398>
- [28] P. Paris and F. Erdogan, "A critical analysis of crack propagation laws," *Journal of Fluids Engineering*, vol. 85, no. 4, pp. 528–533, 1963.
- [29] N. Brown and X. Lu, "A fundamental theory for slow crack growth in polyethylene," *Polymer*, vol. 36, no. 3, pp. 543–548, 1995.
- [30] J. Teh, J. White, and E. Andrews, "Fatigue of viscoelastic polymers: 1. crack-growth characteristics," *Polymer*, vol. 20, no. 6, pp. 755–763, 1979. [Online]. Available: <http://www.sciencedirect.com/science/article/pii/0032386179902519>
- [31] N. Haddaoui, A. Chudnovsky, and A. Moet, "Ductile fatigue crack propagation in polycarbonate," *Polymer*, vol. 27, no. 9, pp. 1377–1384, 1986. [Online]. Available: <http://www.sciencedirect.com/science/article/pii/0032386186900376>
- [32] A. Frank, W. Freimann, G. Pinter, and R. W. Lang, "A fracture mechanics concept for the accelerated characterization of creep crack growth in PE-HD pipe grades," *Engineering Fracture Mechanics*, vol. 76, no. 18, pp. 2780–2787, 2009, fracture of

- Polymers, Composites and Adhesives 5th ESIS TC4 Conference. [Online]. Available: <http://www.sciencedirect.com/science/article/pii/S0013794409001891>
- [33] S. Sternstein and L. Ongchin, "Yield criteria for plastic deformation of glassy high polymers in general stress fields," *Polymer Preprints*, vol. 10, pp. 1117–1124, 1969.
- [34] R. Oxborough and P. Bowden, "A general critical-strain criterion for crazing in amorphous glassy polymers," *Philosophical Magazine*, vol. 28, no. 3, pp. 547–559, 1973.
- [35] J. Hessel, "Minimum service-life of buried polyethylene pipes without sand-embedding," *3R international*, vol. 40, pp. 4–12, 2001.
- [36] M. Haager, G. Pinter, and R. Lang, "Ranking of pe-hd pipe grades by fatigue crack growth performance," *Plastics Pipe XII*, 2006. [Online]. Available: <https://www.plasticpipe.org/pdf/htd-rank-pe-pipe-grades-crack-growth-performance.pdf>
- [37] X. Lu and N. Brown, "Abnormal slow crack growth in polyethylene," *Polymer*, vol. 38, no. 23, pp. 5749–5753, 1997. [Online]. Available: <http://www.sciencedirect.com/science/article/pii/S0032386197001304>
- [38] G. Pinter, M. Haager, W. Balika, and R. W. Lang, "Cyclic crack growth tests with CRB specimens for the evaluation of the long-term performance of PE pipe grades," *Polymer Testing*, vol. 26, no. 2, pp. 180–188, 2007. [Online]. Available: <http://www.sciencedirect.com/science/article/pii/S0142941806001784>
- [39] DIN 8075, "Polyethylene (PE) pipes - PE 80, PE 100 - General quality requirements, testing," 2011.
- [40] ISO 1167-1, "Thermoplastics pipes, fittings and assemblies for the conveyance of fluids – determination of the resistance to internal pressure – part 1: General method." International Organization for Standardization, 2006.
- [41] H. Nishimura and I. Narisawa, "Fatigue behavior of medium-density polyethylene pipes," *Polymer Engineering and Science*, vol. 31, no. 6, pp. 339–403, 1991.
- [42] H. Nishimura, A. Nakashiba, M. Nakakura, and K. Sasai, "Fatigue behavior of medium-density polyethylene pipes for gas distribution," *Polymer Engineering and Science*, vol. 33, no. 14, pp. 895–900, 1993.
- [43] C. J. Plummer, A. Goldberg, and A. Ghanem, "Micromechanisms of slow crack growth in polyethylene," in *ccc*, ser. European Structural Integrity Society, A. P. B.R.K. Blackman and J. Williams, Eds. Elsevier, 2003, vol. 32, pp. 3–14. [Online]. Available: <http://www.sciencedirect.com/science/article/pii/S1566136903800791>
- [44] V. Favier, T. Giroud, E. Strijko, J. Hiver, C. G'Sell, S. Hellinckx, and A. Goldberg, "Slow crack propagation in polyethylene under fatigue at controlled stress intensity," *Polymer*, vol. 43, no. 4, pp. 1375–1382, 2002. [Online]. Available: <http://www.sciencedirect.com/science/article/pii/S0032386101007017>
- [45] A. Frank, "Fracture mechanics based lifetime assessment and long-term failure behavior of polyethylene pressure pipes," Ph.D. dissertation, Montanuniversitat Leoben, 2010.

- [46] R. Land, G. Pinter, and W. Balika, "Konzept zur nachweisführung für nutzungsdauer und sicherheit von pe-druckrohren bei beliebiger einbausituation," in *3R International*, vol. 44, 01 2005, pp. 33–41.
- [47] R. Land, G. Pinter, W. Balika, and M. Haager, "A novel qualification concept for lifetime and safety assessment of pe pressure pipes for arbitrary installation conditions," in *Plastics Pipes XIII*, Washington DC, USA, 10 2006, pp. 01–10.
- [48] A. A. Griffith, "The Phenomena of Rupture and Flow in Solids," *Royal Society of London Philosophical Transactions Series A*, vol. 221, pp. 163–198, 1921.
- [49] M. L. Williams, "On the stress distribution at the base of a stationary crack," *Journal of Applied Mechanics*, vol. 24, no. 1, pp. 109–114, 1956.
- [50] R. S. Barsoum, "On the use of isoparametric finite elements in linear fracture mechanics," *International Journal for Numerical Methods in Engineering*, vol. 10, no. 1, pp. 25–37, 1976. [Online]. Available: <http://dx.doi.org/10.1002/nme.1620100103>
- [51] H. Rhee and M. M. Salama, "Mixed-mode stress intensity factor solutions of a warped surface flaw by three-dimensional finite element analysis," *Engineering Fracture Mechanics*, vol. 28, no. 2, pp. 203–209, 1987. [Online]. Available: <http://www.sciencedirect.com/science/article/pii/0013794487902141>
- [52] H. Rhee, "Stress intensity factor evaluation from displacements along arbitrary crack tip radial lines for warped surface flaws," *Engineering Fracture Mechanics*, vol. 32, no. 5, pp. 723–730, 1989. [Online]. Available: <http://www.sciencedirect.com/science/article/pii/0013794489901689>
- [53] ANSYS INC. ANSYS 13.0 Help, 2012.
- [54] S. Chan, I. Tuba, and W. Wilson, "On the finite element method in linear fracture mechanics," *Engineering Fracture Mechanics*, vol. 2, no. 1, pp. 1–17, 1970. [Online]. Available: <http://www.sciencedirect.com/science/article/pii/0013794470900263>
- [55] J. R. Rice, "A path independent integral and the approximate analysis of strain concentration by notches and cracks," *Journal of applied mechanics*, vol. 35, no. 2, pp. 379–386, 1968.
- [56] J. R. Rice, "Mathematical analysis in the mechanics of fracture," *Fracture: an advanced treatise*, vol. 2, pp. 191–311, 1968.
- [57] F. Erdogan and G. Sih, "On the crack extension in plates under plane loading and transverse shear," *Journal of Fluids Engineering*, vol. 85, no. 4, pp. 519–525, 1963.
- [58] G. Sih, "Some basic problems in fracture mechanics and new concepts," *Engineering Fracture Mechanics*, vol. 5, no. 2, pp. 365–377, 1973. [Online]. Available: <http://www.sciencedirect.com/science/article/pii/0013794473900271>
- [59] E. E. Gdoutos, "Problems of mixed mode crack propagation," 1984.
- [60] M. Hussain, S. Pu, and J. Underwood, "Strain energy release rate for a crack under combined mode I and mode II," *Fracture Analysis*, p. 2–28, 1974.

- [61] D. Dugdale, "Yielding of steel sheets containing slits," *Journal of the Mechanics and Physics of Solids*, vol. 8, no. 2, pp. 100–104, 1960. [Online]. Available: <http://www.sciencedirect.com/science/article/pii/0022509660900132>
- [62] G. I. Barenblatt, "The mathematical theory of equilibrium cracks in brittle fracture," *Advances in applied mechanics*, vol. 7, no. 55-129, p. 104, 1962.
- [63] J. C. Newman and I. Raju, "Stress-intensity factor equations for cracks in three dimensional finite bodies subjected to tension and bending loads," *NASA Technical Memorandum 85793*, 1984.
- [64] M. Janssen, J. Zuidema, and R. Wanhill, *Fracture Mechanics, Second Edition*. CRC Press, 2004, ISBN 978-0-415-34622-1.
- [65] E. Folias, "An axial crack in a pressurized cylindrical shell," *Int. J. Fract. Mech*, vol. 1, pp. 104–113, 1965.
- [66] R. Schouwenaars, V. Jacobo, E. Ramos, and A. Ortiz, "Slow crack growth and failure induced by manufacturing defects in hdpe-tubes," *Engineering Failure Analysis*, vol. 14, no. 6, pp. 1124–1134, 2007, papers presented at the Second International Conference on Engineering Failure Analysis (Toronto, Canada, 12-15 September 2006) Part I. [Online]. Available: <http://www.sciencedirect.com/science/article/pii/S1350630706002068>
- [67] Z. Bazant and L. Estenssoro, "Surface singularity and crack propagation," *International Journal of Solids and Structures*, vol. 15, pp. 405–426, 1979.
- [68] L. Pook, "Some implications of corner point singularities," *Engineering Fracture Mechanics*, vol. 48, pp. 367–378, 1994.
- [69] P. Hutař, L. Náhlík, and Z. Knésl, "Quantification of the influence of vertex singularities on fatigue crack behavior," *Computational Materials Science*, vol. 45, no. 3, pp. 653–657, 2009.
- [70] M. Ševčík, P. Hutař, and L. Náhlík, "Crack behavior in a welded polyolefin pipe," *Mechanics of Composite Materials*, vol. 47, no. 3, pp. 263–270, 2011. [Online]. Available: <http://dx.doi.org/10.1007/s11029-011-9206-x>
- [71] M. Ševčík, P. Hutař, L. Náhlík, R. Lach, Z. Knesl, and W. Grellmann, "Crack propagation in a welded polyolefin pipe," *International Journal of Structural Integrity*, vol. 3, pp. 148–157, 2012.
- [72] S.-h. Chi and Y.-L. Chung, "Cracking in coating-substrate composites with multi-layered and fgm coatings," *Engineering Fracture Mechanics*, vol. 70, no. 10, pp. 1227–1243, 2003.
- [73] F. J. Arbeiter, G. Pinter, and A. Frank, "Impact of single and dual pressure butt-welding procedures on the reliability of PE 100 pipe welds," 2013.
- [74] A. Florian, G. Pinter, and A. Frank, "The applicability of the pennsylvania notch test for a new generation of pe pipe grades," *Polymer Testing*, vol. 32, pp. 106–114, 2013.

- [75] E. Nezbedová, P. Hutař, M. Zouhar, Z. Knésl, J. Sadílek, and L. Náhlík, “The applicability of the pennsylvania notch test for a new generation of PE pipe grades,” *Polymer Testing*, vol. 32, no. 1, pp. 106–114, 2013. [Online]. Available: <http://www.sciencedirect.com/science/article/pii/S0142941812001882>
- [76] O. Juseok, O. Youngjin, L. Seunggun, K. Jungsung, and C. Sunwoong, “Enhancement of butt fusion joints integrity against slow crack growth,” *Barcelona (Spain): Proceedings Plastic Pipes XVI*, 2012.
- [77] E. M. Hoang and D. Lowe, “Lifetime prediction of a blue PE100 water pipe,” *Polymer Degradation and Stability*, vol. 93, no. 8, pp. 1496 – 1503, 2008. [Online]. Available: <http://www.sciencedirect.com/science/article/pii/S0141391008001547>
- [78] A. Stern, “Fracture mechanical characterization of the long-term behavior of polymers under static loads,” diploma thesis, Leoben (Austria): University of Leoben, 1995.
- [79] G. Pinter, “Rißwachstumsverhalten von pe-hd unter statischer belastung,” diploma thesis, Leoben (Austria): University of Leoben, 1999.
- [80] A. Frank, P. Hutař, and G. Pinter, “Numerical assessment of PE 80 and PE 100 PipeLifetime based on Paris-Erdogan equation,” *Macromol. Symp.*, no. 311, p. 112–121, 2012.
- [81] P. Hutař, M. Ševčík, A. Frank, L. Náhlík, J. Kučera, and G. Pinter, “The effect of residual stress on polymer pipe lifetime,” *Engineering Fracture Mechanics*, vol. 108, no. 0, pp. 98–108, 2013, crack Paths 2012. [Online]. Available: <http://www.sciencedirect.com/science/article/pii/S0013794413001732>



# List of Abbreviations

APDL	Ansys Parametric Design Language
CCG	Creep Crack Growth
CNC	Computer Numerical Control
COD	Crack Opening Displacement
CRB	Cracked Round Bar
DENT	Double Edge Notched Tensile
FCG	Fatigue Crack Growth
FEM	Finite Element Method
FNCT	Full Notch Creep Test
EPFM	Elasto Plastic Fracture Mechanics
FGM	Functionally Graded Material
GSIF	Generalized Stress Intensity Factor
HDPE	High Density Polyethylene
LDPE	Low Density Polyethylene
LEFM	Linear Elastic Fracture Mechanics
MDPE	Medium Density Polyethylene
MRS	Minimal Required Stress
MTS	Maximal Tangential Stress
NPT	Notch Pipe Test
PE	Polyethylene
PENT	Pennsylvania Edge Notched Tensile
PP	Polypropylene
SCG	Slow Crack Growth
SDR	Standard Dimensional Ratio
SIF	Stress Intensity Factor
SSY	Small Scale Yielding





# List of Symbols and Physical Constants

$\beta$	$MPa$	parameter (Oxborough and Bowden's craze criterion)
$\delta a$	$mm$	crack increment
$\gamma$	$MPa$	parameter (Oxborough and Bowden's craze criterion)
$\mu$	—	Poisson's ratio
$\pi$	—	Ludolph's number
$\rho$	$mm$	size of plastic zone (strip yield model)
$\sigma$	$MPa$	stress
$\sigma_{axial}$	$MPa$	stress in axial direction
$\sigma_{hoop}$	$MPa$	tangential stress
$\sigma_{ij}$	$MPa$	stress tensor
$\sigma_m$	$MPa$	hydrostatic stress
$\sigma_y$	$MPa$	yield stress
$\tau_j$	$N/mm^2$	resistance against the stable crack propagation
$\Theta$	—	elliptical integral of the second kind
$\varepsilon$	—	strain
$\varphi$	$RAD$	polar coordinate (angle)
$a$	$mm$	crack length, length of the major axis of an ellipse
$a_0$	$mm$	initial crack size
$a_f$	$mm$	final crack size
$B$	$mm$	solid body thickness
$b$	$mm$	minor axis of ellipse
$C$	$\frac{mm/s}{(MPa \cdot m^{1/2})^m}$	Paris-Erdogan constant
$C$	—	Raju and Newman constant
$COD$	$mm$	crack opening displacement
$d$	$mm$	pipe outer diameter
$E$	$MPa$	Young's modulus
$E_{max}$	$MPa$	maximum Young's modulus in the weld
$E_{min}$	$MPa$	Young's modulus of the basic pipe material
$E_C$	$MPa$	Creep modulus
$F$	$N$	force
$f_{ij}$	—	goniometric functions

$F_{max}$	$N$	maximum applied force
$F_{min}$	$N$	minimum applied force
$G$	$J/mm^2$	crack driving force
$h_{1,2}$	—	functions of material inhomogeneity function
$J_{0,2}$	$N/mm$	resistance against the stable crack initiation
$K$	$MPa.m^{1/2}$	stress intensity factor
$K_{I,max}$	$MPa.m^{1/2}$	maximum applied stress intensity factor
$K_{I,min}$	$MPa.m^{1/2}$	minimum applied stress intensity factor
$K_{II}$	$MPa.m^{1/2}$	stress intensity factor (second mode)
$K_{III}$	$MPa.m^{1/2}$	stress intensity factor (third mode)
$K_I$	$MPa.m^{1/2}$	stress intensity factor (first mode)
$L$	$mm$	length
$m$	—	Paris-Erdogan constant
$M_f$	—	Follias correction factor for bulging of the crack flanks
$p$	—	singularity exponent
$p$	—	exponent of material inhomogeneity function
$p_{axial}$	$MPa$	applied axial pressure
$p_{in}$	$MPa$	pipe internal pressure
$r$	$mm$	polar coordinate (distance from the crack tip)
$R$	$mm$	pipe min-surface radius
$r$	$mm$	weld bead notch radius
$r_p$	$mm$	size of plastic zone (the second approximation)
$r_y$	$mm$	size of plastic zone (the first approximation)
$s$	$mm$	pipe wall thickness
$t$	$s$	time
$T$	$^{\circ}C$	temperature
$t_{SCG}$	$h$	time of slow crack growth
$t_f$	$h$	time to failure
$u$	$mm$	displacement in x-direction
$U$	$J$	strain energy
$v$	$mm$	displacement in y-direction
$w$	$J/mm^3$	strain energy density
$w$	$mm$	half weld width
$Y$	—	shape function

# List of Appendices

<b>A Flow Diagrams</b>	<b>109</b>
A.1 Algorithm of Axial Crack Propagation . . . . .	109
A.2 Algorithm of Circumferential Crack Propagation . . . . .	110
<b>B APDL Scripts</b>	<b>111</b>
B.1 Material Inhomogeneity Implementation . . . . .	111



# A Flow Diagrams

## A.1 Algorithm of Axial Crack Propagation

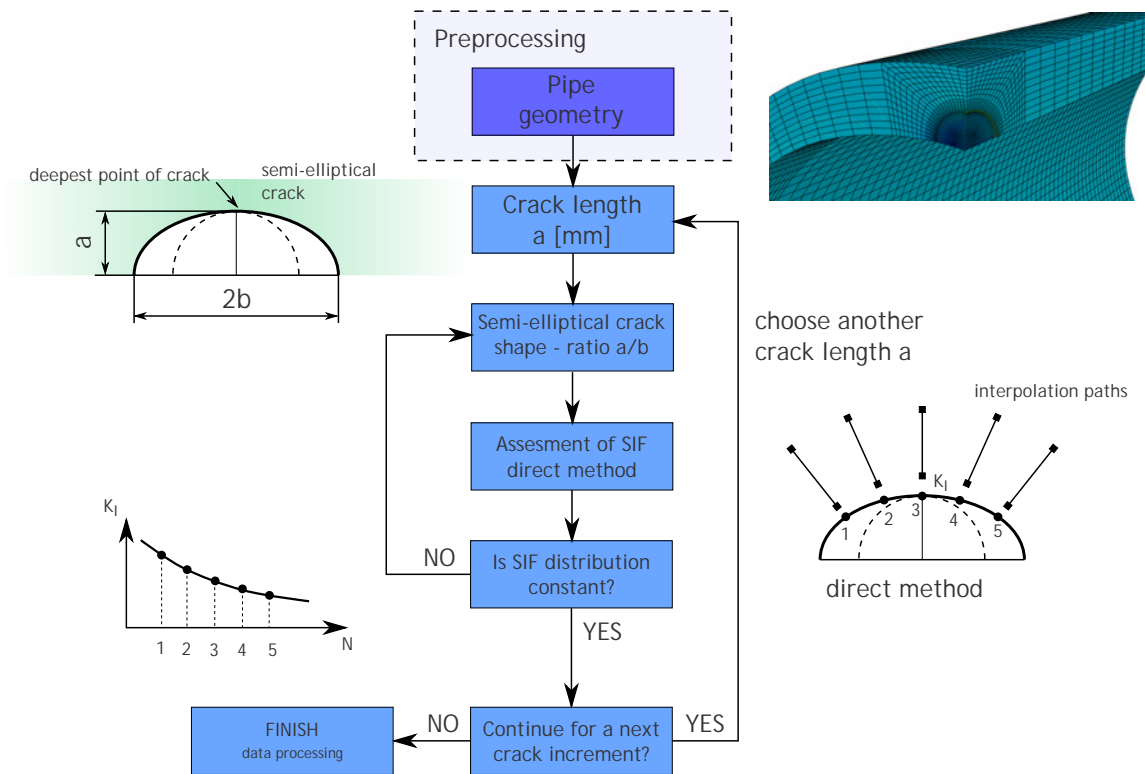


FIGURE 13.1: Flow diagram of solving axial crack propagation (3D case)

## A.2 Algorithm of Circumferential Crack Propagation

The presented algorithm was described in the author's bachelor's thesis [4]. The algorithm was extended of solving axisymmetric bodies.

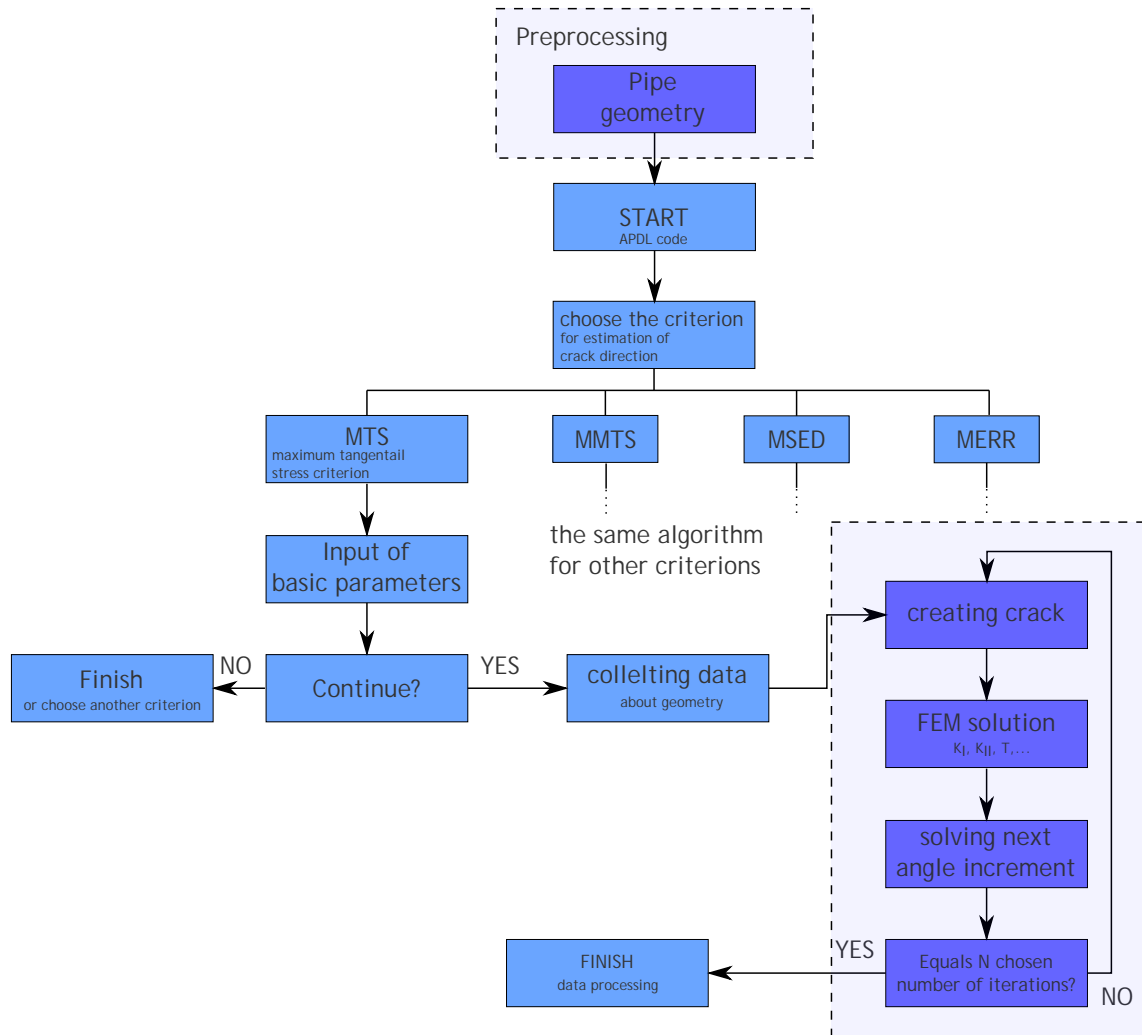


FIGURE 13.2: Flow diagram of solving circumferential crack propagation (2D case)

# B APDL Scripts

## B.1 Material Inhomogeneity Implementation

---

```
1 !Implementation of the inhomogeneous distribution of Young's modulus
2 !Global coordinate system (CS) is in the middle of the weld bead (x axis)
3
4 /prep7
5
6 !Read the function 'm1750_15.mat' describing the Inhomogeneous distrubution
7 !(E_min = 1750 MPa, E_max/E_min = 1.5)
8
9 MPREAD, 'm1750_15', 'mp', 'C:\Users\mikula\Documents'
10
11 !Select everything
12 allsel, all
13
14 !Import the inhomogeneity into the positive y-axis direction with respect to the global CS
15
16 *DO, i, 1, 20, 1 !function is discretized into 21 values
17   NSEL, S, LOC, Y, (i-1)*0.30, 0.35*i !select nodes
18   BF, all, TEMP, i !prescribe a temperature (i-th value) to the selected nodes
19 *ENDDO
20
21   NSEL, S, LOC, Y, 20*0.30, +600 !21st value
22   BF, all, TEMP, 21
23
24 !Import the inhomogeneity into the negative y-axis direction with respect to the global CS
25
26 *DO, i, 1, 20, 1 !function is discretized into 21 values
27   NSEL, S, LOC, Y, -(i-1)*0.30, -0.35*i !select nodes
28   BF, all, TEMP, i !prescribe a temperature (i-th value) to the selected nodes
29 *ENDDO
30
31   NSEL, S, LOC, Y, -20*0.30, -600 !21st value
32   BF, all, TEMP, 21
33
34 !Each temperature is connected with a Young's modulus value (defined in 'm1750_15.mat')
35 !Continue with the solution
36 !/sol
```

---